GNSS Precise Point Positioning with Application of the Equivalence Principle

---

Das Verfahren des GNSS Precise Point Positioning unter Anwendung des Äquivalenzprinzips

vorgelegt von
M. Sc.
Yan Xu
geb. in Fujian, China

von der Fakultät VI – Planen Bauen Umwelt
der Technischen Universität Berlin
zur Erlangung des akademischen Grades

Doktorin der Ingenieurwissenschaften
- Dr. –Ing -

genehmigte Dissertation

Promotionsausschuss:
Vorsitzender: Prof. Jürgen Oberst
Gutachter: Prof. Harald Schuh
Gutachterin: Prof. Luísa Bastos (Universität Porto)
Gutachter: Prof. Roman Galas

Tag der wissenschaftlichen Aussprache: 08. September 2016

Berlin 2016

Abstract

In the last decade Precise Point Positioning (PPP) has become a powerful and widely used technique for positioning by means of Global Navigation Satellite System (GNSS) in geodetic/scientific and civil/daily applications. Meanwhile, the equivalence principle of GNSS data processing has been developed and can now be easily explained and accepted since it was firstly algebraically pointed out in 2002. The objective of this thesis is to explore high-performance PPP algorithms and to develop GNSS algorithms with application of the equivalence principle. The core research and contributions of this thesis are summarized as follows.

In this thesis it is the first time that the specific equivalence of un-differenced and time differencing PPP algorithms is proved theoretically on the basis of the equivalence principle and the equivalence property of un-differenced and differencing algorithms. Meanwhile, as a supplement to the equivalence property of the triple differences, an alternative method is proposed and derived to prove the equivalence between triple differences and zero-difference which up to now was missing.

As a consequence of above conducted theoretical study, a time differencing PPP algorithm based on the equivalence principle is derived and can be used to obtain the coordinates difference and average velocity between two adjacent epochs. Such a time differencing PPP algorithm is able to provide both position and velocity results from the phase and code observations and is expected to be beneficial for applications, such as airborne gravimetry or earthquake monitoring, and could also be an efficient method to detect cycle slips in data processing.

The influence of tropospheric delay on PPP, especially in the context of observations in the polar region or with low elevation cut-off angles, where the position results of the observations are more significantly affected by tropospheric delay, is analyzed and a methodology for minimizing its effect is proposed. Actual meteorological data are used and proved to be beneficial for improving PPP precision in the Antarctic region. The effect of

tropospheric horizontal gradient correction on PPP is also analyzed and verified to remarkably improve PPP precision under lower elevation cut-off angles and higher humidity conditions.

A priori constrained PPP algorithms are proposed and derived in this thesis to improve the efficiency and precision of PPP. The a priori information concerning the geometric and physical properties of observations, which is known with a certain a priori precision, is applied in the PPP algorithms. The contribution of different a priori information constraints on different parameters to PPP solution is analyzed and validated. The a priori constraints as employed in the PPP are specified according to coordinates-, receiver clock offset-, tropospheric delay- and ambiguities-constraints, respectively. The validation of the derived PPP algorithms shows a significant improvement concerning convergence time and positioning accuracy. Moreover, the applications of different constraints under specific conditions are discussed and validated.

A multi-constellation combined PPP algorithm based on the equivalence principle is proposed and derived in this thesis. With such an algorithm, the exponentially increased computational load of the traditional multi-GNSS PPP algorithm can be reduced to the single linear increase when more GNSS satellites are available and used for combined computation. In case of GPS/BDS combination, a method which can speed up the determination of the ambiguities parameters of BDS through applying the contribution of GPS observations is proposed to significantly reduce the convergence time in BDS PPP. The GPS/BDS combined PPP algorithm with inter-system bias (ISB) parameter is also derived. Using the estimated ISB as a priori constraint in the GPS/BDS combined PPP is proposed. The result demonstrates that the a priori constraint of ISB shows superiority in the convergence time of PPP processing and can mainly improve the positioning accuracy in E component.

In traditional combined PPP it is difficult to adaptively adjust the contribution of each single system to the combination through constructing total calculation, and it will lead to the deterioration in the combination accuracy. In this context, the adaptively combined PPP algorithms based on the equivalence principle are proposed and derived, which can easily achieve an adaptive adjustment of weight ratio of each system in the multi-GNSS combination. By using the posteriori covariance matrix of the shared parameters of each

single system and the Helmert variance components to adaptively adjust the weight ratio of each system, the derived algorithms can improve the accuracy of combination significantly, compared to combined PPP with identical weight ratio.

The developed algorithms are net applicable and can be used for cloud computation for internet GNSS service which is considered relevant for possible commercial applications.

Keywords: GNSS; Precise Point Positioning; Sequential Least Squares; Equivalence Principle; Equivalently Eliminated Equation; Time Differencing PPP; Triple Differences; Tropospheric Delay; Meteorological Data; Horizontal Gradient; A Priori Constraint; Coordinates Constraint; Receiver Clock Offset Constraint; Tropospheric Delay Constraint; Ambiguities Constraint; Multi-GNSS Combined PPP; Fast BDS Ambiguity Determination; Inter-system Bias; Adaptively Combined PPP; Posteriori Covariance; Variance Component Estimation

Zusammenfassung

In den letzten zehn Jahren entwickelte sich das Verfahren des Precise Point Positioning (PPP) zu einer leistungsstarken und weit verbreiteten Technik in der Positionsbestimmung mittels des Global Navigation Satellite System (GNSS) in geodätischen/wissenschaftlichen und zivilen/täglichen Anwendungen. Ein wichtiges Grundprinzip der GNSS-Datenverarbeitung ist das Äquivalenzprinzip der GNSS-Datenverarbeitung, das 2002 erstmals beschrieben wurde. Das Ziel dieser Arbeit ist die Untersuchung von Hochleistungs-PPP-Algorithmen und die Entwicklung von GNSS-Algorithmen unter Anwendung des Äquivalenzprinzips. Der Kern der Untersuchungen und die Beiträge dieser Arbeit lassen sich wie folgt zusammengefassen.

Aufbauend auf dem Äquivalenzprinzip und den Äquivalenz-Eigenschaften von nicht-differenzierenden und differenzierenden GNSS-Algorithmen wird in dieser Arbeit zum ersten Mal die spezifische Gleichwertigkeit von nicht-differenzierenden und zeitdifferenzierenden PPP-Algorithmen theoretisch bewiesen. In diesem Zusammenhang beschreiben wir – als Ergänzung zu den Äquivalenz-Eigenschaften der Tripel-Differenzen - eine bis jetzt noch nicht existierende alternative Methode zum Beweis der Äquivalenz von Tripel-Differenzen und undifferenzierten Beobachtungen.

Aufbauend auf der oben erwähnten theoretischen Untersuchung wurde ein zeitlich differenzierender PPP-Algorithmus abgeleitet, der auf dem Äquivalenzprinzip beruht und der dazu benutzt werden kann, die Koordinatendifferenz und die mittlere Geschwindigkeit zwischen benachbarten Beobachtungszeitpunkten zu bestimmen. Ein solcher zeitlich differenzierender PPP-Algorithmus ist in der Lage, sowohl Position als auch Geschwindigkeit aus Phasen- und Code-Beobachtungen zu liefern. Dieser Algorithmus sollte für Anwendungen wie Fluggravimetrie oder Erdbeben-Überwachung nützlich sein und stellt eine effiziente Methode zur Erkennung von Cycle-Slips dar.

Diese Arbeit umfasst auch Analysen des Einflusses der Troposphärischen Signalverzögerung auf das PPP, vor allem im Blick mit Beobachtungen in den Polarregionen oder im Fall niedriger Höhengrenzwinkel (sog. Cut-off-Winkel), wo die Positionsbestimmung

sehr stark von der Troposphärischen Signalverzögerung beeinflusst ist. In diesem Zusammenhang wird eine Methodologie zur Minimierung des Troposphäreneinflusses vorgeschlagen. Es werden reale meteorologische Daten verwendet und es wird gezeigt, dass dies zur Verbesserung der Präzision des PPP in antarktischen Regionen von Vorteil ist. Außerdem wird der Effekt der troposphärischen Horizontalgradienten-Korrektur analysiert und es wurde bewiesen, dass diese Methode zu einer deutlichen Verbesserung des PPP im Fall niedriger Cut-off-Winkel und hoher Luftfeuchtigkeit führt.

In dieser Arbeit werden PPP-Algorithmen mit A-priori-Nebenbedingungen (sog. Constraint) vorgeschlagen und abgeleitet, um die Effizienz und Präzision des PPP zu verbessern. Die in den PPP-Algorithmen angewandten A-priori-Informationen betreffen die geometrischen und physikalischen Eigenschaften von Beobachtungen, von denen vorab eine bestimmte Genauigkeit bekannt ist. Der Einfluss von verschiedenen A-priori-Nebenbedingungen auf verschiedene Parameter innerhalb der PPP-Lösung wird analysiert und validiert. Diese in den PPP-Algorithmen angewandten A-priori-Bedingungen sind aus Nebenbedingungen für Koordinaten, Empängeruhren-Offsets, Troposphären-Verzögerung und Ambiguities abgeleitet. Die Validierung dieser Algorithmen zeigt eine deutliche Verbesserung bezüglich der Konvergenzzeit und der Genauigkeit in der Positionsbestimmung. Ferner wird die Anwendung verschiedener Constraints unter spezifischen Bedingungen diskutiert unf validiert.

In dieser Arbeit wurde ein kombinierter PPP-Algorithmus für Multi-Satellitensysteme vorgeschlagen und abgeleitet, der auf dem genannten Äquivalenzprinzip beruht. Mit einem solchen Algorithmus kann die exponentiell ansteigende Computerlast des traditionellen Multi-GNSS-PPP dahingehend reduziert werden, dass es nur einen einfachen linearen Anstieg gibt, wenn mehr GNSS-Satelliten einbezogen werden. Für den Fall der Kombination von GPS mit dem chinesischen Beidou-System (BDS) wird eine Methode vorgeschlagen, die die Berechnung der Ambiguity-Parameter für das BDS-System durch Beitrag von GPS-Beobachtungen schneller beschleunigt. Diese Methode reduziert die Konvergenzzeit im BDS-PPP deutlich. Außerdem wird im Fall der Kombination von GPS und BDS ein Inter-System-Bias (ISB) abgeleitet. Es wird vorgeschlagen, diesen ISB als

A-priori-Nebenbedingung in das PPP bei der Kombination von GPS und BDS einzuführen. Dadurch ergeben sich überlegene Resultate für die Konvergenzzeit in der PPP-Prozessierung und die Positionsgenauigkeit in der Ost-Komponente kann verbessert werden.

Im traditionellen kombinierten PPP-Verfahren ist es schwierig, den Beitrag jedes einzelnen Systems zur Kombination durch Konstruktion einer Gesamtlösung adaptiv anzugleichen, was zur Verschlechterung in der Kombinationsgenauigkeit führt. In diesem Zusammenhang wurde ein adaptiv kombinierter PPP-Algorithmus vorgeschlagen und entwickelt, der auf dem Äquivalenzprinzip beruht. Dieser Algorithmus ermöglicht eine einfache adaptive Ausgleichung der relativen Wichtungen für jedes Satelliten-System in der Multi-GNSS-Kombination. Durch Nutzung der a-posteriori Kovarianz-Matrix, die für alle gemeinsamen Parameter der einzelnen Satelliten-Systeme aufgestellt wurde und durch die Anwendung der Helmertschen Varianzkomponenten-Schätzung zur adaptiven Ausgleichung der relativen Wichtungen der einzelnen Systeme kann die Genauigkeit der Kombination im Vergleich zum PPP mit identischen Relativgewichten deutlich gesteigert werden.

Die entwickelten Algorithmen sind über das Internet anwendbar und könnten für Cloud-Berechnungen im Rahmen eines Internet-GNSS-Dienstes verwendet werden, was für mögliche kommerzielle Anwendungen von Bedeutung sein könnte.

Stichworte: GNSS; Precise Point Positioning; Sequenzielle Kleinste Quadrate; Äquivalenzprinzip; Äquivalent eliminierte Gleichung; Zeitlich differenzierendes PPP; Trip-Differenzen; Troposphärische Verzögerung; Meteorogische Daten; Horizontaler Gradient; A-priori-Nebenbedingung; Koordinaten-Nebenbedingung; Empfängeruhren-Offset-Nebenbedingung; Troposphären-Verzögerungs-Nebenbedingung; Ambiguity-Nebenbedingung; Kombiniertes Multi-GNSS-PPP; Schnelle BDS-Ambiguity-Bestimmung; Intersystem-Bias; Adaptiv kombiniertes PPP; A-prosteriori Kovarianz; Varianzkomponenten-schätzung

Table of Contents

List of Abbreviations

BDS	the Chinese BeiDou Navigation Satellite System
CNAGA	China National Administration of GNSS and Applications
DD	Double Differences
DIA	Detection Identification and Adaptation
ESA	European Space Agency
ERP	Earth Rotation Parameter
FOC	Full Operational Capability
Galileo	the European Union Satellite Navigation System
GEO	Geostationary Earth Orbit
GFZ	GFZ German Research Centre for Geosciences
GLONASS	the Russian GLObal NAvigation Satellite System
GMF	Global Mapping Function
GNSS	Global Navigation Satellite System
GPS	Global Positioning System
GPT	Global Pressure and Temperature model
GPT2	the improved Global Pressure and Temperature model
IERS	International Earth Rotation Service
IGG	Institute of Geodesy and Geophysics
IGS	International GNSS Service
IGSO	Inclined Geo-Synchronous Orbit
IMU	Inertial Measurement Unit
INS	Inertial Navigation System
IOV	In-Orbit Validation
ISB	Inter-System Bias
ITRF	International Terrestrial Reference Frame
LEO	Low Earth Orbit
MEO	Medium Earth Orbit
MGEX	Multi-GNSS Experiment
NMF	Niell Mapping Function

PCO	Phase Centre Offset
PCV	Phase Centre Variation
PPP	Precise Point Positioning
RMS	Root Mean Square
RTCM	Radio Technical Commission for Maritime Services
RTS	Real-Time Service
SD	Single Difference
TD	Triple Differences
UKF	Unscented Kalman Filter
VMF1	Vienna Mapping Function 1
ZHD	Zenith Hydrostatic Delay
ZPD	Zenith Path Delay
ZTD	Zenith Total Delay
ZWD	Zenith Wet Delay

List of Figures

List of Tables

1 Introduction

1.1 Research Background and Motivation

Global Navigation Satellite System (GNSS) refers to a constellation of satellites providing signals from space transmitting positioning and timing data. It is playing a significant role in offering high-precision navigation, positioning and timing service for global users (Hoffmann-Wellenhof et al., 2008; Someswar et al., 2013). Positioning by means of GNSS is one of the most widely used techniques in geodetic and geodynamics applications (Gandolfi et al., 2015). In the last decade Precise Point Positioning (PPP) has become a powerful technique for determining a point's coordinates using GNSS (Kouba and Héroux, 2001; Zumberge et al., 1997) and it also has become increasingly significant in high-precision positioning applications. With PPP technique, observations produced by a single receiver without the requirement of a nearby reference station are used to determine its three coordinate components, along with other parameters such as the receiver clock error and the tropospheric delay of observations (Leandro et al., 2010). Currently it is being strongly considered as a solution wherever precise positioning and navigation are required in isolated locations or wide areas, where reference station infrastructure is not available (Bisnath and Gao, 2009). During recent years PPP has been widely applied in many spots, such as precise orbit determination of Low Earth Orbiters (Bisnath and Langley, 2002), marine applications (Bisnath et al., 2003; Geng et al., 2010), airborne mapping (Gao et al., 2005), atmosphere remote sensing (Gao et al., 2004), land surveying (Dixon, 2006), precise time-transfer (Defraigne et al., 2007; Defraigne et al., 2008), ionospheric (Leandro et al., 2007) and tropospheric characterization (Kjørsvik et al., 2006), biases calibration (Leandro et al., 2010), etc. During the past few years, PPP has achieved performance levels comparable to those obtainable through differencing approach (Bisnath and Gao, 2009; Griffiths and Ray, 2009), especially for GNSS permanent stations. By using the precise orbit and clock products generated by the International GNSS Service (IGS) through a dense global network and several contributing analysis centers (Dow et al., 2009), static absolute positioning can

achieve an accuracy of mm-cm in post processing and a cm-dm precision level can be attained in kinematic applications (Hesselbarth, 2011; Kouba and Héroux, 2001; Wang, 2014). For real-time application, with the availability of the IGS real-time service (RTS), it becomes possible for the users to obtain precise satellite orbit and satellite clock corrections via RTCM streams in real-time. Recent research has shown that the availability of GPS IGS RTS products is at least 95%, which makes it possible to perform real-time PPP with high accuracy (Caissy et al., 2012; Elsobeiey and Al-Harbi, 2015). Furthermore, with the rapid development of PPP technique (Bertiger et al., 2010; Grinter and Roberts, 2011; Grinter and Roberts, 2013), several PPP software packages are developed and online PPP processing services are released (Moreno Monge et al., 2013). Such online PPP services are open to users and are available 24 hours per day. Besides precise coordinates and quality information of user stations in the International Terrestrial Reference Frame (ITRF) the results also include ionospheric delays, tropospheric delays, and receiver clock corrections (Guo, 2014).

Although for many applications the PPP approach presents definite advantages regarding operational flexibility and cost-effectiveness, it requires a relatively long initialization time as phase ambiguities converge to constant values and the solution reaches its optimal precision. The convergence time of PPP will vary because it is affected by a number of factors, such as the number and geometry of visible satellites, observation quality and sampling rate, user tracking conditions, and environment (Bisnath and Gao, 2009). Furthermore, due to the influence of pseudorange noise and tropospheric delay (etc.), the accuracy and reliability of PPP are still limited (Li, 2013). The unknown tropospheric delay parameter is usually estimated along with the position and ambiguity parameters. Ingestion of precise tropospheric models could reduce the total number of unknown parameters that need to be estimated from the observation model, potentially remove the need for noise propagating linear combinations of observables, and potentially improve positioning performance (Dodd et al., 2006). In this case, the influence of tropospheric delay on PPP is studied in this thesis. Especially in the context of polar region or with low elevation cut-off angles, where the position results of the observations are more significantly affected by tropospheric delay (Ren et al., 2011; She et al., 2011; Xu et al., 2014), the actual meteorological data are used and proved to be beneficial for

improving PPP precision. The effect of the tropospheric horizontal gradient correction on PPP is also analyzed and verified to have remarkable improvement on PPP under lower elevation cut-off angles and higher humidity conditions. Moreover, a priori constrained PPP algorithms are proposed and derived to improve the efficiency and precision of PPP. The a priori information concerning the geometric and physical properties of observations, which is known with a certain a priori precision, is applied in the PPP algorithms. In this thesis the a priori constraints as employed in PPP are specified according to coordinates-, receiver clock offset-, tropospheric delay- and ambiguities-constraints, respectively, and are validated to be superior both in convergence time and positioning accuracy of PPP.

During the past decades of GPS research, advantages and disadvantages of differencing and un-differenced, combined and uncombined GPS algorithms have been discussed in detail in many publications. However, the equivalence principle can now be easily explained and accepted, since the differencing and un-differenced GPS algorithms were algebraically proved to be equivalent in Xu (2002) and the equivalence of combined and uncombined algorithms were also proved in Xu (2007). As the information, including the used GPS data and model and adjustment method, are the same, the results should also be equivalent. The equivalence properties are summarized in a theorem in Xu (2007) and Xu et al. (2010) as follows. First, for any GNSS survey with definitive space-time configuration, the results obtained by using any GNSS data processing algorithms or any mixture of the algorithms are identical. Second, the diagonal elements of the covariance matrix and the precision of the solutions are identical. And third, suitable algorithms or mixtures of the algorithms will be specifically beneficial for special kinds of data dealings. The theorem indicates that if the data used are the same and the model is parameterized identically and regularly, then the results must be identical and the precision should be equivalent. On the basis of the equivalence principle and the equivalence property of un-differenced and differencing algorithms pointed out in Xu (2007) and Xu et al. (2010), the specific equivalence of un-differenced and time differencing PPP algorithms is proved theoretically in this thesis for the first time. Meanwhile, an alternative method to prove the equivalence between triple differences and zero-difference is proposed and derived in this thesis as a supplement to the equivalence property of the triple differences stated in Xu

(2007) and Xu et al. (2010). Then as a consequence of this theoretical study, a time differencing PPP algorithm based on the equivalence principle is also derived.

As summarized in Xu et al. (2010), one of the most important inference of the equivalence principle is the diagonalization algorithm (Xu, 2003). Based on the parameter equivalent reduction principle, the equivalently eliminated normal equation can be constructed and thus the normal equation can be diagonalised. This has a great significance for sequential adjustment and Kalman filter used in real-time data processing, since the nuisance parameter from the past can be eliminated and given up to keep the updated problem as small as possible. Generally, the observation equation can be separated into two diagonal parts, respectively. Each part uses the original observation vector and the original weight matrix, while the equation owns only a part of the unknown parameters. The normal equation of the original observation equation can also be separated into two parts. Only the interested unknown part is needed to be accumulated into the present normal equation to solve the problem. Therefore the nuisance parameters are eliminated during sequential data processing so that the data processing problem remains as small as possible. Applying this method, it is realistic to make an exact and effective real-time data sequential processing (Shen et al., 2008; Shen and Xu, 2007; Xu et al., 2010).

With the rapid development of multiple GNSS systems, PPP technique is also advancing forward from mainly using GPS measurements towards using multi-GNSS combinations. With newly available precise orbit and clock data for GLONASS and BDS satellites, additional GLONASS and BDS observations can be applied to augment GPS for improved positioning accuracy, reliability, and availability using PPP. Many studies on multi-GNSS combination have been conducted during recent years (Cai and Gao, 2013; Dach et al., 2007; Jokinen et al., 2011). Nevertheless, these studies focus mainly on validation of precision and reliability superiority of multi-GNSS combination, while the combined algorithm itself and the weight ratio of each single system in the combination are seldom involved. The traditional combined PPP algorithm directly constructs observation equations using all GNSS observables to obtain the solution. However, with the advance of other available systems and satellites, as well as the wide utilization of high-frequency (1-50 Hz) recording receivers, the

computational load of the traditional algorithm increases exponentially, while the efficiency of the algorithm decreases significantly at the same time (Huang et al., 2013). This is highly undesirable in high performance systems. Therefore, on the basis of the equivalence principle and its inference described above, a multi-GNSS combined PPP algorithm is derived in this thesis to improve the computation efficiency by decreasing the exponentially increased computation load to single linear increase. In case of GPS/BDS combination, a method which can speed up the determination of the ambiguities parameters of BDS through applying the contribution of GPS observations is proposed and analyzed. The GPS/BDS combined PPP algorithm with inter-system bias parameter is also derived. Furthermore, the usage of estimated ISB as a priori constraint in the GPS/BDS combined PPP is proposed to improve the convergence time and positioning accuracy. In addition, in the traditional combined PPP it is difficult to adaptively adjust the contribution of each single system to the combination through constructing total calculation, which will lead to the deterioration in the combination accuracy. In this context, the adaptively combined PPP based on the equivalence principle, which can easily achieve an adaptive adjustment of the weight ratio of each system in the multi-GNSS combination is proposed and derived. Compared to combined PPP with identical weight ratio the derived algorithms can significantly improve the accuracy of combination.

1.2 The Main Research Contents and Overview of the Dissertation

This thesis mainly explores high-performance PPP algorithms and develops GNSS algorithms with application of the equivalence principle, it includes the following chapters:

First, Chapter 1 presents the background and the motivation of this thesis and specifies the contributions of this research.

In Chapter 2 commonly used adjustment and filtering algorithms in PPP are outlined. Then the equivalence principle is described and developed. The specific equivalence of un-differenced and time differencing PPP algorithms is proved theoretically. An alternative method to prove the equivalence between triple differenced and zero-difference is proposed and derived. An algorithm of time differencing PPP based on the equivalence principle is derived and a numerical example is given.

Chapter 3 explores the influence of tropospheric delay on PPP. The effects of using actual meteorological data on positioning, especially in the context of observations in the polar region or with low elevation cut-off angles, are highlighted. The influence and improvement by applying horizontal gradient correction on PPP is also studied in this chapter. Several practical and enlightening conclusions are given.

In Chapter 4 a priori constrained PPP algorithms are researched and derived. A priori information concerning geometric and physical properties of observations, which is known with a certain a priori precision, is applied in the PPP algorithms. The contribution of different a priori information constraints on different parameters to PPP solution is studied and validated. The a priori constrained PPP algorithms are specified according to coordinates-, receiver clock offset-, tropospheric delay- and ambiguities-constraints, respectively, and are validated to have great superiority in convergence time and positioning accuracy. Moreover, the applications of different constraints under specific conditions are also discussed.

Chapter 5 proposes and derives a multi-constellation combined PPP algorithm based on the equivalence principle. The advantages of the algorithm, the computation efficiency and accuracy of the algorithm are validated through several numerical examples. Then a method which can speed up the determination of the ambiguities parameters of BDS through applying the contribution of GPS observations is proposed and analyzed in case of GPS/BDS combination. The GPS/BDS combined PPP algorithm with inter-system bias parameter is also derived. Furthermore, the usage of estimated ISB as a priori constraint in the GPS/BDS combined PPP is proposed to improve the convergence time and positioning accuracy.

In Chapter 6 the principle, developments and application of the adaptively robust filter, are summarized and introduced. Then the adaptively robust PPP of a single system based on the equivalence principle is derived. Moreover, due to the defect of the multi-GNSS combination with equal weight ratio, two kinds of adaptively multi-GNSS combined PPP algorithms based on the equivalence principle are derived, which can easily achieve an adaptive adjustment of the weight ratio of each system in the multi-GNSS combination. The posteriori covariance matrix of the shared parameters of each single system and the Helmert variance components are used to adaptively adjust the weight ratio of each system in the multi-GNSS combination,

respectively. Numerical examples are conducted to validate the derived algorithms.

Finally, Chapter 7 summarizes the main results as obtained in the previous chapters, presents the final conclusions and suggests recommendations for future work.

1.3 The Main Contributions of the Dissertation

The main contributions of this thesis can be summarized as follows.

1. In this thesis it is the first time that the specific equivalence of un-differenced and time differencing PPP algorithms is proved theoretically on the basis of the equivalence principle and the equivalence property of un-differenced and differencing algorithms. Meanwhile, as a supplement to the equivalence property of the triple differences, an alternative method is proposed and derived to prove the equivalence between triple differences and zero-difference, which up to now was missing.

2. As a consequence of above conducted theoretical study, a time differencing PPP algorithm based on the equivalence principle is derived and can be used to obtain the coordinates difference and average velocity between two adjacent epochs. Such a time differencing PPP algorithm is able to provide both position and velocity results from the phase and code observations and is expected to be beneficial for different types of applications, such as airborne gravimetry, earthquake monitoring, and could also be an efficient method to detect cycle slips in data processing.

3. The influence of tropospheric delay on PPP, especially in the context of observations in the polar region or with low elevation cut-off angles, where the position results of observations are more significantly affected by tropospheric delay, is analyzed and a methodology for minimizing its effect is proposed. Due to the specificity of Antarctic positioning, the actual meteorological data are used and proved to be beneficial for improving PPP precision in the Antarctic region. The effect of tropospheric horizontal gradient correction on PPP is also analyzed and verified to remarkably improve PPP precision under lower elevation cut-off angles and higher humidity conditions.

4. A priori constrained PPP algorithms are proposed and derived in this thesis to improve the efficiency and precision of PPP. The a priori information concerning the geometric and

physical properties of observations, which is known with a certain a priori precision, is applied in the PPP algorithms. The contribution of different a priori information constraints on different parameters to PPP solution is analyzed and validated. The a priori constrained PPP algorithms are specified according to coordinates-, receiver clock offset-, tropospheric delay- and ambiguities-constraints, respectively, and not only the efficiency and accuracy improvement by applying constraints but also their applications under specific conditions are discussed and validated.

5. A multi-GNSS combined PPP algorithm based on the equivalence principle is proposed and derived in this thesis. With such an algorithm, the exponentially increased computational load of the traditional multi-GNSS PPP algorithm can be reduced to the single linear increase when more GNSS satellites are available and used for combined computation. In case of GPS/BDS combination, a method which can speed up the determination of the ambiguities parameters of BDS through applying the contribution of GPS observations is proposed to significantly reduce the convergence time in BDS PPP. The GPS/BDS combined PPP algorithm with inter-system bias parameter is also derived. Using the estimated ISB as a priori constraint in the GPS/BDS combined PPP is proposed. The result demonstrates that the a priori constraint of ISB shows superiority in the convergence time of PPP processing and can mainly improve the positioning accuracy in E component.

6. In traditional combined PPP it is difficult to adaptively adjust the contribution of each single system to the combination through constructing total calculation, and it will lead to the deterioration in the combination accuracy. In this context, the adaptively combined PPP algorithms based on the equivalence principle are proposed and derived, which can easily achieve an adaptive adjustment of weight ratio of each system in multi-GNSS combination. By using the posteriori covariance matrix of the shared parameters of each single system and the Helmert variance components to adaptively adjust the weight ratio of each system, the derived algorithms can improve the accuracy of combination significantly, compared to combined PPP with identical weight ratio.

2 Equivalence Principle of Precise Point Positioning

2.1 Introduction

Commonly used adjustment and filtering algorithms in Precise Point Positioning (PPP) are outlined in this chapter. Adjustment algorithms discussed here include the least squares adjustment and the sequential least squares adjustment. The filtering algorithm discussed here is the classic Kalman filter. The equivalence principle is described and developed. On the basis of the equivalence principle and the equivalence property of un-differenced and differencing algorithms, the specific equivalence of un-differenced and time differencing PPP algorithms is proved theoretically. Meanwhile, as a supplement to the equivalence property of the triple differences, an alternative method is proposed and derived to prove the equivalence between triple differences and zero-difference which up to now was missing. As a consequence of the conducted theoretical study, an algorithm of time differencing PPP based on the equivalence principle is derived and a numerical example is given. Such a time differencing PPP algorithm is able to provide both position and velocity results from the phase and code observations.

2.2 Commonly Used Adjustment and Filtering Algorithms in PPP

In PPP, precise ephemeris and precise satellite clock errors are usually immediately substituted into the observation equation to fix the satellite orbits and remove the satellite clock errors. Furthermore, the first-order effects of ionospheric delay is eliminated via dual-frequency observations. Therefore the calculation model of PPP can be written as (Ye et al., 2008; Zumberge et al., 1997)

$$v_{\Phi} = \rho + c \cdot \Delta t + \delta + \lambda \cdot N - \lambda \cdot \Phi + \varepsilon_{\Phi} \tag{2.1}$$

where ρ is the geometric distance between the satellite at the emission time and the receiver antenna at the reception time; c denotes the speed of light; Δt denotes the receiver clock error; δ denotes the tropospheric delay; λ denotes the wavelength; Φ is the ionosphere-free combined observation; N denotes its ambiguity; ε_{Φ} denotes the not modeled

remaining errors like multipath and observation noise; and v_Φ is the corresponding observation error.

To solve the unknowns, like coordinates, clock error, and tropospheric delay parameters the commonly used adjustment and filtering algorithms in PPP are outlined in the next sections.

2.2.1 Least Squares Adjustment

The principle of least squares adjustment can be summarized as follows (Leick et al., 2015; Xu, 2007).

The system of the linearized error equation of Eq. (2.1) can be represented as

$$V = AX - L, \quad P \tag{2.2}$$

where L is the observational vector of dimension n; A is the coefficient matrix of dimension $n \times m$; X is the unknown parameter vector of dimension m; V is the residual vector of dimension n; m is the number of unknown parameters; n is the number of observations; P is the symmetric and definite weight matrix of dimension $n \times n$.

The least squares principle for solving the error equation is well-known as

$$V^T PV = \min \tag{2.3}$$

where V^T is the transpose of vector V.

Solving the minimum value of $V^T PV$ with respect to X and take Eq. (2.2) into account, one has

$$A^T PV = 0 \tag{2.4}$$

where A^T is the transpose matrix of A.

Substituting Eq. (2.2) into Eq. (2.4), one has

$$A^T PAX - A^T PL = 0 \tag{2.5}$$

Therefore, the least squares solution of Eq. (2.2) is

$$X = (A^T PA)^{-1} A^T PL \tag{2.6}$$

where superscript $^{-1}$ is an inverse operator. Denoting $M = A^T PA$, $Q_X = (A^T PA)^{-1}$, where M is usually called normal matrix and Q_X is the cofactor matrix.

The covariance matrix $\sum_X$ of the estimated parameter X is

$$\sum_X = Q_X \sigma_0^2 \tag{2.7}$$

where σ_0 is the standard deviation, which can be computed by

$$\sigma_0 = \sqrt{\frac{V^T PV}{n-m}} \quad (n > m) \tag{2.8}$$

2.2.2 Sequential Least Squares Adjustment

Suppose L_i is an observational vector of dimension n_i at epoch i, and the corresponding weight matrix is P_i. At epoch i-1, the estimation value of the unknown parameters and its weight matrix are obtained and denoted as X_{i-1} and $P_{X_{i-1}}$. The error equation at epoch i can be represented as

$$V_i = A_i X_i - L_i \ , \quad P_i \tag{2.9}$$

where subscript i denotes epoch i; A_i is the coefficient matrix of dimension $n_i \times m$; V_i is the residual vector of dimension n_i; m is the number of unknown parameters; n_i is the number of observations at epoch i. Since the unknown parameter X_i has the a priori expectation and variance, the least squares principle of the parameter estimation is (Yang, 2006)

$$V_i^T P_i V_i + (X_i - X_{i-1})^T P_{X_{i-1}} (X_i - X_{i-1}) = \min \tag{2.10}$$

Solving the minimum value of Eq. (2.10) with respect to X_i and taking Eq. (2.9) into account, one has

$$A_i^T P_i V_i + P_{X_{i-1}} (X_i - X_{i-1}) = 0 \tag{2.11}$$

Substituting Eq. (2.9) into Eq. (2.11), one has

$$(A_i^T P_i A_i + P_{X_{i-1}}) X_i - (A_i^T P_i L_i + P_{X_{i-1}} X_{i-1}) = 0 \tag{2.12}$$

Therefore, the sequential least squares solution of Eq. (2.9) is

$$X_i = (A_i^T P_i A_i + P_{X_{i-1}})^{-1}(A_i^T P_i L_i + P_{X_{i-1}} X_{i-1}) \tag{2.13}$$

Denoting

$$P_{X_i} = A_i^T P_i A_i + P_{X_{i-1}} \tag{2.14}$$

one has

$$X_i = P_{X_i}^{-1}(A_i^T P_i L_i + P_{X_{i-1}} X_{i-1}) \tag{2.15}$$

$$Q_{X_i} = P_{X_i}^{-1} = (A_i^T P_i A_i + P_{X_{i-1}})^{-1} \tag{2.16}$$

Eq. (2.15) is the recurrence formula of the sequential least squares solution, that

$$\begin{cases} X_1 = P_{X_1}^{-1} A_1^T L_1 \\ X_2 = P_{X_2}^{-1}(A_2^T P_2 L_2 + P_{X_1} X_1) \\ \vdots \\ X_i = P_{X_i}^{-1}(A_i^T P_i L_i + P_{X_{i-1}} X_{i-1}) \end{cases} \tag{2.17}$$

$$\begin{cases} P_{X_1} = A_1^T P_1 A_1 \\ P_{X_2} = P_{X_1} + A_2^T P_2 A_2 \\ \vdots \\ P_{X_i} = P_{X_{i-1}} + A_i^T P_i A_i \end{cases} \tag{2.18}$$

The posteriori covariance matrix $\sum_{X_i}$ of X_i is

$$\sum_{X_i} = Q_{X_i} \sigma_{0_i}^2 = P_{X_i}^{-1} \sigma_{0_i}^2 \tag{2.19}$$

where σ_{0_i} is the standard deviation, which can be computed by (Yang, 2006)

$$\sigma_{0_i} = \sqrt{\frac{V_i^T P_i V_i + (X_i - X_{i-1})^T P_{X_{i-1}} (X_i - X_{i-1})}{n_i}} \tag{2.20}$$

where n_i is the number of observations at epoch *i*.

2.2.3 Kalman Filter

The Kalman filter is known to estimate the state vector based on a sequence of observations and its state equation. The principle of the classic Kalman filter is outlined as follows (Brown and Hwang, 1992; Gelb, 1986; Koch and Yang, 1998; Schwarz et al., 1989; Xu, 2007; Yang, 2006).

The observation equation and the state equation can be expressed as

$$V_i = A_i X_i - L_i \ , \quad P_i \tag{2.21}$$

$$X_i = \Phi_{i,i-1} X_{i-1} + W_i \tag{2.22}$$

where subscript *i* and *i*-1 denote epoch time; X_{i-1} and X_i are the simplified state vectors of dimension *m* at epoch *i*-1 and epoch *i*, respectively; $\Phi_{i,i-1}$ is the state transition matrix of dimension $m \times m$; W_i is the residual vector of the system state model of dimension *m* with zero expectation and covariance matrix $\sum_{W_i}$; L_i is the observational vector of dimension n_i; A_i is the coefficient matrix of dimension $n_i \times m$; V_i is the residual vector of observational vector of dimension n_i; *m* is the number of unknown parameters; n_i is the number of observations at epoch *i*; P_i is the weight matrix of observational vector of dimension $n_i \times n_i$.

According to Eq. (2.22), the predicted value of the state vector $\overline{X}_i$ at epoch *i* can be obtained through the estimated state vector X_{i-1} and the transition matrix as

$$\overline{X}_i = \Phi_{i,i-1} X_{i-1} \tag{2.23}$$

The covariance matrix $\sum_{\overline{X}_i}$ of the predicted state vector $\overline{X}_i$ can be obtained by using the covariance propagation law as

$$\sum_{\overline{X}_i} = \Phi_{i,i-1} \sum_{X_{i-1}} \Phi_{i,i-1}^T + \sum_{W_i} \tag{2.24}$$

The residual vector $V_{\overline{X}_i}$ of the predicted state vector $\overline{X}_i$ is

$$V_{\overline{X}_i} = X_i - \overline{X}_i \tag{2.25}$$

Therefore a least squares principle of the parameter estimation is formed as

$$V_i^T P_i V_i + V_{\overline{X}_i}{}^T P_{\overline{X}_i} V_{\overline{X}_i} = \min \tag{2.26}$$

where $P_i = \sum_i^{-1}$ is the weight matrix of L_i and $P_{\overline{X}_i} = \sum_{\overline{X}_i}^{-1}$ is the weight matrix of $\overline{X}_i$.

Making the partial differentiation of Eq. (2.26) with respect to X_i equals zero, one has

$$A_i^T P_i V_i + P_{\bar{X}_i} V_{\bar{X}_i} = 0 \tag{2.27}$$

Substituting Eq. (2.21) and (2.25) into Eq. (2.27), one has

$$(A_i^T P_i A_i + P_{\bar{X}_i}) X_i - (A_i^T P_i L_i + P_{\bar{X}_i} \bar{X}_i) = 0 \tag{2.28}$$

Therefore, the least squares solution of state vector X_i is

$$X_i = (A_i^T P_i A_i + P_{\bar{X}_i})^{-1} (A_i^T P_i L_i + P_{\bar{X}_i} \bar{X}_i) \tag{2.29}$$

The covariance matrix of X_i is

$$\sum_{X_i} = (A_i^T P_i A_i + P_{\bar{X}_i})^{-1} \sigma_0^2 \tag{2.30}$$

Denoting

$$P_{X_i} = A_i^T P_i A_i + P_{\bar{X}_i} \tag{2.31}$$

one has

$$\sum_{X_i} = P_{X_i}^{-1} \sigma_0^2 \tag{2.32}$$

According to the principle of the matrix identity transformation (Yang et al., 2001), that

$$X_i = \bar{X}_i + K_i (L_i - A_i \bar{X}_i) \tag{2.33}$$

where K_i is called the gain matrix of the Kalman filter and is formed as

$$K_i = \sum_{\bar{X}_i} A_i^T (A_i \sum_{\bar{X}_i} A_i^T + \sum_i)^{-1} \tag{2.34}$$

or in accordance with the matrix identity equation

$$K_i = (A_i^T P_i A_i + P_{\bar{X}_i})^{-1} A_i^T P_i \tag{2.35}$$

The covariance matrix of X_i can be obtained by using the covariance propagation law to Eq. (2.33) as

$$\sum_{X_i} = \sum_{\bar{X}_i} - \sum_{\bar{X}_i} A_i^T (A_i \sum_{\bar{X}_i} A_i^T + \sum_i)^{-1} A_i \sum_{\bar{X}_i} \tag{2.36}$$

or

$$\sum_{X_i} = (I - K_i A_i) \sum_{\bar{X}_i} \tag{2.37}$$

where I is the identity matrix.

The main difference between Kalman Filter and Sequential Least Squares Adjustment is that Kalman filter is applied in kinematic case, taking into account the state equation, the velocity and acceleration information of the carriers; while sequential least squares adjustment is usually applied in static processing. Kalman filter is a general form of sequential least squares adjustment, and the sequential least squares adjustment is a special case of Kalman filter. Kalman filter estimation uses the predicted values computed by the state equation at current epoch, while sequential least squares adjustment uses the estimated values of last epoch.

As introduced Kalman filter assumes a state equation, which is formed by a system transition matrix and a cofactor. Therefore, the estimated values in Kalman filter process are dependent on the transition matrix and cofactor. The transition matrix should be based on strengthened physical models, and the cofactor should be well-known or reasonably given. If the system description is accurate enough, of course Kalman filter will lead to a more precise result. However, if the system is not sufficiently well-known, the result of Kalman filter will sometimes not converge to the true values (divergence). Furthermore, a kinematic process is generally difficult to be precisely represented by theoretical system equations. Another problem of Kalman filter is the strong dependency of the given initial values.

2.3 Equivalence Principle and Equivalently Eliminated Observation Equation

The equivalence properties are summarized in a theorem in Xu (2007) and Xu et al. (2010) as follows. First, for any GNSS survey with definitive space-time configuration, the results obtained by using any GNSS data processing algorithms or any mixture of the algorithms are identical. Second, the diagonal elements of the covariance matrix and the precision of the solutions are identical. And third, suitable algorithms or mixtures of the algorithms will be specifically beneficial for special kinds of data dealings. The theorem indicates that if the data used are the same and the model is parameterized identically and regularly, then the results

must be identical and the precision should be equivalent. As we know that the observation equations of the differencing methods or combined algorithms can be obtained by carrying out a related linear transformation to the original equations. All methods are theoretically equivalent, since the weight matrix is similarly transformed according to the law of covariance propagation. Any combinations of the solutions must be equivalent to each other and to the original observation equation, none of the combinations will lead to better solutions or better precision of the solutions. However, suitable algorithms or combination of the algorithms will lead to convenience in the computation and software realization and may decrease the risk for wrong computation as well. Nevertheless, theoretically the final result should be equivalent even if the efficiency or the error tolerance capacity of computation will be improved. From this rigorous theoretical aspect, such as the traditional wide-lane ambiguity fixing technique (Petrovello, 2006; Teunissen, 2003; Teunissen, 2005; Teunissen et al., 1997) may lead to a more effective search, but not a better solution and precision of the ambiguity. The equivalent observation equation approach based on the derivation of Zhou (1985) can be used to unify the differencing and un-differenced methods as well as uncombined and combined algorithms.

As summarized in Xu et al. (2010), one of the most important inference of the equivalence principle is the diagonalization algorithm (Xu, 2003). Based on the parameter equivalent reduction principle, the equivalently eliminated normal equation can be constructed and thus the normal equation can be diagonalised. This has a great significance for sequential adjustment and Kalman filter used in real-time data processing, since the nuisance parameter from the past can be eliminated and given up to keep the updated problem as small as possible. Generally, the observation equation can be separated into two diagonal parts, respectively. Each part uses the original observation vector and the original weight matrix, while the equation owns only a part of the unknown parameters, where the nuisance parameters have been eliminated during the sequential data processing. Therefore in least squares adjustment, the unknown parameters are divided into two groups: interested unknowns and uninterested unknowns in practice. It is better to eliminate the group of uninterested unknowns because of its size. In this case, through using the equivalently eliminated observation equation, the

uninterested unknown parameters can be eliminated directly from the observation equations instead of from the normal equations.

The linearized observation equation can be represented as

$$V = \begin{pmatrix} A & B \end{pmatrix} \begin{pmatrix} X_1 \\ X_2 \end{pmatrix} - L, \quad P \tag{2.38}$$

where L is the observational vector of dimension n; A and B are the coefficient matrices of dimension $n \times (m-r)$ and $n \times r$; X_1 and X_2 are the unknown vectors of dimension m-r and r; V is the residual vector of dimension n; m is the number of total unknowns; n is the number of observations; P is the symmetric and definite weight matrix of dimension $n \times n$.

Then the normal equation of the least squares can be formed as

$$\begin{pmatrix} M_{11} & M_{12} \\ M_{21} & M_{22} \end{pmatrix} \begin{pmatrix} X_1 \\ X_2 \end{pmatrix} = \begin{pmatrix} B_1 \\ B_2 \end{pmatrix} \tag{2.39}$$

where

$$\begin{pmatrix} M_{11} & M_{12} \\ M_{21} & M_{22} \end{pmatrix} = \begin{pmatrix} A^T PA & A^T PB \\ B^T PA & B^T PB \end{pmatrix} \tag{2.40}$$

$$B_1 = A^T PL, \quad B_2 = B^T PL \tag{2.41}$$

The elimination matrix is formed as

$$\begin{pmatrix} I & 0 \\ -Z & I \end{pmatrix} \tag{2.42}$$

where I is the identity matrix; 0 is a zero matrix; $Z = M_{21} M_{11}^{-1}$, M_{11}^{-1} is the inversion of M_{11}.

Multiplying the normal Eq. (2.39) by the elimination matrix Eq. (2.42) one has

$$\begin{pmatrix} I & 0 \\ -Z & I \end{pmatrix} \begin{pmatrix} M_{11} & M_{12} \\ M_{21} & M_{22} \end{pmatrix} \begin{pmatrix} X_1 \\ X_2 \end{pmatrix} = \begin{pmatrix} I & 0 \\ -Z & I \end{pmatrix} \begin{pmatrix} B_1 \\ B_2 \end{pmatrix}$$

or

$$\begin{pmatrix} M_{11} & M_{12} \\ 0 & M_2 \end{pmatrix}\begin{pmatrix} X_1 \\ X_2 \end{pmatrix}=\begin{pmatrix} B_1 \\ R_2 \end{pmatrix} \tag{2.43}$$

where

$$\begin{aligned} M_2 &= -M_{21}M_{11}^{-1}M_{12} + M_{22} = B^T PB - B^T PAM_{11}^{-1}A^T PB \\ &= B^T P(I - AM_{11}^{-1}A^T P)B \end{aligned} \tag{2.44}$$

$$R_2 = B_2 - M_{21}M_{11}^{-1}B_1 = B^T P(I - AM_{11}^{-1}A^T P)L \tag{2.45}$$

If only the unknown vector X_2 is of interest, then only the second equation of Eq. (2.43) needs to be solved. The solution is identical to that of solving the whole Eq. (2.43).

Denoting

$$J = AM_{11}^{-1}A^T P \tag{2.46}$$

and it has properties of

$$J^2 = (AM_{11}^{-1}A^T P)(AM_{11}^{-1}A^T P) = AM_{11}^{-1}A^T PAM_{11}^{-1}A^T P = AM_{11}^{-1}A^T P = J$$

$$(I - J)(I - J) = I^2 - 2IJ + J^2 = I - 2J + J = I - J$$

$$[P(I - J)]^T = (I - J^T)P = P - (AM_{11}^{-1}A^T P)^T P = P - PAM_{11}^{-1}A^T P = P(I - J)$$

Matrices *J* and (*I*-*J*) are idempotent and $(I - J)^T P$ is symmetric, that is

$$J^2 = J\,,\ \ (I - J)^2 = (I - J)\,,\quad (I - J^T)P = P(I - J) \tag{2.47}$$

Using the above derived properties, M_2 in Eq. (2.44) and R_2 in Eq. (2.45) can be rewritten as

$$M_2 = B^T P(I - J)B = B^T P(I - J)(I - J)B = B^T P(I - J)^T P(I - J)B \tag{2.48}$$

$$R_2 = B^T P(I - J)L = B^T (I - J)^T PL \tag{2.49}$$

Denoting

$$D_2 = (I - J)B \tag{2.50}$$

then the eliminated normal equation (the second equation of Eq. (2.43)) can be rewritten as

$$B^T(I-J)^T P(I-J)BX_2 = B^T(I-J)^T PL \tag{2.51}$$

or

$$D_2^T PD_2 X_2 = D_2^T PL \tag{2.52}$$

which is the least squares normal equation of the following linear observation equation

$$U_2 = D_2 X_2 - L, \quad P \tag{2.53}$$

or

$$U_2 = (I-J)BX_2 - L, \quad P \tag{2.54}$$

where L and P are the original observational vector and the weight matrix, U_2 is the residual vector, which has the same property as V in Eq. (2.37).

The advantage of using Eq. (2.54) is that the unknown vector X_1 has been eliminated. However, L vector and P matrix remain the same as in the originals. In this case, the correlation problems can be avoided.

2.4 Equivalence of Un-differenced and Time Differencing PPP Algorithms

In this section, the equivalent equations are formed to eliminate the ambiguities from the original un-differenced equations, then the equivalence of the time differencing and original un-differenced equations is proved theoretically.

The linearized PPP observation equation can be expressed as

$$V = \begin{pmatrix} A & B \end{pmatrix} \begin{pmatrix} X_1 \\ X_2 \end{pmatrix} - L, \quad P \tag{2.55}$$

Suppose at one station n common satellites $(k_1, k_2, \cdots, k_n)$ are observed at time $t1$ and $t2$, thus the original observation equation can be written as

$$\begin{pmatrix} V_{t1} \\ V_{t2} \end{pmatrix} = \begin{pmatrix} I & B_{t1} \\ I & B_{t2} \end{pmatrix} \begin{pmatrix} X_1 \\ X_2 \end{pmatrix} - \begin{pmatrix} L_{t1} \\ L_{t2} \end{pmatrix}, \; P = \frac{1}{\sigma^2} \begin{pmatrix} I & 0 \\ 0 & I \end{pmatrix} \tag{2.56}$$

where if no cycle slip exists, X_1 denotes the ambiguity and X_2 represents other unknown

parameters. For simplicity, ambiguity is scaled by the ionosphere-free combined wavelength λ and directly used as unknown. Thus the coefficient matrix of X_1 is an identity matrix *I*.

Comparing Eq. (2.55) with Eq. (2.56), one has (cf. Sect. 2.3)

$$A=\begin{pmatrix} I \\ I \end{pmatrix}, \qquad B=\begin{pmatrix} B_{t1} \\ B_{t2} \end{pmatrix}, \qquad L=\begin{pmatrix} L_{t1} \\ L_{t2} \end{pmatrix}, \qquad V=\begin{pmatrix} V_{t1} \\ V_{t2} \end{pmatrix}$$

$$M_{11}=A^T PA=\begin{pmatrix} I & I \end{pmatrix}\frac{1}{\sigma^2}\begin{pmatrix} I & 0 \\ 0 & I \end{pmatrix}\begin{pmatrix} I \\ I \end{pmatrix}=\frac{2}{\sigma^2}I$$

$$J=AM_{11}^{-1}A^T P=\begin{pmatrix} I \\ I \end{pmatrix}\frac{\sigma^2}{2}I\begin{pmatrix} I & I \end{pmatrix}\frac{1}{\sigma^2}\begin{pmatrix} I & 0 \\ 0 & I \end{pmatrix}=\frac{1}{2}\begin{pmatrix} I & I \\ I & I \end{pmatrix}$$

$$I_{2n\times 2n}-J=\frac{1}{2}\begin{pmatrix} I & -I \\ -I & I \end{pmatrix}$$

$$\left(I_{2n\times 2n}-J\right)B=\frac{1}{2}\begin{pmatrix} B_{t1}-B_{t2} \\ B_{t2}-B_{t1} \end{pmatrix}$$

Therefore the equivalently eliminated equation of Eq. (2.56) is

$$\begin{pmatrix} U_{t1} \\ U_{t2} \end{pmatrix}=\frac{1}{2}\begin{pmatrix} B_{t1}-B_{t2} \\ B_{t2}-B_{t1} \end{pmatrix}X_2-\begin{pmatrix} L_{t1} \\ L_{t2} \end{pmatrix}, \quad P=\frac{1}{\sigma^2}\begin{pmatrix} I & 0 \\ 0 & I \end{pmatrix} \tag{2.57}$$

where the ambiguity parameter X_1 has been eliminated, and the observable vector and weight matrix remain unchanged. Denoting $B_{TD}=B_{t2}-B_{t1}$, the least squares normal equation of Eq. (2.57) can be formed as

$$\frac{1}{2}\begin{pmatrix} -B_{TD}^T & B_{TD}^T \end{pmatrix}P\begin{pmatrix} -B_{TD} \\ B_{TD} \end{pmatrix}X_2=\begin{pmatrix} -B_{TD}^T & B_{TD}^T \end{pmatrix}P\begin{pmatrix} L_{t1} \\ L_{t2} \end{pmatrix}$$

or

$$B_{TD}^T B_{TD}X_2=B_{TD}^T\left(L_{t2}-L_{t1}\right) \tag{2.58}$$

Alternatively, a time differencing equation can be obtained by multiplying Eq. (2.56) with a transformation matrix $C_{TD}=\begin{pmatrix} -I & I \end{pmatrix}$ or directly by subtracting the common observables of

time $t1$ from that of time $t2$, which can be formed as

$$C_{TD}\begin{pmatrix} V_{t1} \\ V_{t2} \end{pmatrix} = C_{TD}\begin{pmatrix} I & B_{t1} \\ I & B_{t2} \end{pmatrix}\begin{pmatrix} X_1 \\ X_2 \end{pmatrix} - C_{TD}\begin{pmatrix} L_{t1} \\ L_{t2} \end{pmatrix}$$

or

$$V_{t2} - V_{t1} = \left(B_{t2} - B_{t1}\right) X_2 - \left(L_{t2} - L_{t1}\right) \tag{2.59}$$

Therefore the covariance $\sum_{TD}$ and weight matrix P_{TD} of time differencing observational equation can be represented as

$$\sum_{TD} = C_{TD}\sigma^2\begin{pmatrix} I & 0 \\ 0 & I \end{pmatrix}C_{TD}^T = 2\sigma^2 I \tag{2.60}$$

and

$$P_{TD} = \sum_{TD}^{-1} = \frac{1}{2\sigma^2} I \tag{2.61}$$

Supposing Eq. (2.59) is solvable, its least squares normal equation is then

$$\left(B_{t2} - B_{t1}\right)^T \left(B_{t2} - B_{t1}\right) X_2 = \left(B_{t2} - B_{t1}\right)^T \left(L_{t2} - L_{t1}\right) \tag{2.62}$$

It is obvious that Eq. (2.62) and Eq. (2.58) are identical. Therefore in case of two epochs, the time differencing Eq. (2.59) is equivalent to the equivalently eliminated Eq. (2.57) and consequently equivalent to the original zero-difference equation. In practice, it should be noted that the precondition of the equivalence of time differencing and zero-difference is that the sample rate of the observations used in the computation should be high enough, then the common error between two epochs can be expected to be the same or similar enough and the result of the time differencing obtained is considered as precise and reliable enough and should be equivalent to that of zero-difference.

2.5 Equivalence of Un-differenced and Triple Differences Algorithms

It is known that data differentiations are methods of combining GNSS observations of different stations (Xu, 2007). As we know, single difference can be formed by observations between two stations, two satellites or two epochs. Here we take the case that single difference is the difference formed by data observed at two stations on the same satellite as

$$\mathrm{SD}_{i1,i2}^{k}(O) = O_{i2}^{k} - O_{i1}^{k} \tag{2.63}$$

where O is the original observable, $i1$ and $i2$ are two id numbers of the two stations.

Double differences are formed between two single differences related to two observed satellites as

$$\begin{aligned} \mathrm{DD}_{i1,i2}^{k1,k2}(O) &= \mathrm{SD}_{i1,i2}^{k2}(O) - \mathrm{SD}_{i1,i2}^{k1}(O) \\ &= (O_{i2}^{k2} - O_{i1}^{k2}) - (O_{i2}^{k1} - O_{i1}^{k1}) \end{aligned} \tag{2.64}$$

where $k1$ and $k2$ are two id numbers of the satellites.

Triple differences are formed between two double differences related to the same stations and satellites at the two adjacent epochs as

$$\begin{aligned} \mathrm{TD}_{i1,i2}^{k1,k2}(O(t1,t2)) &= \mathrm{DD}_{i1,i2}^{k1,k2}(O(t2)) - \mathrm{DD}_{i1,i2}^{k1,k2}(O(t1)) \\ &= O_{i2}^{k2}(t2) - O_{i1}^{k2}(t2) - O_{i2}^{k1}(t2) + O_{i1}^{k1}(t2) \\ &\quad - O_{i2}^{k2}(t1) + O_{i1}^{k2}(t1) + O_{i2}^{k1}(t1) - O_{i1}^{k1}(t1) \end{aligned} \tag{2.65}$$

where $t1$ and $t2$ are two adjacent epochs.

In order to prove the equivalence of triple differences and zero-difference, the eight terms of triple differences in Eq. (2.65) should be rearranged to the new order as

$$\begin{aligned} \mathrm{TD}_{i1,i2}^{k1,k2}(O(t1,t2)) &= \left\{\left[O_{i2}^{k2}(t2) - O_{i2}^{k2}(t1)\right] - \left[O_{i1}^{k2}(t2) - O_{i1}^{k2}(t1)\right]\right\} \\ &\quad - \left\{\left[O_{i2}^{k1}(t2) - O_{i2}^{k1}(t1)\right] - \left[O_{i1}^{k1}(t2) - O_{i1}^{k1}(t1)\right]\right\} \\ &= (D^{t} \cdot O_{i2}^{k2} - D^{t} \cdot O_{i1}^{k2}) - (D^{t} \cdot O_{i2}^{k1} - D^{t} \cdot O_{i1}^{k1}) \end{aligned} \tag{2.66}$$

where D^{t} represents the time difference observables between time $t1$ and $t2$.

From Eq. (2.66) triple differences can be regarded as to make time differencing of the same satellite between two adjacent epochs at the station firstly, then to be formed by double differences between two single differences related to two observed satellites. The time differenced observable between two adjacent epochs has the same property as the original one, which is still uncorrelated (cf. Eq. (2.56) and Eq. (2.60)-(2.61)). And it is generally accepted that the single difference as well as double differences equation are equivalent to the zero-difference equation, which has been explained and proved in Xu (2007). Moreover, with consideration of the equivalence of un-differenced and time differencing proved in Sect. 2.4,

it can be concluded that the triple differences equation is equivalent to the zero-difference equation.

2.6 Time Differencing PPP Based on the Equivalence Principle

As a result of the theoretical study, a time differencing PPP based on the equivalence principle is derived.

Referring to Sect. 2.3, one has

$$V = \begin{pmatrix} A & B \end{pmatrix} \begin{pmatrix} X_1 \\ X_2 \end{pmatrix} - L, \quad P \tag{2.67}$$

where X_1 denotes the receiver clock error parameter; X_2 denotes the coordinates, tropospheric delay and ambiguity parameters. Therefore the equivalently eliminated observation equation of the receiver clock error parameter can be formed as

$$U_2 = D_2 X_2 - L, \quad P \tag{2.68}$$

where the characters in Eq.(2.68) have the same meaning as in Eq. (2.53).

If no cycle slip exists, the ambiguities can be eliminated through the difference of two adjacent epochs. The tropospheric delay can also be eliminated between epochs. Generally the tropospheric delay can be deemed as fixed and unchanged during a certain period, typically as two hours. However, when the weather at the observed station changes drastically and constanly, or there are high variations in the atomosphere humidity, then the unchanged duration should be considered much less. Therefore the time differencing of Eq. (2.68) at epoch *i* and *i*-1 can be formed as

$$U_2^{i,i-1} = D_2^i X_2^i - D_2^{i-1} X_2^{i-1} - \left(L_i - L_{i-1} \right), \quad P \tag{2.69}$$

Denoting

$$dX_2^i = X_2^i - X_2^{i-1} \tag{2.70}$$

thus Eq. (2.69) can be expressed as

$$U_2^{i,i-1} = D_2^i \cdot dX_2^i + dD_2^i \cdot X_2^{i-1} - \left(L_i - L_{i-1} \right), \quad P \tag{2.71}$$

where $dD_2^i = D_2^i - D_2^{i-1}$ and can be ignored (Chen and Wang, 2007; Li et al., 2010). It means when the high-rate recording observations are used, then the coefficients of the linearized observation equations at two epochs are highly similar or nearly the same, thus the difference between them can be small enough to be ignored. In this case Eq. (2.71) can be simplified to

$$U_2^{i,i-1} = D_2^i \cdot dX_2^i - \left(L_i - L_{i-1}\right), \quad P \tag{2.72}$$

where dX_2^i denotes the coordinates difference between two epochs.

Thus the coordinates difference can be estimated through solving Eq. (2.72). The average velocity of the station can also be obtained in accordance with the sample interval of the observations.

To validate the derived time differencing PPP algorithm, the GPS observations of IGS station GMSD (30.56º N, 131.02 º E, located in Japan) on GPS day 334 with sample intervals of 1 s and 30 s were used, respectively. In principle, the position coordinates difference between epochs is zero for the static observations. Thus the coordinates difference between epochs obtained in the static time differencing PPP can be regarded as the computational error and reflect the precision of the computation method. The coordinates difference between epochs of interval 1 s and 30 s are shown in Fig. 2.1 and Fig. 2.2, respectively. The mean value and the standard deviation of the coordinates difference are given in Table 2.1.

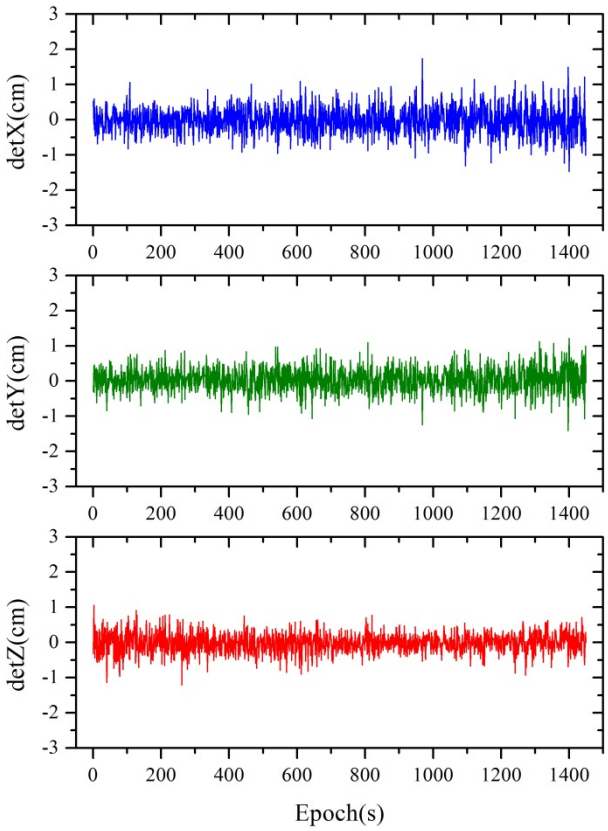

Fig. 2.1. Coordinates difference between epochs (1 s interval)

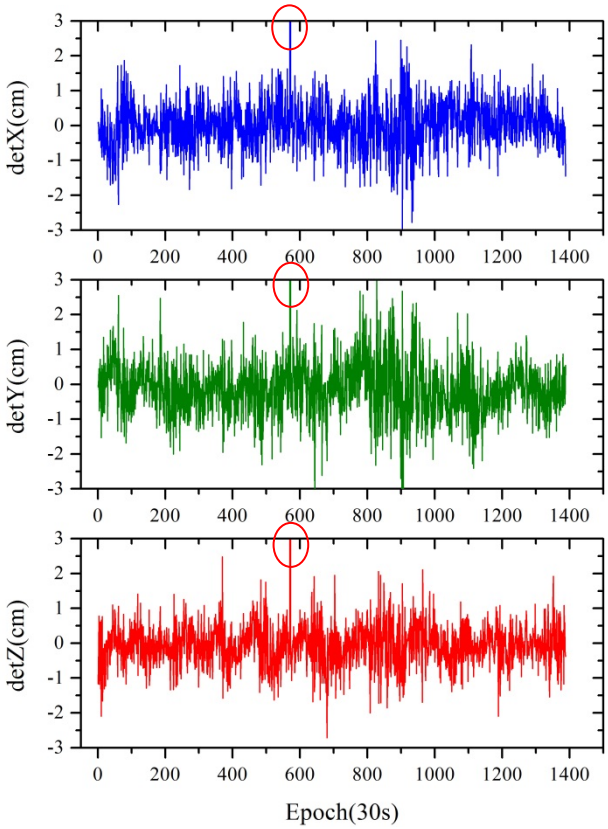

Fig. 2.2. Coordinates difference between epochs (30 s interval)

Table 2.1 Mean and STD of the coordinates difference (units: cm)

Interval	1 s			30 s		
	detX	detY	detZ	detX	detY	detZ
Mean (cm)	-0.02	0.03	-0.01	0.02	-0.13	-0.06
STD (cm)	0.38	0.34	0.28	0.70	0.83	0.62

From Fig. 2.1-2.2 and Table 2.1 it can be found that the precisions of the coordinates difference are different with different sample intervals of the observations. The coordinates differences between epochs of observations with a 1 s interval are within 1 cm in most instances while that of observations with a 30 s interval are within 2 cm. The coordinates difference between epochs of observations with a 1 s interval has higher precision than that of a 30 s interval. That is because the smaller the interval is, the more similar the common error between two epochs will be. Therefore the error elimination in the time differencing is much better. In case of a 1 s interval, the coordinates difference between epochs is just the velocity of the station between epochs. The obtained coordinates difference as well as velocity, which can be obtained by making differential of the coordinate difference with respect to the interval, can keep stable from the beginning of computation. This approach is superior to making position difference of PPP which always needs some convergence time. Thus the results can be useful in applications, such as airborne gravimetry, which needs reliable velocity and acceleration solutions. It is known that in airborne gravimetry, the external information related to the acceleration of the platform which carries the sensors (a classical air gravimeter or a strapdown system), is needed to allow the correct discrimination of accelerations that are not due to the Earth gravity field. The coordinate difference can also be useful for earthquake monitoring. It makes the integration for the obtained coordinate difference to compute the final position at each epoch. In case of a 30 s interval (cf. Fig. 2.2) it is noted that there is a big jump (red circle) where the coordinates difference in X, Y and Z components reached 2 m, 5 m and 1 m, respectively. This is caused by an existing cycle slip in the phase measurement from one of the satellites during the observations. In this case the ambiguity of the satellite changed between these two adjacent epochs, which would not be eliminated through differencing, and caused the big error in coordinates difference computation. Therefore the coordinates difference between epochs could be an efficient method to detect cycle slips.

2.7 Conclusions

In this chapter, the basic algorithms used in the thesis were described. The commonly used adjustment and filtering algorithms in PPP including least squares adjustment, sequential least squares adjustment and Kalman filter were introduced. Then the equivalence principle and the equivalently eliminated observation equation approach were described. It has a great significance in eliminating the nuisance unknown parameters directly through the observation equations, which can reduce the size problem in the computation. On the basis of the equivalence principle and the equivalence property of un-differenced and differencing algorithms, the specific equivalence of un-differenced and time differencing PPP algorithms is proved theoretically for the first time. Moreover, through regarding triple differences as to make time differencing of the same satellite between two adjacent epochs at one station first and then to be formed by double differences, the equivalence of zero-difference and triple differences is proved. Finally, as a consequence of the conducted theoretical study, a time differencing PPP algorithm based on the equivalence principle was derived and a numerical example was given. Through such a time differencing PPP algorithm the coordinates difference and average velocity between epochs can be obtained. The obtained coordinates difference can keep stable from the beginning of computation, which is superior to making position difference of PPP because that always needs a certain convergence time. Thus the results could be useful in the applications, such as airborne gravimetry, as well as earthquake monitoring. Results also show that the time differencing PPP could be an efficient method to detect cycle slips.

3 Influence of Tropospheric Delay on Precise Point Positioning

3.1 Introduction

As known, due to the influence of pseudorange noise, tropospheric delay and other error sources, the accuracy and reliability of PPP are still limited (Li, 2013). Tropospheric delay is one of the key factors which affect the precision of GPS positioning (Dai et al., 2011). The unknown tropospheric delay parameter is usually estimated along with the position and ambiguity parameters. Ingestion of precise tropospheric models can reduce the total number of unknown parameters that need to be estimated from the observation model, potentially remove the need for noise propagating linear combinations of observables, and potentially improve positioning performance (Dodd et al., 2006). In this case, the influence of tropospheric delay on PPP is studied in this chapter.

The tropospheric delay in satellite navigation positioning usually refers to the signal delay generated when the electromagnetic waves get through the non-ionized neutral atmosphere below 80 km. The tropospheric delay could be about 2 m in the zenith direction and a few tens of meters in the case of a lower satellite elevation (Xu, 2007). There are two methods for dealing with the tropospheric delay in single point positioning. One is using a tropospheric model to calculate and correct the delay immediately. The other one is to treat the delay as an unknown parameter which will be estimated in the adjustment (Ge and Liu, 1996). However, in high-precision GPS positioning it is difficult to obtain optimal positioning results by only using the first method. That is because of the existence of model errors and measurement errors of the meteorological parameters along the signal transmission path. It is better to regard the computed value of the tropospheric model as an approximation, and then to estimate the exact tropospheric delay by a stricter adjustment procedure.

The effects of using a tropospheric model on GPS PPP was researched by Kouba (2009b). In that study the global pressure and temperature model GPT (Boehm et al., 2007) was used

to compute a priori zenith hydrostatic delay and demonstrated to perform well for low and mid latitude stations. However, in the polar region or with low elevation angles, the GPS height solution errors can sometimes reach more than 10 mm. Nevertheless, it should be noted that the station height time series based on simple GPT model have a better repeatability than those based on more realistic tropospheric a priori delay derived from surface pressure if atmosphere loading correction is not included, since the a priori hydrostatic part of the zenith delay derived from the empirical pressure can partially compensate for the atmospheric loading displacement (Kouba, 2009b; Wanninger, 2012). According to Xu et al. (2014), there are more visible satellites with lower elevation angles in the Antarctic region comparing with the low-latitude observatories. And researches show that the observations with lower elevation angles are more significantly influenced by the tropospheric delay (Ren et al., 2011; She et al., 2011). Thus the residual errors of the tropospheric model can greatly affect the precision of the positioning there. Both zenith delay model and mapping function play an important role. In recent years, there are some most commonly used models. An improved global pressure and temperature empirical model GPT2 (Lagler et al., 2013) was proposed in 2013. In this chapter, the impact of the tropospheric delay on the Antarctic positioning, especially the effect of the meteorological data derived from GPT2 model and actual meteorological data on global positioning are analyzed and compared. The existing tropospheric models are proposed usually based on the assumption that the atmosphere is homogeneous in all directions (Xu and Wu, 2009). However, the tropospheric delay is anisotropic in the horizontal direction (Cao et al., 2014; Miyazaki et al., 2003). Thus the influence of horizontal gradient correction on PPP is studied in this chapter.

3.2 Tropospheric Delay Model

The tropospheric delay can be represented as the product of the tropospheric refraction in zenith direction and a mapping function related to the elevation angle. It is separated into hydrostatic (about 90%, caused by dry gas in the atmosphere) and wet (about 10%, caused by water vapor) parts, which can be defined according to Hoffmann-Wellenhof et al. (2001), Leick (2004) as

$$\delta = \delta_h + \delta_w = Z_h \times MF_h + Z_w \times MF_w \tag{3.1}$$

where δ denotes the tropospheric delay; the subscript *h* and *w* denote hydrostatic and wet; Z_h and Z_w denote the tropospheric zenith hydrostatic delay and zenith wet delay; MF_h and MF_w are mapping functions related to the hydrostatic and wet components. The residual influence of the wet component of the tropospheric delay still exists while more than 90% of the hydrostatic component can be corrected immediately by using a tropospheric model (Brunner and Welsch, 1993; Collins and Langley, 1997; Tsujii et al., 2000).

3.2.1 Zenith Tropospheric Delay

The hydrostatic zenith delay Z_h can be accurately modeled based on the surface pressure as (Saastamoinen, 1972)

$$Z_h = \frac{0.0022768P}{1 - 0.00266\cos(2B) - 0.00028 \times 10^{-3} H} \tag{3.2}$$

where Z_h is the zenith hydrostatic delay (in units of meters); *P* is the atmospheric pressure (in units of millibars); *B* is geodetic latitude at the station (in units of radians) and *H* is the geodetic height at the station (in units of meters).

On the other hand, the zenith wet delay component is more difficult to model accurately due to its temporally unpredictable changes and is therefore estimated as an unknown along with other unknowns in the adjustment in precise point positioning. The zenith wet delay could also be computed by Saastamoinen formula with a loss of precision:

$$Z_w = \frac{0.0022768 \times \left(\frac{1255}{T} + 0.05 \right) \times e}{1 - 0.00266\cos(2B) - 0.00028 \times 10^{-3} H} \tag{3.3}$$

where Z_w is the zenith wet delay (in units of meters); *T* is the temperature at the station (in units of Kelvin); *e* is the partial pressure of water vapor (in units of millibars).

With the approximate position and the meteorological data, the hydrostatic and wet zenith

delay could be easily computed by Eqs. (3.2) and (3.3). According to Eq. (3.2), 1 mbar pressure change at sea level can cause a change of about 2.3 mm in a priori zenith hydrostatic delay, it is essential to use as accurate meteorological data as possible (Tregoning and Herring, 2006).

Generally, the meteorological data needed by Eqs. (3.2) and (3.3) can be obtained from actual observations, or derived from using a standard atmospheric value at sea level and the height of the station (Berg, 1948). Meteorological data can also be determined by empirical models called GPT (Boehm et al., 2007) or the later GPT2 model (Lagler et al., 2013). In this chapter, the meteorological data derived from GPT2 models and the actual meteorological observations were used.

3.2.2 Mapping Functions

To obtain the slant tropospheric delay, a mapping function which describes the variation of the slant tropospheric delay with respect to satellite elevation angle is needed. Many mapping functions were proposed in the past, such as NMF (Niell Mapping Function, (Niell, 1996)), VMF1 (Vienna Mapping Function 1, (Boehm et al., 2006b)), GMF (Global Mapping Function, (Boehm et al., 2006a)), which were commonly researched in the recent years. By comparison, a general form of the hydrostatic and wet mapping functions can be outlined as (Herring, 1992)

$$MF = \frac{1+\dfrac{a}{1+\dfrac{b}{1+c}}}{\sin\varepsilon+\dfrac{a}{\sin\varepsilon+\dfrac{b}{\sin\varepsilon+c}}} \tag{3.4}$$

where MF is the mapping function; ε is the elevation angle; a, b and c are empirical coefficients with different values in various mapping functions. (a_h, b_h, c_h) and (a_w, b_w, c_w) are used for the hydrostatic and wet components, respectively.

The accuracy of the mapping function would definitely affect the precision of the slant delay, thus affecting the positioning precision. And when the elevation cut-off angle is lower, the impact is more significant. Applying a rule of thumb (Boehm et al., 2006b; MacMillan

and Ma, 1994), an error in the wet mapping function of 0.01 or in the hydrostatic mapping function of 0.001 would cause an error of 4 mm in the station height under 5° elevation cut-off angle at 2000 mm ZHD and 200 mm ZWD, respectively. In this study, the GMF mapping function was applied to make the analysis.

3.3 Comparison of Tropospheric Delays Based on GPT2 and Actual Meteorological Observations

3.3.1 Data Preparation

The data of a globally distributed set of 9 IGS (International GNSS Service, www.igs.org) stations during 2013 were used to make the analysis. This set of 9 IGS stations (DAV1, OHI2, OUS2, HRAO, NURK, MANA, FUNC, YAKT and SCOR) would represent high-latitude, mid-latitude, and low-latitude areas in both southern and northern hemispheres. The distribution of these stations is shown in Fig. 3.1.

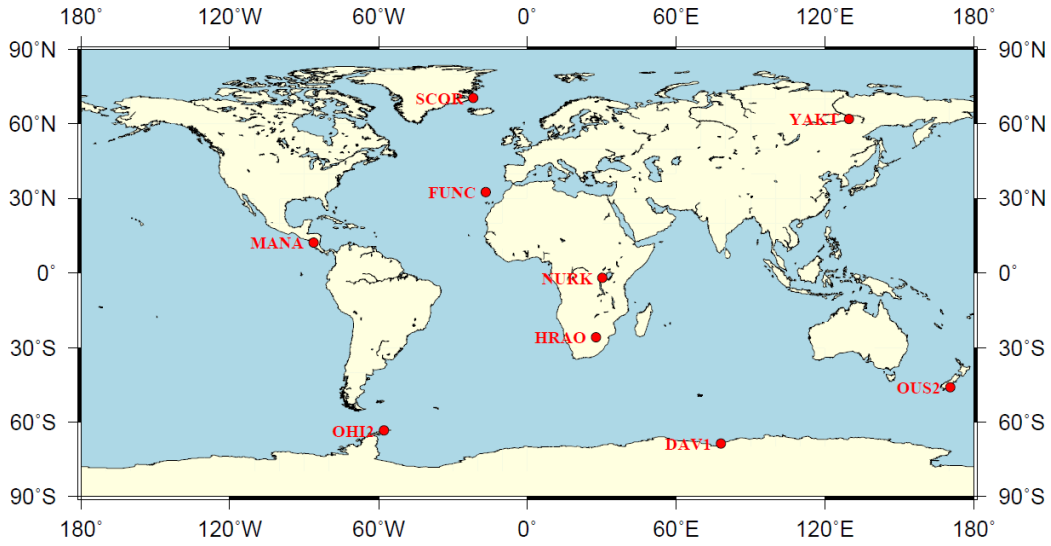

Fig. 3.1. Distribution of the selected IGS stations used for analysis

3.3.2 Comparison of Zenith Hydrostatic Delays

A priori zenith hydrostatic delay (ZHD) derived from a tropospheric model, which is proportional to the surface pressure at the station, will greatly affect the precision of positioning. Furthermore, the higher percentage of low-elevation observations at high latitude stations amplifies the effect of an a priori ZHD error (Tregoning and Herring, 2006). Thus a

comparison of pressures and ZHD derived from GPT2 and the actual meteorological data for Antarctic stations is presented here.

The surface atmosphere pressure (denoted as M, once-daily) and pressure time series derived from GPT2 model for stations in Antarctic region (e.g. DAV1 and OHI2) in 2013 are given in Fig. 3.2.

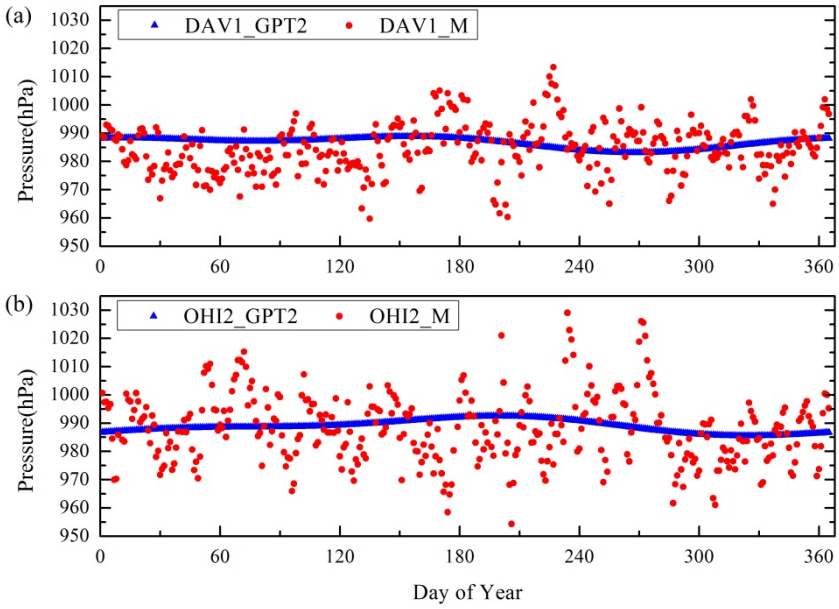

Fig. 3.2. Comparison of surface pressure and pressure derived from GPT2 for stations DAV1 (a) and OHI2 (b)

Fig. 3.2 shows that the pressure time series derived from GPT2 model is a smooth scatter diagram while the actual surface pressure time series is more discrete, which could better reflect the temporal variation of the pressure.

Fig. 3.3 shows the zenith hydrostatic delay derived from GPT2, actual meteorological observations and VMF1, which are plotted in blue scatters, olive scatters and red ones, respectively. The statistics of their differences are given in Table 3.1. The interval of the ZHD derived from GPT2 and actual meteorological data are set as 6 hours, in accordance with the interval of VMF1 ZHD.

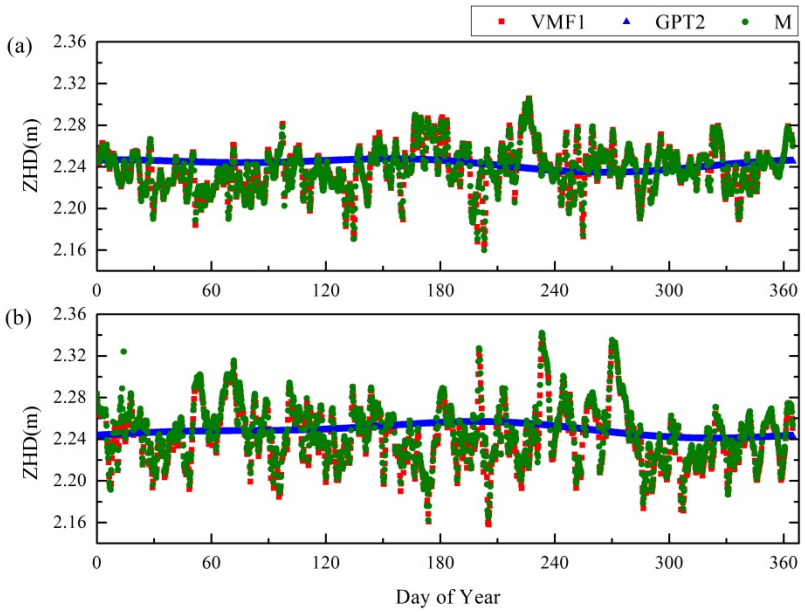

Fig. 3.3. Comparison of zenith hydrostatic delays for stations DAV1 (a) and OHI2 (b)

Table 3.1 Statistics of zenith hydrostatic delay difference (units: mm)

Stations	GPT2-VMF1		M-VMF1	
	Mean	RMS	Mean	RMS
DAV1	4.0	22.2	-0.7	3.7
OHI2	4.9	29.4	2.9	5.6

From Fig. 3.3 and Table 3.1 it can be found that, the ZHD derived from actual meteorological observations agrees well with the one derived from VMF1 model, which is considered as the true value here. The difference of ZHD at these two stations has an average of -0.7 mm and 2.9 mm, and their RMS (Root Mean Square) are 3.7 mm and 5.6 mm (cf. Table 3.1), which is much more less than the difference between GPT2 and VMF1. Moreover, the ZHD series derived from GPT2 model is a nearly slippy scatter diagram, it is known that ZHD is in proportion to the pressure at one station, thus the pressures derived from GPT2 model can hardly reflect the temporal variation, especially in case of dramatic changes in weather. Therefore a priori ZHD derived from actual meteorological observation is recommended if it is available in the position processing.

3.4 Effect of Meteorological Data on Precise Point Positioning

3.4.1 Tropospheric Delay Estimation

As mentioned before, the residual influence of the wet component of the tropospheric delay

still exists while more than 90% of the hydrostatic component can be corrected immediately by using the tropospheric model. Therefore, the tropospheric delay is regarded as an unknown parameter and will be estimated by the adjustment in precise point positioning. The value calculated by the tropospheric model is regarded as an initial approximation in the estimation.

As mentioned in Sect. 3.3.1, the same 9 stations are selected in this part. Combined with GMF mapping function, GPT2-derived meteorological data and the actual meteorological observations (denoted as M in Table 3.3 and Fig. 3.4) were used to calculate the tropospheric delay, respectively, which were treated as a priori values. Then the tropospheric delay was estimated as an unknown parameter along with position coordinates, receiver clock offsets and carrier phase ambiguities in the precise point positioning. Finally the position results both in horizontal and vertical directions were obtained. The details in the PPP processing are listed in Table 3.2.

Table 3.2 Observation models and data processing strategies for PPP

Item	Models and Strategies
Observations	Undifferenced ionosphere-free code and phase combination
Observation weight	Elevation dependent weight
Elevation angle cutoff	5°/10°
Sampling rate	30s
Precise orbit	Fixed, IGS final precise ephemeris
Precise clock biases	Fixed, IGS precise clock
Tropospheric delay	Saastamoinen model (real meteorological data/GPT2) & random walk process
Mapping function	Global Mapping Function (GMF)
Ionospheric delay	First order effect eliminated by ionosphere-free linear combination
Phase-windup effect	Corrected
Earth rotation parameter	Fixed, IGS ERP product
PCO & PCV	Satellite antenna and receiver antenna Applied
Relativistic effects	IERS Convention 2010
Tidal displacement	Solid Earth tides, pole tides, ocean tides (IERS Convention 2010)
Receiver clock biases	Estimated as white noise for each epoch
Phase ambiguity	Estimated as constant for each ambiguity arc
Time system	GPS Time
Terrestrial frame	ITRF2008

3.4.2 Data Analysis and Results

To make a comparison, the position coordinates published by IGS were regarded as standard values to compute the RMS of the position results with following formula.

$$RMS\_(N,E,U)=\sqrt{\frac{\sum_{i=1}^{n}\left(X_{i\_(N,E,U)}-X_{\text{standard}\_(N,E,U)}\right)^2}{n}} \tag{3.5}$$

where i denotes the epoch, n is the number of epochs; $X_{i\_(N,E,U)}$ represents the computed position result of N, E or U directions at epoch i respectively; $X_{\text{standard}\_(N,E,U)}$ represents the IGS published position coordinates in corresponding direction.

The RMS with respect to IGS published results are given in Table 3.3. The RMS results in U direction are shown in Fig. 3.4.

Table 3.3 RMS with respect to IGS results during 2013 (units: mm)

Stations	5°						10°					
	GPT2/GMF-IGS			M/GMF-IGS			GPT2/GMF-IGS			M/GMF-IGS		
	N	E	U	N	E	U	N	E	U	N	E	U
DAV1	2.4	4.2	12.5	2.3	4.2	9.3	1.8	3.6	5.3	1.8	3.6	4.1
OHI2	6.2	7.6	22.4	6.2	7.6	19.6	6.3	5.8	11.6	6.3	5.8	11.1
OUS2	5.3	4.8	6.6	5.3	4.8	6.8	4.5	4.3	7.0	4.5	4.3	7.1
HRAO	4.0	8.7	17.9	4.0	8.7	17.9	4.3	8.3	13.9	4.3	8.3	13.9
NURK	5.7	9.4	22.0	5.7	9.4	22.5	6.5	6.1	14.0	6.5	6.1	14.2
MANA	2.4	6.7	17.6	2.4	6.7	17.7	2.1	6.9	15.2	2.1	6.9	15.2
FUNC	4.3	4.3	5.7	4.3	4.2	5.3	4.1	3.9	3.9	4.1	3.9	3.6
YAKT	3.8	6.9	5.5	3.8	6.9	6.0	3.3	7.2	4.6	3.3	7.2	4.8
SCOR	2.2	3.6	8.9	2.2	3.6	8.4	2.1	3.8	5.9	2.1	3.8	5.8

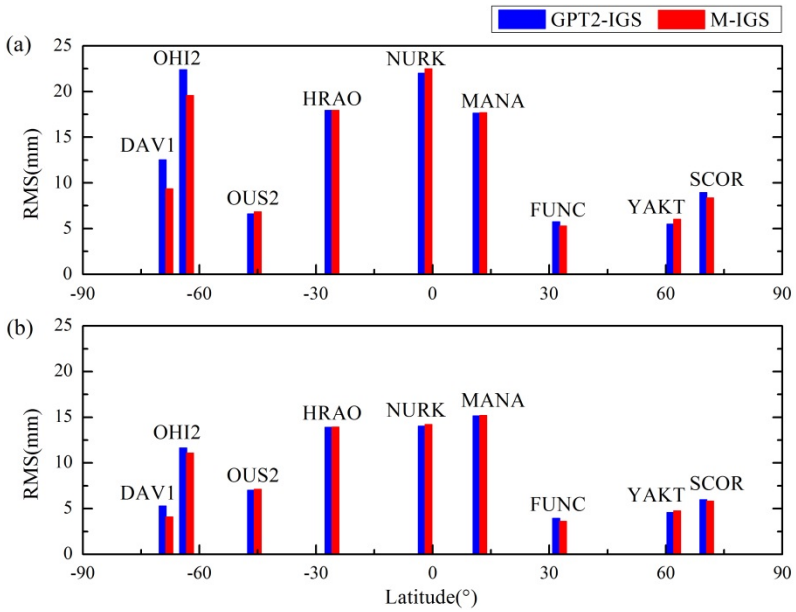

Fig. 3.4. RMS in U direction under 5° elevation cut-off angle (a) and 10° elevation cut-off angle (b) during 2013

In order to analyze the results intuitively, the visible satellite trajectories connected to the elevation angles for Antarctic stations (e.g. DAV1 and OHI2) are shown in Fig. 3.5.

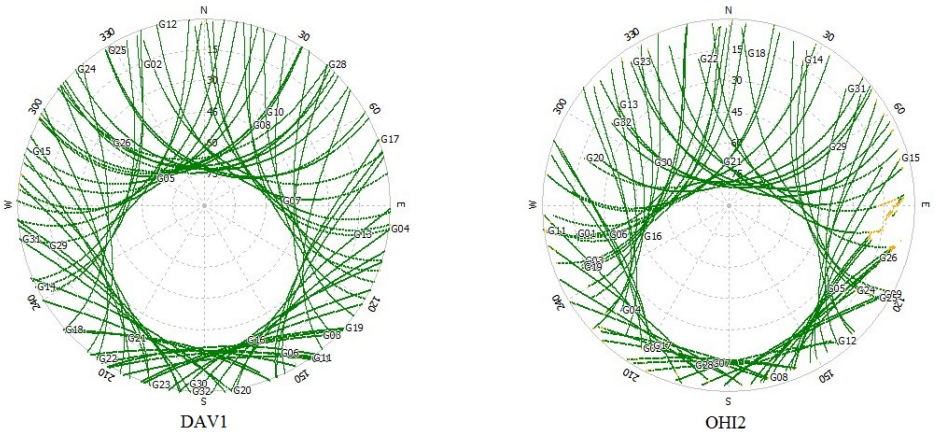

Fig. 3.5. Skyplots of the observations for Antarctic stations DAV1 and OHI2

From Table 3.3 and Fig. 3.4 - Fig. 3.5 it can be found that: (1) There is a high variability in U direction under different elevation cut-off angles in Table 3.3. That is because when the elevation cut-off angle was set from 10° to 5°, the tropospheric errors of the observations which increase significantly, are included and used in the computation. Due to the specificity of Antarctic region, there are more observations with lower elevation angles. And the lower the elevation angles are, the larger the height solution errors will be, since observations with lower elevation angles are more significantly influenced by the tropospheric delay. Thus the

residual errors of the tropospheric model can greatly affect the precision of positioning there. (2) Using GPT2-derived meteorological data and actual meteorological observations the same positioning precision can be achieved in most areas of the world except for the Antarctic region (e.g. DAV1 and OHI2). Thus in most instances GPT2 model is meaningful and useful in case of a priori tropospheric delay is required but the actual measured meteorological data is not available. (3) The improvement of the actual meteorological observations on the positioning result is significant in the Antarctic region (e.g. DAV1 and OHI2) compared to using GPT2-derived meteorological data. That is because in the Antarctic positioning more visible satellites are in lower elevation angles (cf. Fig. 3.5; (Xu et al., 2012)), which has a significant influence on the tropospheric delay. Therefore, the improvement of the more accurate tropospheric model with actual measured meteorological data on the positioning precision is certainly more obvious. (4) When the elevation cut-off angle was set to 5°, the precision in U direction of DAV1 and OHI2 improved by 25% and 13%, respectively. While under 10° elevation cut-off angle, the precision in U direction improved by 23% and 5%, respectively. Therefore when the cut-off angle is lower, the effect of the actual meteorological observations on the positioning precision is also more significant in Antarctic due to the retention of low elevation angle observations. (5) For high-precision positioning in the Antarctic region, actual meteorological data is suggested to be measured and used.

In order to have a better understanding of the result, the standard deviations *STD* and average difference μ with respect to IGS results were additionally computed by Eq. (3.6). The symbols have the same meanings as that of Eq. (3.5).

$$\begin{aligned} STD\_(N,E,U) &= \sqrt{\frac{\sum_{i=1}^{n}\left(\Delta X_{i\_(N,E,U)} - \mu\right)^2}{n}} \\ \Delta X_{i\_(N,E,U)} &= X_{i\_(N,E,U)} - X_{\text{standard}\_(N,E,U)} \\ \mu &= \frac{1}{n}\sum_{i=1}^{n}\Delta X_{i\_(N,E,U)} \end{aligned} \tag{3.6}$$

It is found that the standard deviations of using GPT2/GMF with respect to IGS are the same as that of using M/GMF on the whole. However, the values of μ are different when using different models, which have the same tendency as the RMS results given in Table 3.3.

Therefore it is inferred that the difference between GPT2/GMF and M/GMF can influence the tropospheric delay, thus affect the values of μ, which also reflect in the values of RMS. When using M/GMF, smaller μ can be obtained comparing to that of GPT2/GMF, which means the average difference of the computed coordinates and IGS coordinates is reduced.

3.5 Effects of A Tropospheric Horizontal Gradient Model

3.5.1 Tropospheric Horizontal Gradient Model

The tropospheric model of Eq. (3.1) was proposed usually based on the assumption that the atmosphere is homogeneous in all directions. However, the tropospheric delay is anisotropic in the horizontal direction. Thus a tropospheric delay model which has added a horizontal gradient correction was proposed by various researchers (Chen and Herring, 1997; MacMillan, 1995; Miyazaki et al., 2003; Teke et al., 2011) as

$$\delta = Z_h \times MF_h + Z_w \times MF_w + (G_N \cos\phi + G_E \sin\phi) \times MF_g \tag{3.7}$$

where ϕ is the azimuth angle from north; G_N and G_E are the gradient vectors in north-south and east-west directions, respectively. MF_g denotes the gradient mapping function, which can be set as $MF_w \cot\varepsilon$ due to the anisotropic water vapor distributions (Li et al., 2011); ε denotes the elevation angle.

3.5.2 Data Analysis and Results

The same IGS stations mentioned in Sect. 3.3.1 were selected to test the effects of horizontal gradients under different weather conditions and different elevation cut-off angles. The data of January and July 2013 were used to make the analysis. The elevation cut-off angles were set to 5° and 10°, respectively. The mean and RMS of difference between position results with and without horizontal gradients under different elevation cut-off angles are given in Table 3.4-3.5. Similarly with Sect. 3.4.2, the position results with and without horizontal gradients were compared with the standard values from IGS. The RMS with respect to IGS published results under different elevation cut-off angles are given in Table 3.6-3.7. For an intuitive analysis, the RMS under 5° elevation cut-off angle in January and July were plotted and are

shown in Fig. 3.6-3.7.

Table 3.4 Mean and RMS of difference between position results with and without horizontal gradients in January 2013 (units: mm)

Stations	5°						10°					
	Mean			RMS			Mean			RMS		
	N	E	U	N	E	U	N	E	U	N	E	U
DAV1	3.6	1.6	-1.1	3.6	1.6	1.1	2.7	0.7	-1.2	2.7	0.7	1.3
OHI2	3.0	0.2	-2.3	3.1	0.5	2.6	2.1	-0.6	-0.5	2.1	0.6	0.7
OUS2	4.1	-0.6	-2.8	4.1	0.7	2.8	2.9	-1.2	-0.1	2.9	1.2	0.3
HRAO	-2.3	-1.3	-5.5	2.4	1.5	5.7	-2.2	-1.4	-3.9	2.2	1.6	4.2
NURK	-1.9	-0.8	-1.4	1.9	1.0	1.5	-0.8	-0.7	-1.3	0.8	0.9	1.3
MANA	-3.6	-0.1	-8.7	3.7	1.4	8.8	-4.3	0.8	-4.3	4.3	1.3	4.4
FUNC	1.8	0.1	-1.1	1.8	0.3	1.3	1.6	0.3	-0.1	1.6	0.3	0.3
YAKT	2.8	-2.1	0.3	2.9	2.2	0.4	2.0	-0.9	-0.6	2.1	1.0	0.6
SCOR	-1.1	0.8	0.9	1.1	0.9	0.9	-0.6	0.4	-0.1	0.6	0.5	0.1

Table 3.5 Mean and RMS of difference between position results with and without horizontal gradients in July 2013 (units: mm)

Stations	5°						10°					
	Mean			RMS			Mean			RMS		
	N	E	U	N	E	U	N	E	U	N	E	U
DAV1	4.3	-1.6	-4.9	4.3	1.7	4.9	2.6	-0.8	-2.1	2.6	0.8	2.1
OHI2	1.7	-0.4	-2.4	1.8	0.5	2.5	1.0	-0.5	-0.8	1.0	0.5	0.8
OUS2	2.0	0.3	-0.1	2.0	0.3	0.2	0.4	-0.1	0.3	0.4	0.23	0.3
HRAO	-0.3	-0.1	-0.1	0.3	0.1	0.1	-0.2	-0.1	-0.2	0.2	0.2	0.2
NURK	3.3	-0.1	-6.5	3.3	0.5	6.5	2.1	0.6	-0.1	2.1	0.7	0.4
MANA	-0.6	1.7	-3.4	0.6	1.8	3.5	-1.0	1.2	-2.8	1.0	1.4	2.8
FUNC	1.8	-0.6	-3.3	1.8	0.7	3.4	1.5	-0.5	-2.1	1.6	0.6	2.1
YAKT	-1.2	2.1	0.9	1.0	1.8	0.8	-1.0	0.8	0.6	0.8	0.8	0.5
SCOR	-0.4	-1.9	0.4	0.5	2.0	0.5	-0.4	-1.0	-0.1	0.4	1.0	0.1

Table 3.6 RMS with respect to IGS results in January 2013 (units: mm)

Stations	5°						10°					
	NoGrad-IGS			Grad-IGS			NoGrad-IGS			Grad-IGS		
	N	E	U	N	E	U	N	E	U	N	E	U
DAV1	3.3	4.2	5.9	0.4	2.7	4.8	2.7	4.2	3.1	0.3	3.5	4.3
OHI2	3.7	12.2	15.2	0.6	12.0	12.8	3.5	6.5	8.0	1.4	6.0	7.5
OUS2	10.2	4.9	5.0	6.1	4.3	2.3	8.6	4.8	5.1	5.8	3.7	5.1
HRAO	8.0	7.1	13.1	5.7	5.9	10.0	8.1	7.1	19.6	5.9	5.9	15.7
NURK	2.3	13.9	7.3	0.5	13.1	5.9	1.5	11.7	4.4	0.7	10.9	3.1
MANA	1.9	13.0	12.0	1.9	13.2	7.2	2.8	14.2	10.7	1.7	13.4	6.5

FUNC	2.6	9.3	7.0	0.8	9.3	6.0	2.5	9.1	5.5	0.9	8.9	5.5
YAKT	11.0	7.9	2.4	9.5	5.7	2.1	10.1	6.2	2.4	9.1	5.2	1.9
SCOR	2.0	2.7	2.8	0.9	1.8	2.7	1.6	2.3	4.9	1.1	1.9	4.7

Table 3.7 RMS with respect to IGS results in July 2013 (units: mm)

Stations	5°						10°					
	NoGrad-IGS			Grad-IGS			NoGrad-IGS			Grad-IGS		
	N	E	U	N	E	U	N	E	U	N	E	U
DAV1	2.5	5.8	17.5	1.8	4.1	15.2	1.8	3.5	9.1	0.9	2.8	7.0
OHI2	2.2	2.1	14.4	0.6	2.4	11.9	2.2	1.8	0.8	1.2	2.2	0.6
OUS2	5.2	4.3	7.3	3.2	4.6	7.2	4.4	3.7	6.5	4.0	3.6	6.8
HRAO	2.7	6.8	15.9	2.4	6.8	15.8	2.9	6.3	12.9	2.7	6.2	12.7
NURK	7.6	5.0	6.6	4.3	5.1	1.1	7.1	5.5	2.5	5.0	5.1	2.6
MANA	1.7	5.4	5.3	2.0	4.0	2.0	2.2	4.8	8.4	1.3	3.9	5.7
FUNC	6.8	2.2	5.7	5.0	2.8	2.5	6.2	1.3	1.9	4.7	1.3	0.7
YAKT	5.3	5.9	1.0	4.1	3.9	0.7	4.6	6.7	4.7	3.7	5.9	4.1
SCOR	0.9	3.6	9.1	0.5	1.8	8.7	0.7	3.6	5.1	0.4	2.7	5.1

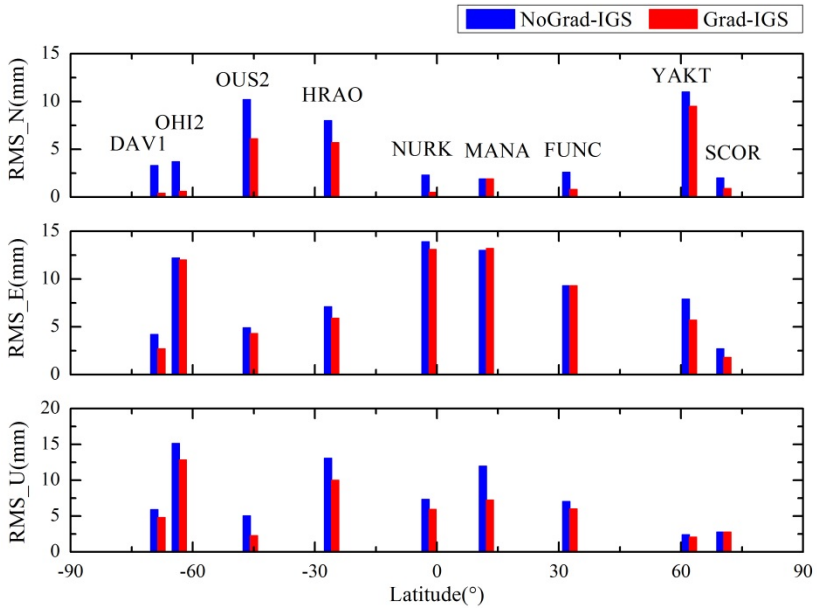

Fig. 3.6. RMS with respect to IGS results under 5° elevation cut-off angle in January 2013

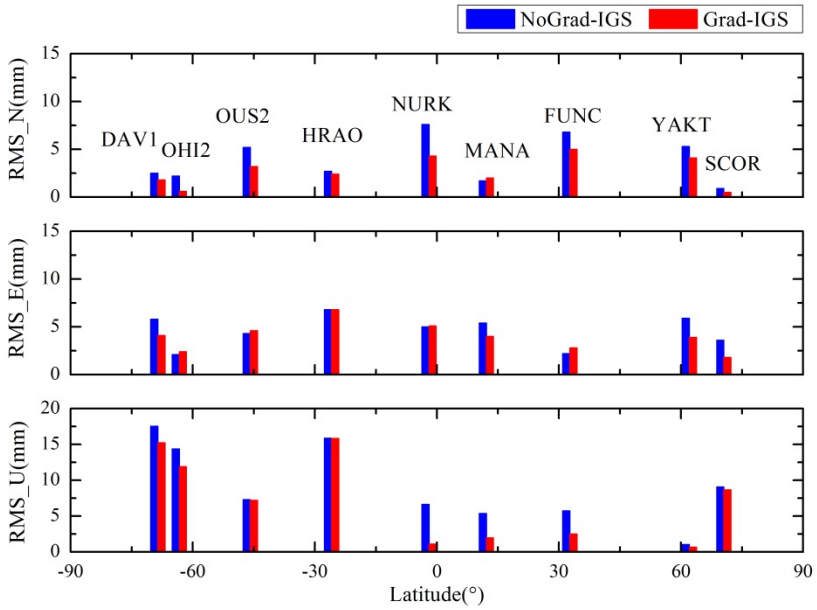

Fig. 3.7. RMS with respect to IGS results under 5° elevation cut-off angle in July 2013

Results in Table 3.4-3.5 show the difference between position results with and without horizontal gradients under 5° elevation cut-off angle is more significant than that under 10° elevation cut-off angle. Moreover, the impact of adding gradient estimation in horizontal direction is generally bigger than in vertical direction.

From Table 3.6-3.7 and Fig. 3.6-3.7 it can be found that: (1) Generally the precision of precise point positioning can be improved when the tropospheric horizontal gradient correction is added in the calculation. (2) Comparing the results under different elevation cut-off angles, it shows when the elevation cut-off angle was set to 5°, that the positioning precision can be improved more significantly by adding tropospheric horizontal gradient correction than for elevation cut-off angle of 10°. (3) Comparing the results between July and January (cf. Fig. 3.6-3.7), the positioning precision of the stations located in southern hemisphere especially in the mid-latitudes area (e.g. OUS2, HRAO) has bigger improvement in January than in July. An opposite situation can be found to the northern hemisphere stations (e.g. MANA, FUNC). That is because the weather conditions of the mid-latitudes area in southern hemisphere in January are much more variable than in July, so does the condition in northern hemisphere in July. It might cause remarkable azimuth dependency of water vapor distribution. Thus, adding the horizontal gradient correction can have a more significant effect on the positioning. (4) Comparing the results of all these stations, when adding tropospheric

horizontal gradient corrections, the average improvement of N, E and U directions can reach up to 51%, 15% and 30%, respectively. The positioning precision of low-latitudes stations had the larger improvement than the high-latitudes stations. This may be because of the different humidity conditions in different latitudes. The effect of horizontal gradients is generally larger at low-latitudes sites because of higher humidity. And due to the lesser amount of humidity at higher latitudes, the effect decreases with increasing northern and southern latitudes.

3.6 Conclusions

In most instances and areas worldwide, GPT2 model is meaningful and useful in case of a priori tropospheric delay is required but the actual measured meteorological data is not available. However, in the Antarctic region the improvement of the actual meteorological observations on the positioning result is significant compared to using GPT2-derived meteorological data. Furthermore, when the elevation cut-off angle is lower, the effect of the actual meteorological observations on the positioning precision is more significant in Antarctic due to the retention of low elevation angle observations. Thus for high-precision positioning in the Antarctic region, actual meteorological data is suggested to be measured and used.

The effect of the tropospheric horizontal gradient correction on the precise point positioning was also analyzed. Results show that adding horizontal gradient corrections can generally improve the positioning precision. Under the lower elevation cut-off angles and higher humidity conditions, especially in summer time and low-latitudes area, the improvement of horizontal gradient correction on PPP is remarkable. The average improvement of N, E and U directions could reach up to 51%, 15% and 30%, respectively.

4 A Priori Constrained Precise Point Positioning Algorithms

4.1 Introduction

Although for many applications the PPP approach presents definite advantages regarding operational flexibility and cost-effectiveness, it requires a relatively long initialization time as phase ambiguities converge to constant values and the solution reaches its optimal precision. The convergence time of PPP will vary because it is affected by a number of factors, such as the number and geometry of visible satellites, observation quality and sampling rate, user tracking conditions, and environment (Bisnath and Gao, 2009). Furthermore, due to the influence of pseudorange noise and atmospheric delay (etc.), the accuracy and reliability of PPP are still limited (Li, 2013). As scientists gain increasingly deeper and more complete understanding of the geometric and physical properties of observations, a multitude of a priori information can be obtained and utilized in the data processing (Chen, 2010; Xie, 2014). A priori information, which is known with a certain a priori precision, could be expected to improve the efficiency and precision of PPP. In PPP, generally the a prior constraints are mainly focus on the error models corrections on the domain of observation equation. In this chapter the a priori information constraints concerning the different estimated parameters on the domain of normal equation rather than the error models on the domain of observation equation are emphasized on. The contribution of different a priori information constraints concerning different parameters to PPP solution is studied and validated. The a priori constraints employed are comprehensively specified according to coordinates-, receiver clock offset-, tropospheric delay- and ambiguities-constraints. Furthermore, not only the efficiency and accuracy improvement by applying constraints but also their applications under specific conditions are discussed. Numerical examples were also conducted.

4.2 Analytic Contribution of Different Constraints on Parameters to PPP Solution

4.2.1 A Priori Constrained PPP Algorithms

As we know, after applying precise orbit and clock corrections, ionosphere-free code and phase observations for GNSS satellites in traditional PPP can be written as

$$P_{IF} = \frac{f_1^2 \cdot P_1 - f_2^2 \cdot P_2}{f_1^2 - f_2^2} = \rho + c \cdot dt + d_{trop} + dm_{IF} + \varepsilon_{P_{IF}} \tag{4.1}$$

$$\Phi_{IF} = \frac{f_1^2 \cdot \Phi_1 - f_2^2 \cdot \Phi_2}{f_1^2 - f_2^2} = \rho + c \cdot dt + d_{trop} + \lambda_{IF} \cdot N_{IF} + \delta m_{IF} + \varepsilon_{\Phi_{IF}} \tag{4.2}$$

where P_{IF} is the ionosphere-free code observation; Φ_{IF} is the ionosphere-free phase observation; f_1 and f_2 are the different frequencies of the dual-frequency observations; ρ is the geometric distance between the satellite and the receiver; dt denotes the receiver clock offset; d_{trop} denotes the tropospheric delay; dm_{IF} and δm_{IF} denote a series of error corrections including relativistic effect, earth tide, ocean tide and hardware delay; λ_{IF} denotes the wavelength; N_{IF} denotes its ambiguity; $\varepsilon_{P_{IF}}$ and $\varepsilon_{\Phi_{IF}}$ denote the not modeled remaining errors like multipath and observation noise of code and phase.

Thus the linearized error equation of PPP can be expressed as

$$V = AX - L \,, \quad P \tag{4.3}$$

where the terms in Eq. (4.5) have the same meaning as Eq. (2.2) in Sect. 2.2.

In PPP, generally the unknown parameter vector X in Eq. (4.3) can be separately divided into four groups, $X = \begin{pmatrix} X_1 & X_2 & X_3 & X_4 \end{pmatrix}^T$, where X_1 denotes the coordinates; X_2 denotes the receiver clock offset; X_3 denotes the tropospheric delay and X_4 denotes the ambiguities in PPP. And similarly we can set $A = \begin{pmatrix} A_1 & A_2 & A_3 & A_4 \end{pmatrix}$. Thus the linearized error equation can be rewritten as

$$V = \begin{pmatrix} A_1 & A_2 & A_3 & A_4 \end{pmatrix} \begin{pmatrix} X_1 \\ X_2 \\ X_3 \\ X_4 \end{pmatrix} - L, \qquad P \tag{4.4}$$

As we know, the satellite orbits can be fixed and satellite clock errors can be removed by using precise ephemeris and precise satellite clock offset products. And the first-order effect of ionospheric delay can be eliminated by using dual-frequency ionosphere-free combined observations. Furthermore, these four groups of parameters have different properties. The coordinate parameter is a constant in the static positioning, while in the kinematic case it changes every epoch. And the coordinate parameter is independent of a satellite. The parameter of troposphere delay is a piece-wise constant, we normally estimate it every 2 hours. The station clock is a random error, which should be estimated every epoch. The ambiguity parameter is dependent on a specific satellite, it is a constant if there is no cycle slip of this satellite during the observing period.

The least squares normal equation can be formed as

$$\begin{pmatrix} N_{11} & N_{12} & N_{13} & N_{14} \\ N_{21} & N_{22} & N_{23} & N_{24} \\ N_{31} & N_{32} & N_{33} & N_{34} \\ N_{41} & N_{42} & N_{43} & N_{44} \end{pmatrix} \begin{pmatrix} X_1 \\ X_2 \\ X_3 \\ X_4 \end{pmatrix} = \begin{pmatrix} B_1 \\ B_2 \\ B_3 \\ B_4 \end{pmatrix} \tag{4.5}$$

where

$$N = \begin{pmatrix} N_{11} & N_{12} & N_{13} & N_{14} \\ N_{21} & N_{22} & N_{23} & N_{24} \\ N_{31} & N_{32} & N_{33} & N_{34} \\ N_{41} & N_{42} & N_{43} & N_{44} \end{pmatrix} = \begin{pmatrix} A_1^T PA_1 & A_1^T PA_2 & A_1^T PA_3 & A_1^T PA_4 \\ A_2^T PA_1 & A_2^T PA_2 & A_2^T PA_3 & A_2^T PA_4 \\ A_3^T PA_1 & A_3^T PA_2 & A_3^T PA_3 & A_3^T PA_4 \\ A_4^T PA_1 & A_4^T PA_2 & A_4^T PA_3 & A_4^T PA_4 \end{pmatrix} \tag{4.6}$$

$$B = \begin{pmatrix} B_1 \\ B_2 \\ B_3 \\ B_4 \end{pmatrix} = \begin{pmatrix} A_1^T PL \\ A_2^T PL \\ A_3^T PL \\ A_4^T PL \end{pmatrix} \tag{4.7}$$

According to Xu (2007), it is known that the a priori constraints may be interpreted as additional observations or fictitious observations and will cause two additional terms in both sides of the normal Eq. (4.5). The difference between the common normal equation and the

normal equation of the a priori constraint is that the a priori terms will be added to the corresponding elements of the normal equation coefficient matrices *N* and *B*, which can be expressed as

$$0 = CX_i - W, \quad P_i \quad (i = 1,2,3,4) \tag{4.8}$$

$$N_{ii(constrain)} = N_{ii} + C^T P_i C \tag{4.9}$$

$$B_{i(constrain)} = B_{ii} + C^T P_i W \tag{4.10}$$

where Eq. (4.8) is the representation of the a priori constrain to parameter X_i; C is the coefficient matrix; W is the constant vector; P_i is the a priori weight matrix; $N_{ii(constrain)}$ and $B_{i(constrain)}$ are the newly updated normal equation coefficients with respect to parameter X_i.

Substituting Eq. (4.9) and Eq. (4.10) into Eq. (4.5), the new normal equation matrix with a priori constrain to the corresponding parameter is obtained. Thus the a priori constrained PPP can be applied.

4.2.2 Contribution Analysis of the Constraints to PPP

On the basis of the equivalence principle, an equivalently eliminated normal equation can be formed as (refer to Sect. 2.3, the second equation of Eq. (2.43))

$$M_2 X_2 = R_2 \tag{4.11}$$

Thus a priori constraint to the parameter X_2 in Eq. (4.11) can be represented as

$$0 = CX_2 - W, \quad P_2 \tag{4.12}$$

$$M_2' = M_2 + C^T P_2 C \tag{4.13}$$

$$R_2' = R_2 + C^T P_2 W \tag{4.14}$$

where M_2' and R_2' are the new normal equation coefficients with respect to parameter X_2 in Eq. (4.11).

According to Eq. (4.11), the PPP solution can be expressed as

$$X_2 = (M_2)^{-1} R_2 \tag{4.15}$$

$$Q_{X_2} = (M_2)^{-1} \tag{4.16}$$

where X_2 includes the coordinates, tropospheric delay and ambiguities parameters, Q_{X_2} denotes the coefficient matrix of X_2.

In accordance with Eq. (4.13) and Eq. (4.14), the new PPP solution by applying constraints can be expressed as

$$X_2' = \left(M_2 + C^T P_2 C\right)^{-1} \left(R_2 + C^T P_2 W\right) \tag{4.17}$$

$$Q_{X_2}' = \left(M_2 + C^T P_2 C\right)^{-1} \tag{4.18}$$

Therefore, the analytic contribution of the constraints to PPP solution can be expressed as

$$dX_2 = X_2' - X_2 = \left(M_2 + C^T P_2 C\right)^{-1} \left(R_2 + C^T P_2 W\right) - (M_2)^{-1} R_2 \tag{4.19}$$

To assess the precision, the covariance matrix $\sum_{X_2}$ of the parameter can be formed as

$$\sum_{X_2} = Q_{X_2} \sigma^2 \tag{4.20}$$

$$\sum_{X_2}' = Q_{X_2}' \sigma^2 \tag{4.21}$$

where σ denotes the standard deviation and can be computed by

$$\sigma = \sqrt{\frac{V^T P V}{n - m}} \tag{4.22}$$

where *n* is the number of observations; *m* is the number of estimated parameters.

Therefore, the contribution of the constraints to the estimation precision of PPP can be expressed as

$$\Delta \sum_{X_2} = \sum_{X_2} - \sum_{X_2}' \tag{4.23}$$

4.3 Applications of Different Constraints under Specific Conditions

4.3.1 Application of A Priori Constrain to Coordinates

In practice, the a priori constrain to coordinates in PPP solutions can reduce the convergence

time and avoid divergent positioning results. The a priori constraint of the coordinates X_1 of Eq. (4.8) can be known and formed in many cases.

1. A priori three-dimensional coordinates constraint

In applications for atmosphere research and long distance network RTK, the precise coordinates of the reference station are known in advance. In this case, the coefficient matrix *C* and constant vector *W* in Eq. (4.8) turn to be

$$C = I, \quad W = \begin{pmatrix} x_0 & y_0 & z_0 \end{pmatrix}^T \tag{4.24}$$

where I is an three-dimensional identity matrix; $\begin{pmatrix} x_0 & y_0 & z_0 \end{pmatrix}$ are the precisely known three-dimensional coordinates.

P_1 in Eq. (4.8) can be given by variance matrix $\sum_W$ and

$$P_1 = \sum_W^{-1}, \quad \sum_W = \begin{pmatrix} \sigma_{x_0}^2 & & \\ & \sigma_{y_0}^2 & \\ & & \sigma_{z_0}^2 \end{pmatrix} \tag{4.25}$$

Therefore, large weight indicates strong constraint and small weight indicates loose constraint. The strongest constraint is to keep the datum fixed. In this case, the three-dimensional coordinates are fixed in the estimation. P_1 can be set to a really large value such as

$$P_1 = \sum_W^{-1} = \begin{pmatrix} 10^{10} & & \\ & 10^{10} & \\ & & 10^{10} \end{pmatrix} \tag{4.26}$$

This a priori constrain to the coordinates can be used to resolve float ambiguities, since the coordinate parameters and ambiguity parameters are highly correlated and it is difficult to fix the ambiguities correctly (Li and Shen, 2009).

On the other hand, in the real-time slow-motion kinematic positioning, the precise a priori coordinates of the slow-motion carrier can be considered as stationary during a certain time period. Thus the coordinates estimated at epoch *i*-1 can be inherited directly at epoch *i*. In this case, the coefficient matrix C^i and constant vector W^i at epoch *i* in Eq. (4.8) turn to be

$$C^i = I, \quad W^i = X_1^{i-1} = \begin{pmatrix} x_0^{i-1} & y_0^{i-1} & z_0^{i-1} \end{pmatrix}^T \tag{4.27}$$

where X_1^{i-1} is the estimated coordinates at epoch *i*-1, and

$$P_1^i = P_{X_1^{i-1}} \tag{4.28}$$

where $P_{X_1^{i-1}}$ is the posteriori weight matrix of X_1^{i-1} at epoch *i*-1 (cf. Sect. 2.2, Eq. (2.18)).

The a priori constrain to coordinates is particularly beneficial to real-time disasters monitoring, such as landslide, urban land subsidence, and structural monitoring (Zang et al., 2014). In these cases, the slow-motion carriers have in common that the monitoring stations are continuously and long-term tracked with precise a priori information on coordinates. In addition, the deformation during or preceding geological disasters is generally continuous and in slow-motion, thus the monitoring station can be considered as stationary and the coordinates between epochs can be considered like static positioning during a certain period. The coordinates will be constrained to fluctuate only in a definitive range, which can remove the influence of other noises and improve the precision. However, it should be noted that the a priori constraints applied should be well-formulated mathematically and well-reasoned physically, in other words, the a priori information is considered as exactly known. And the information is known with certain a priori precision. Otherwise it will lead to the wrong or unreasonable results.

2. A priori horizontal coordinates constraint

In some deformation monitoring applications, such as bridge deformation, solar radiation and vehicles are major factors in causing the height variation while the horizontal coordinates remain unchanged. Therefore constraits can be applied to the horizontal coordinates. In this case, the coefficient matrix *C* and constant vector *W* in Eq. (4.8) turn to be

$$C = \begin{pmatrix} -\sin B_0 \cos L_0 & -\sin B_0 \sin L_0 & \cos B_0 \\ -\sin L_0 & \cos L_0 & 0 \end{pmatrix}, \quad W = \begin{pmatrix} x_0 & y_0 \end{pmatrix}^T \tag{4.29}$$

where B_0 and L_0 denote geodetic latitude and longitude of the monitoring station, $\begin{pmatrix} x_0 & y_0 \end{pmatrix}$ are the precisely known horizontal coordinates. And

$$P_1 = \sum\nolimits_W^{-1}, \quad \sum\nolimits_W = \begin{pmatrix} \sigma_{x_0}^2 & \\ & \sigma_{y_0}^2 \end{pmatrix} \tag{4.30}$$

3. A priori height constraint

In horizontal displacement monitoring, such as high building and dam monitoring, the height would remain unchanged. In this case, the coefficient matrix C and constant vector W in Eq. (4.8) turn to be

$$C = \begin{pmatrix} \cos B_0 \cos L_0 & \cos B_0 \sin L_0 & \sin B_0 \end{pmatrix}, \quad W = h_0 \tag{4.31}$$

where B_0 and L_0 denote the geodetic latitude and longitude of the monitoring station, h_0 is the precisely known height. And

$$P_1 = \sum\nolimits_W^{-1}, \quad \sum\nolimits_W = \left(\sigma_{h_0}^2\right) \tag{4.32}$$

4.3.2 A Priori Constrain to Receiver Clock Offset

In many cases the International GNSS Service (IGS) can provide receiver clock offset product. The physical properties of the receiver clocks at the permanent tracking stations for time service can be known previously (Cerretto et al., 2010; Li, 2012). Therefore, the physical model of the clock offset can be used as an a priori constraint. In this case, the coefficient matrix C and constant vector W in Eq. (4.8) turn to be

$$C = I, \quad W = dt_0 = a_0 + a_1(T - T_{oc}) \tag{4.33}$$

where I is identity matrix; dt_0 denotes the receiver clock error calculated by known physical model of the clock; a_0 and a_1 denote clock error and clock speed; T_{oc} is the reference epoch; T is the current epoch. Such constraint can be applied in the stations which have external atomic clocks since the physical model of atomic clock can be well known in advance and used as a priori constraint.

P_2 in Eq. (4.8) can be given by variance matrix $\sum_W$ and

$$P_2 = \sum\nolimits_W^{-1}, \quad \sum\nolimits_W = \left(\sigma_{dt_0}^2\right) \tag{4.34}$$

It is known that the receiver clock sequence obtained by the conventional single-day PPP is

discontinuous at the junction of day and day, which is the so-called day-boundary (Defraigne and Bruyninx, 2007). The day-boundary problem appears because the observation, orbit and satellite clock products are generally provided by one day, however, the initial conditions and error influences (e.g. tropospheric delay, multipath) between days are usually different, which is absorbed by the receiver clock offset in the single-day estimation. Thus there is a system error between the receiver clock offsets of different days. The day-boundary problem can significantly affect the application of PPP technology on precise timing and time transfer service (Huang, 2012). In this case, with the a priori constrain to the receiver clock offset, the day-boundary problem can be suppressed and the receiver clock sequence will become continuous between different days by applying clock offset constraint in the continuous PPP solution. In practice, the receiver clock offset constraint is normally combined with the coordinates constraint, which improves the speed of convergence and suppresses clock slip effectively. The receiver clock offset obtained has better continuity and higher stability.

4.3.3 A Priori Constrain to Tropospheric Delay

IGS has been producing the total troposphere zenith path delay (ZPD) product (Byun and Bar-Sever, 2009). The ZPD product can be selected as the precise external troposphere corrections to calibrate the troposphere zenith delay and as the a priori constraint in PPP. In this case, the coefficient matrix C and constant vector W in Eq. (4.8) turn to be

$$C = I, \quad W = d_{trop0} = ZPD \tag{4.35}$$

where I is identity matrix; d_{trop0} denotes the precise troposphere zenith path delay correction provided by IGS. In case of non-IGS stations, the previously estimated values can be used as the constraint, since the tropospheric delay can be considered as a constant during a certain period under normal weather condition.

P_3 in Eq. (4.8) can be given by variance matrix $\sum_W$ and

$$P_3 = \sum\nolimits_W^{-1}, \quad \sum\nolimits_W = \left(\sigma_{d_{trop0}}^2\right) \tag{4.36}$$

Due to the high precision of the external tropospheric correction, the tropospheric delay can

therefore be strongly constrained with a very small initial standard deviation (cf. $\sigma^2_{d_{trop}0}$ in Eq. (4.36)) in the estimation (Shi and Gao, 2014). It is known that the tropospheric delay will degrade other unknown parameters, especially the height coordinate in PPP (Hadas et al., 2015). Through using the a priori tropospheric delay constraint, the effect of the tropospheric delay on the PPP height solution can be removed because of the reduced correlation between troposphere and height parameters. Consequently, it can be expected that the PPP precision should be improved.

4.3.4 A Priori Constrain to Ambiguities

In practice, when the stations are long-term tracked, the ambiguities of the same visible satellites estimated in the former days can be adopted directly and used as the a priori value for the next days. And as long as there is no cycle slip, this kind of ambiguity constraint based on the values from previous days is reliable. Since the most or at least parts of the ambiguities are known through the a priori constraint, it can be expected that the convergence time of results should be greatly reduced. In this case, the coefficient matrix C^i and constant vector W^i at epoch *i* in Eq. (4.8) turn to be

$$C^i = I, \quad W^i = N^{i-1} \tag{4.37}$$

where N^{i-1} is the estimated ambiguities of the same visible satellites at epoch *i*-1. And

$$P_4^i = P_{X_4^{i-1}} \tag{4.38}$$

where $P_{X_1^{i-1}}$ is the posteriori weight matrix of X_4^{i-1} at epoch *i*-1 (cf. Sect. 2.2, Eq. (2.18)).

4.4 Examples and Analysis

4.4.1 PPP with Coordinates Constraint

As described in Sect. 4.3.1, the a priori constrain to coordinates in PPP solutions is expected to reduce the convergence time and improve positioning accuracy in many circumstances. In case of real-time slow-motion kinematic positioning, such as landslide, urban land subsidence, and structural monitoring, the slow-motion carriers have in common that the monitoring stations are continuously and long-term tracked with precise a priori information on

coordinates. In addition, the deformation during or preceding geological disasters is generally continuous and in slow-motion, thus the monitoring station can be considered as stationary and the coordinates between epochs can be inherited like static positioning during a certain period. The PPP algorithm with coordinates constraint has taken full account of characteristics of the monitoring station. On this basis four schemes were conducted to make comparison and analysis possible.

Scheme 1: Kinematic PPP positioning.

Scheme 2: PPP with a priori coordinates accuracy (cf. Sect. 4.3.1, σ_{x_0}, σ_{y_0} and σ_{z_0} were set as 5 cm here).

Scheme 3: PPP with time period constraint. In this case, the monitoring station is considered as stationary and the coordinates between epochs are inherited like static positioning during a certain period (set as 1 hour here).

Scheme 4: PPP with time period constraint and a priori coordinates accuracy. In this case, the monitoring station is considered as stationary and the coordinates between epochs are inherited like static positioning during a certain period (set as 1 hour here), and a priori coordinates accuracy (set as 5 cm here) is constrained at the first epoch of every time period set.

The GPS/BDS observations of MGEX station GMSD on GPS day 303 in 2014 were used to validate the algorithms. The sample interval of the data is 30 s. The observation models and details of PPP processing are listed in Table 4.1.

Table 4.1 Observation models and data processing strategies for PPP

Item	Models and Strategies
Observations	Un-differenced ionosphere-free code and phase combination
Observation weight	Elevation dependent weight
Elevation angle cutoff	7°
Precise orbit	Fixed, IGS precise ephemeris product and MGEX precise ephemeris from GFZ 15min
Precise clock biases	Fixed, IGS precise clock product and MGEX combined precise clock from GFZ 5min
Tropospheric delay	Saastamoinen model & parameter estimation

Ionospheric delay	First order effect eliminated by ionosphere-free linear combination
Phase-windup effect	Corrected
Earth rotation parameter	Fixed, IGS ERP product
PCO & PCV	Satellite antenna and receiver antenna correction applied for GPS, not applied for BDS
Relativistic effects	IERS Convention 2010
Tidal displacement	Solid Earth tides, pole tides, ocean tides (IERS Convention 2010)
Phase ambiguity	Estimated as constant for each ambiguity arc
Time system	GPS Time
Terrestrial frame	ITRF2008

GPS and BDS observations were used in the computation, respectively. To make a comparison, the position coordinates published by IGS were treated as standard values to compute the bias and RMS of the position results of the four schemes in N, E and U components. The bias of four schemes of GPS and BDS solutions with respect to IGS published results are shown in Fig. 4.1 and Fig. 4.2. The RMS results of GPS and BDS solutions are given in Table 4.2. The convergence time of all four schemes are given in Table 4.3. Due to the different positioning precision of GPS and BDS solutions, the convergence criterion was defined as the bias of the first moment and its following 20 epochs in N, E and U components were always less than 0.05 m for GPS solutions and 0.1 m for BDS solutions in this case.

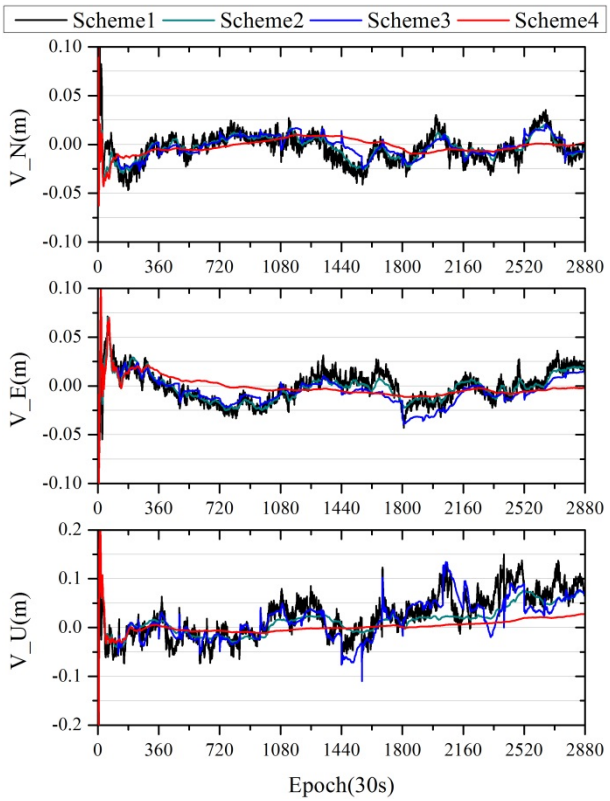

Fig. 4.1. Bias of GPS solutions with respect to IGS published results

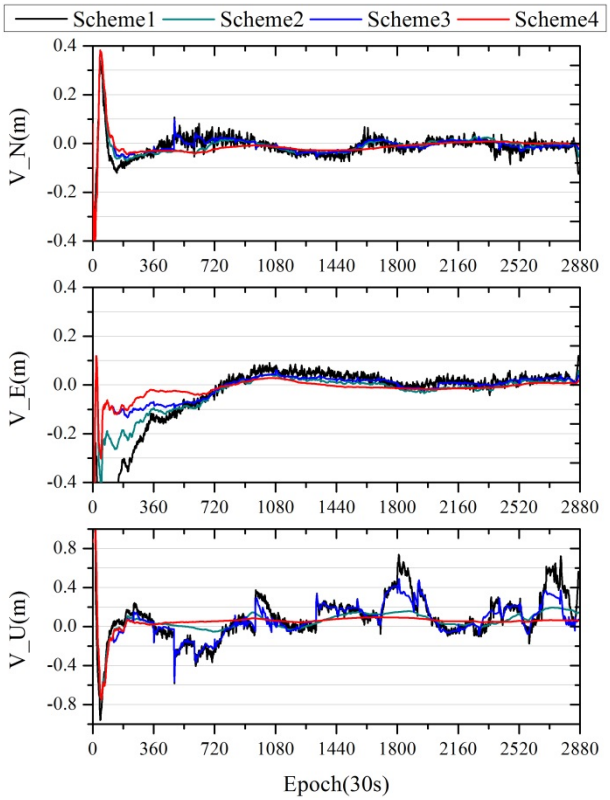

Fig. 4.2. Bias of BDS solutions with respect to IGS published results

Table 4.2 RMS of GPS and BDS solutions with respect to IGS results (units: m)

RMS		Scheme1	Scheme2	Scheme3	Scheme4
GPS	N	0.014	0.011	0.010	0.006
	E	0.015	0.012	0.014	0.008
	U	0.050	0.030	0.042	0.016
BDS	N	0.026	0.018	0.019	0.015
	E	0.034	0.018	0.022	0.013
	U	0.235	0.101	0.180	0.068

Table 4.3 Convergence time of all four schemes

Convergence Time	Scheme1	Scheme2	Scheme3	Scheme4
GPS (<5cm)	1h9min	16min	17min	16min
BDS (<10cm)	4h25min	59min	1h12min	57min

From Fig. 4.1-4.2 and Table 4.2-4.3 it can be found that: (1) Compared to Scheme 1, Schemes 2-4 can reduce the convergence time and improve positioning accuracy significantly, especially in U component. By using Scheme 2, 3, and 4 the accuracy of GPS solutions in U component can be improved by 40%, 16%, and 68%. The accuracy of BDS solutions in U component can be improved by 57%, 23%, and 71%, respectively. That is because the characteristics of the slow-motion carriers described above are taken full account of by PPP with coordinates constraint (Schemes 2-4). The results are constrained to fluctuate only in a definitive range, which can remove the influence of other noises and improve the positioning accuracy. By using Scheme 4, the convergence time of GPS and BDS solutions are decreased by 76% and 78%, respectively. (2) Comparing GPS solutions with BDS solutions, the accuracy and convergence time improvements both illustrate that in this case the effects of coordinates constraint on BDS solutions is more significant than on GPS. (3) The results of PPP with time period constraint and a priori coordinates accuracy (Scheme 4) show that they are superior both in convergence time and positioning accuracy, which is particularly beneficial to such real-time slow-motion monitoring applications.

4.4.2 PPP with Receiver Clock Offset Constraint

The GPS observations of IGS station GMSD during GPS week 1813 were used to validate the algorithms derived in Sect. 4.3.2. The sample interval of the data is 30 s. The precise orbit and satellite clock products from IGS were used. Two computation schemes were conducted to

make comparison and analysis possible.

Scheme 1: The observation data of seven days was processed through PPP day by day, thus the precise receiver clock offset of every single day could be obtained.

Scheme 2: The observation data of seven days was processed continuously through PPP with a priori receiver clock offset constraint. The coordinates and receiver clock offset published by IGS were used as the a priori information when computing the data of the first day, other days used the estimated results of the day before as the a priori information. Thus the continuous precise receiver clock offset could be obtained.

The comparison results of Scheme 1 and Scheme 2 are shown in Fig. 4.3. The differences between Scheme 1 and Scheme 2 were computed and are shown in Fig. 4.4.

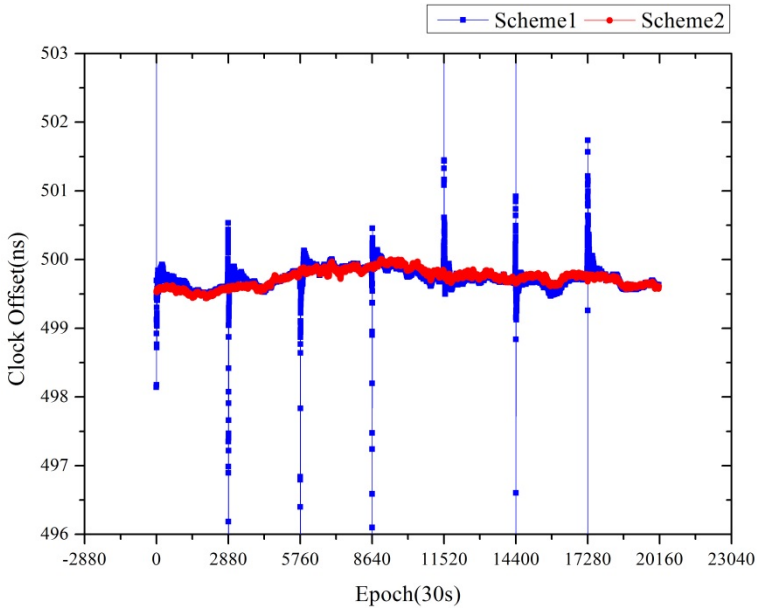

Fig. 4.3. Comparison of Scheme 1 and Scheme 2

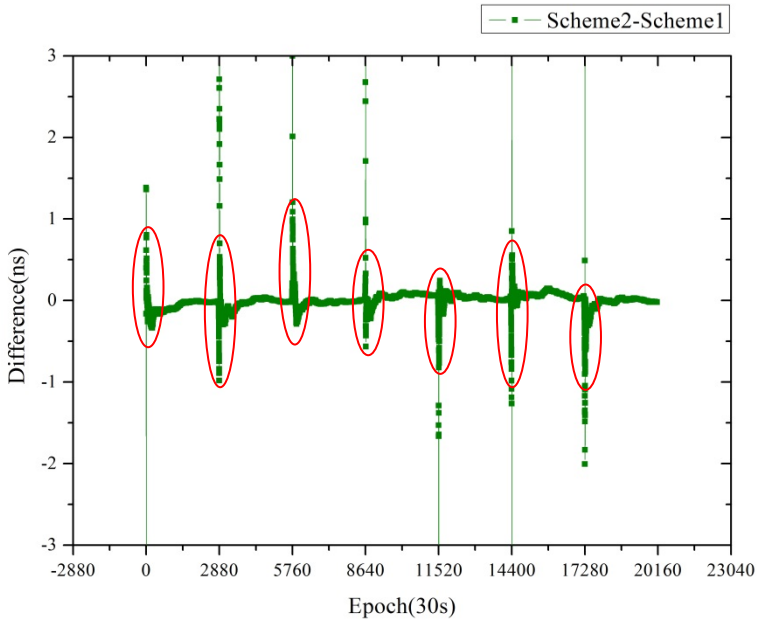

Fig. 4.4. Differences between Scheme 1 and Scheme 2

From Fig. 4.3 and Fig. 4.4 it can be found that: (1) From the comparison of the results of the first day it can be deduced that the result can achieve convergence more quickly with the coordinates and receiver clock offset constraints (Scheme 2) than with the single day solution (Scheme 1). (2) The continuity and stability of the receiver clock offset time series obtained by Scheme 2 is superior to that of Scheme 1. From the discrepancy of Scheme 1 and Scheme 2 (cf. Fig. 4.4), it is obvious that there are day-boundary discontinuities in Scheme 1, which can reach up to a magnitude of ns and is un-neglectable in precise timing and time transfer service. Thus PPP with the receiver clock offset constraint combined with coordinates constraint (Scheme 2) can suppress the day-boundary problem effectively.

4.4.3 PPP with Tropospheric Delay Constraint

The GPS observations of IGS station GMSD during GPS days 278-282 in 2014 were used to validate the algorithms derived in Sect. 4.3.3. The sample interval of the data is 30 s. The ZPD product from IGS was collected and used in this case. Two computation schemes were conducted to make comparison and analysis possible.

Scheme 1: Conventional PPP positioning. The empirical model was applied to calculate the a priori tropospheric delay and the residual tropospheric delay was estimated every hour. The tropospheric delay was considered as constant during one hour.

Scheme 2: Tropospheric delay constrained PPP. ZPD product from IGS was applied and used as an a priori constraint. The ZPD value and the accuracy were constrained at the first epoch of every hour in this case.

To be able to make a comparison, the position coordinates published by IGS were treated as standard values to compute the bias and RMS of the position results of the two schemes in N, E and U components. As an example, the bias of both schemes with respect to IGS published results on GPS day 282 are shown in Fig. 4.5. The RMS with respect to IGS results of both schemes are given in Table 4.4.

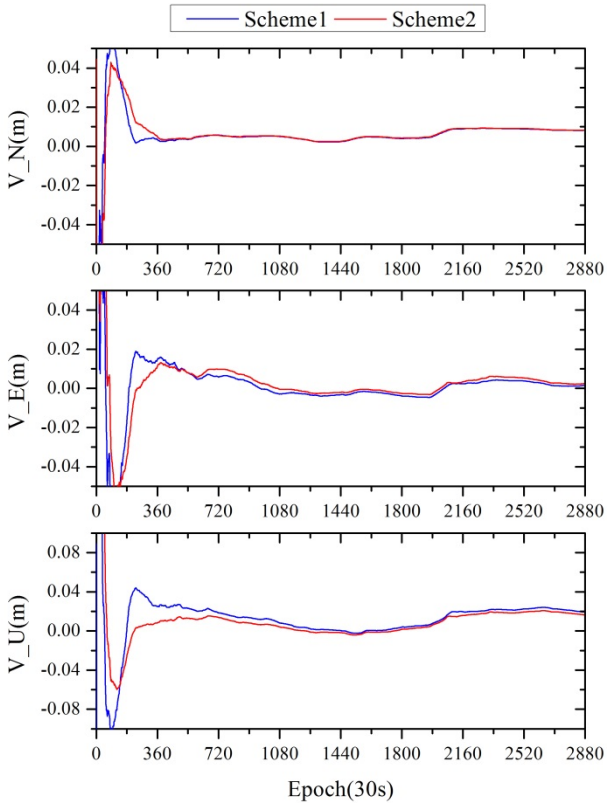

Fig. 4.5. Bias with respect to IGS published results on day 282

Table 4.4 RMS with respect to IGS results (units: mm)

RMS		278	279	280	281	282
Scheme1	N	5.4	5.3	8.2	6.4	6.1
	E	17.3	9.4	12.8	2.7	4.7
	U	29.1	30.4	24.3	22.7	16.2
Scheme2	N	5.4	5.0	7.9	6.2	6.3
	E	17.6	9.2	13.2	3.0	5.1
	U	26.5	28.0	21.9	21.0	12.1

From Fig. 4.5 and Table 4.4 it can be found that: (1) Compared to the conventional method

(Scheme 1) PPP with tropospheric delay constraint (Scheme 2) can mainly reduce the convergence time of the positioning in U component. (2) The position precision in N and E components are nearly identical by using two schemes. However, the positioning accuracy in U components of these five days is improved by 9%, 8%, 10%, 7%, and 25%, respectively. It is obvious, that the tropospheric delay constraint is the most superior in height solution. Owing to the usage of the tropospheric delay constraint, the correlation between troposphere and height coordinate can be solved and the effect of the tropospheric delay on PPP height solution can be removed to some extent, thus the positioning accuracy of the height component is improved most significantly.

4.4.4 PPP with Ambiguities Constraint

The GPS observations of IGS station GMSD during GPS days 302-304 in 2014 were used to validate the algorithms derived in Sect. 4.3.4. The sample interval of the data is 30 s. Two computation schemes were conducted as a basis for comparison and analysis.

Scheme 1: The observation data of three days was processed through conventional PPP day by day.

Scheme 2: The observation data of three days were processed through PPP with an a priori ambiguities constraint. The ambiguities estimated at the day before were used as the a priori value for the next days. In this case, the ambiguities estimated on GPS day 302 were used as the a priori value for day 303; the ambiguities estimated on GPS day 303 were used as the a priori value for day 304.

For comparison, the position coordinates published by IGS were treated as standard values to compute the bias of the position results of the two schemes in N, E and U components. The bias of two schemes with respect to IGS published results on day 303 and 304 are shown in Fig. 4.6 and Fig. 4.7.

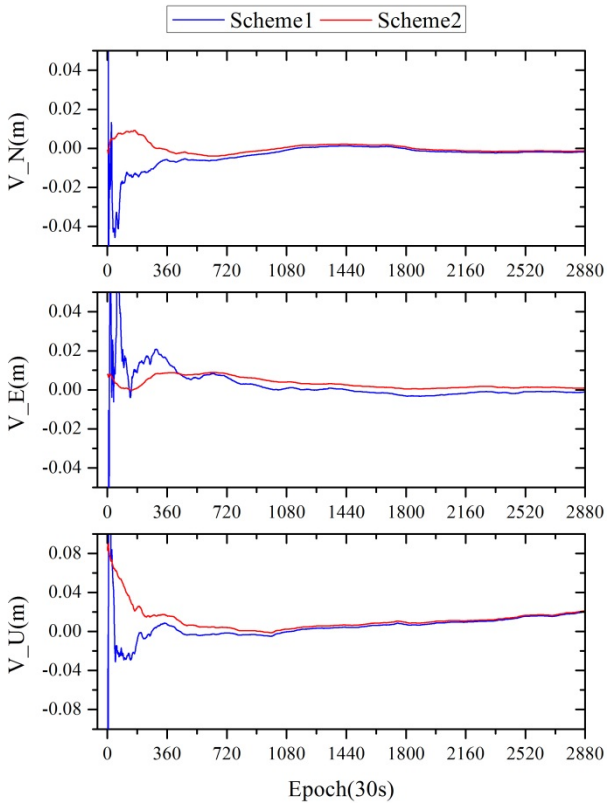

Fig. 4.6. Bias with respect to IGS published results on day 303

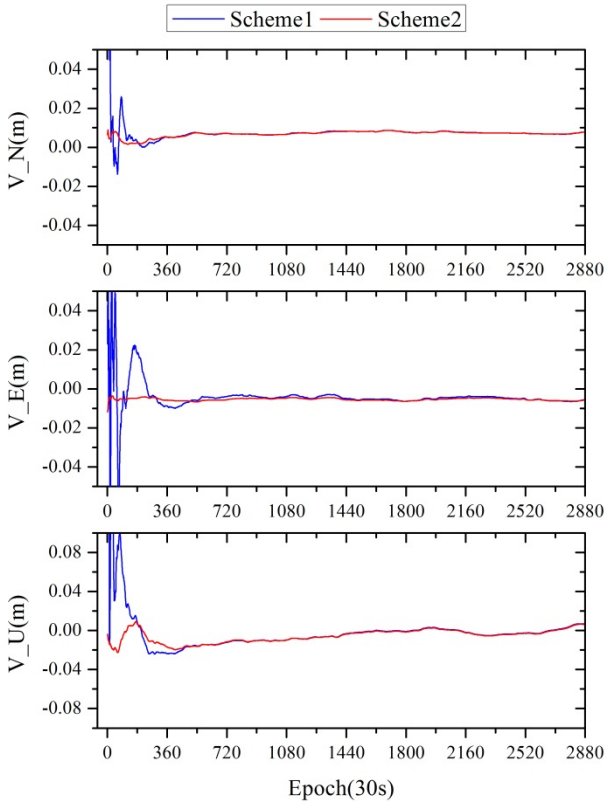

Fig. 4.7. Bias with respect to IGS published results on day 304

From Fig. 4.6 and Fig. 4.7 it can be found that with the ambiguities constraint (Scheme 2),

the result can achieve convergence much more quickly than by using Scheme 1. The reason for this is that in conventional PPP, a period of time is needed to solve the ambiguities parameters. However, Scheme 2 uses the ambiguities estimated at the day before as a priori values at the beginning of the computation. In this case, the ambiguities of the same visible satellites will not need to be solved any more, which significantly reduces convergence time.

4.5 Conclusions

In this chapter, a priori constrained PPP algorithms, which the a priori constraints employed can be comprehensively specified according to coordinates-, receiver clock offset-, tropospheric delay- and ambiguities-constraint, were derived. Numerical examples were conducted to validate that with a priori constraints convergence time of PPP can be reduced and positioning accuracy can be improved. PPP with a priori coordinates accuracy and time period constraints is particularly beneficial to the convergence time and accuracy of the real-time slow-motion carriers positioning, such as landslide, urban land subsidence, and structural monitoring. That is because it fully accounts for characteristics of slow-motion carriers. As deformation during geological disasters is generally continuous and in slow-motion, the monitoring station can be considered as stationary and the coordinates between epochs can be inherited like static positioning during a certain period. The coordinates are constrained to fluctuate only in a definitive range, which can remove the influence of other noises and improve the precision. Results of the example show that with such coordinates constraints, accuracy of GPS and BDS solutions improves and can reach 68% and 71%, while the convergence time is decreased by 76% and 78%, respectively. PPP with receiver clock offset constraint helps to solve the day-boundary discontinuities which are un-neglectable in precise timing and time transfer service. With coordinates and clock offset constraint, the results achieve convergence more quickly and more stable and continuous clock offset series can be obtained. PPP with tropospheric delay constraint removes the effect of the tropospheric delay on PPP height solution to improve the positioning accuracy in height component, which can reach up to 25% in the example. PPP with ambiguities constraint is greatly superior in reducing the convergence time of positioning.

5 Multi-Constellation Combined Precise Point Positioning Based on the Equivalence Principle

5.1 Introduction

The Global Navigation Satellite System (GNSS) has been developed rapidly in recent years and is in constant use nowadays. The Global Positioning System (GPS) is playing an important role now and has made remarkable contributions in both surveying and navigation in the past decades. Since October 2011 Russia's GLONASS system is functional again and is now operating at full capability with 24 satellites in orbits, enabling full global coverage (IAC, 2015). At the moment Europe's Galileo is in its Full Operational Capibility (FOC) phase by following In-Orbit Validation (IOV) and has 12 satellites in orbits (ESA, 2015; ESA, 2016). The Chinese BeiDou navigation satellite system is steadily advancing forward towards being an operational global navigation satellite system, which is planned to be completed by 2020. The first phase of the establishment, consisting of 5 GEO (Geostationary Earth Orbit) satellites, 5 IGSO (Inclined Geo-Synchronous Orbit) satellites and 4 MEO (Medium Earth Orbit) satellites, has been completed at the end of 2012, which provides positioning and navigation service in the Asia-Pacific area (CNAGA, 2014; Yang, 2010; Yang et al., 2014).

Over the past decades, with the rapid development of multiple GNSS systems, the developing features of GNSS precise positioning are being changed from GPS-only to combined multi-GNSS systems positioning. The combination of multi-GNSS systems can be considered as a major milestone in GNSS precise positioning, because it improves the reliability and productivity of GNSS positioning (Wang et al., 2001). The combination of multiple GNSS can significantly increase the number of simultaneous observed satellites, optimize spatial geometry, and therefore better dilution of precision, improve convergence time, accuracy, continuity and reliability of precise positioning, especially in constrained environments such as urban canyons, vegetation areas or deep open-cut mines (Li et al., 2015). Due to its rapidity and flexibility, Precise Point Positioning (PPP) can be one of the most promising application technologies in the combination of multiple GNSS systems. Many

studies on multi-GNSS combination, particularly with focus on GPS and GLONASS combination have been conducted in the last decade (Cai and Gao, 2013; Dach et al., 2007; Jokinen et al., 2011). Nevertheless, these studies focus mainly on validation of precision and reliability superiority of multi-GNSS combination, while the combined algorithm itself is seldom involved. The traditional combined PPP algorithm directly constructs observation equations using all GNSS observables to obtain the solution. However, with the advance of other available systems and satellites, as well as the wide utilization of high-frequency (1-50 Hz) recording receivers, the computational load of the traditional algorithm increases exponentially while at the same time, the efficiency of the algorithm decreases significantly (Huang et al., 2013). This is highly undesirable in high performance systems. Therefore, on the basis of the equivalence principle and its inference discussed formerly in this thesis, a multi-GNSS combined PPP algorithm is derived to improve the computation efficiency as presented in this chapter. In case of GPS/BDS combination, a method which can speed up the ambiguities determination of satellites from BDS through applying the contribution of GPS observations is proposed and analyzed. The GPS/BDS combined PPP algorithm with inter-system bias parameter is also derived. Furthermore, the usage of estimated ISB as a priori constraint in the GPS/BDS combined PPP is proposed to improve the convergence time and positioning accuracy.

5.2 The Conventional Multi-Constellation Combined PPP Algorithm

The observation equations of the traditional PPP have been introduced in Sect. 4.2.1 (refer to Eqs. (4.1)-(4.3)). The linearized observation Eq. (4.3) can be solved by using the sequential least squares adjustment (cf. Sect. 2.2.2) and the Kalman filter (cf. Sect. 2.2.3). In case of static positioning the sequential least squares adjustment is usually applied while the Kalman filter is utilized in the kinematic positioning. Taking sequential least squares PPP as an example, the corresponding solutions can be formed as

$$\begin{cases} X_i = (A_i^T P_i A_i + Q_{X_{i-1}}^{-1})^{-1}(A_i^T P_i L_i + Q_{X_{i-1}}^{-1} X_{i-1}) \\ Q_{X_i} = (A_i^T P_i A_i + Q_{X_{i-1}}^{-1})^{-1} \end{cases} \tag{5.1}$$

where X_{i-1}, X_i and $Q_{X_{i-1}}$, Q_{X_i} are the estimation value of the unknown parameters and

its cofactor matrix at epoch *i*-1 and *i*, respectively.

In case of multiple GNSS systems, the ionosphere-free code and phase observations of GPS, GLONASS, Galileo and BeiDou combination can be expressed as

$$P_{IF}^{G} = \rho^{G} + c \cdot dt^{G} + d_{trop}^{G} + dm_{IF}^{G} + \varepsilon_{P_{IF}}^{G} \tag{5.2}$$

$$\Phi_{IF}^{G} = \rho^{G} + c \cdot dt^{G} + d_{trop}^{G} + \lambda_{IF}^{G} \cdot N_{IF}^{G} + \delta m_{IF}^{G} + \varepsilon_{\Phi_{IF}}^{G} \tag{5.3}$$

$$P_{IF}^{R} = \rho^{R} + c \cdot dt^{R} + d_{trop}^{R} + dm_{IF}^{R} + \varepsilon_{P_{IF}}^{R} \tag{5.4}$$

$$\Phi_{IF}^{R} = \rho^{R} + c \cdot dt^{R} + d_{trop}^{R} + \lambda_{IF}^{R} \cdot N_{IF}^{R} + \delta m_{IF}^{R} + \varepsilon_{\Phi_{IF}}^{R} \tag{5.5}$$

$$P_{IF}^{E} = \rho^{E} + c \cdot dt^{E} + d_{trop}^{E} + dm_{IF}^{E} + \varepsilon_{P_{IF}}^{E} \tag{5.6}$$

$$\Phi_{IF}^{E} = \rho^{E} + c \cdot dt^{E} + d_{trop}^{E} + \lambda_{IF}^{E} \cdot N_{IF}^{E} + \delta m_{IF}^{E} + \varepsilon_{\Phi_{IF}}^{E} \tag{5.7}$$

$$P_{IF}^{C} = \rho^{C} + c \cdot dt^{C} + d_{trop}^{C} + dm_{IF}^{C} + \varepsilon_{P_{IF}}^{C} \tag{5.8}$$

$$\Phi_{IF}^{C} = \rho^{C} + c \cdot dt^{C} + d_{trop}^{C} + \lambda_{IF}^{C} \cdot N_{IF}^{C} + \delta m_{IF}^{C} + \varepsilon_{\Phi_{IF}}^{C} \tag{5.9}$$

where indices *G*, *R*, *E* and *C* represent GPS, GLONASS, Galileo and BeiDou satellites, respectively.

Similar as Eq. (4.3), the linearized error equation of multi-GNSS combined positioning for Eqs. (5.2) to (5.9) can be formed as

$$\begin{bmatrix} V^{G} \\ V^{R} \\ V^{E} \\ V^{C} \end{bmatrix} = \begin{bmatrix} A^{G} \\ A^{R} \\ A^{E} \\ A^{C} \end{bmatrix} X - \begin{bmatrix} L^{G} \\ L^{R} \\ L^{E} \\ L^{C} \end{bmatrix}, \quad \begin{bmatrix} P^{G} & 0 & 0 & 0 \\ 0 & P^{R} & 0 & 0 \\ 0 & 0 & P^{E} & 0 \\ 0 & 0 & 0 & P^{C} \end{bmatrix} \tag{5.10}$$

where indices *G*, *R*, *E* and *C* represent GPS, GLONASS, Galileo and BeiDou satellites, respectively. The unknown parameter vector X to be estimated includes shared parameters as coordinates and tropospheric delay, the self-owned parameters of each system as receiver clock offset and ambiguities. To solve Eq. (5.10), the form of the sequential least squares solution as Eq. (5.1) can also be applied in the conventional way.

However, for the solution and calculation of Eq. (5.10), the traditional method of direct accumulation can hardly meet the demand of rapidly solving an ocean of real-time and

high-rate data. Especially, when considering the preprocessing and iteration calculation in the positioning as well. With a constant increase of the number of available satellites, the exponentially increased computational load has to be taken into the conventional positioning algorithm. To solve this problem, an algorithm based on the equivalence principle which can improve the calculating efficiency, is proposed and derived in the following section. Firstly, the formulas of the parameter solution and its covariance matrix can be rewritten to the form of the accumulation of the coefficient matrix of the normal equation. The coefficient matrix of the normal equation is transferred between epochs by accumulation, so that it can be written as

$$\begin{cases} N_i = A_i^T P_i A_i + N_{i-1} \\ W_i = A_i^T P_i L_i + W_{i-1} \\ X_i = N_i^{-1} W_i \\ Q_{X_i} = N_i^{-1} \end{cases} \tag{5.11}$$

where subscript *i* denotes the epoch; N_i and W_i are the coefficient matrices of normal equation at epoch *i*. Compared to Eq. (5.1), the traditional accumulation form of the parameter vector X_i and its covariance matrix Q_{X_i} are changed to the accumulation form of the coefficient matrices N_i and W_i of the normal equation. N_i and W_i have the same dimension as Q_{X_i} and X_i, thus the computational load of Eq. (5.11) and Eq. (5.1) are identical in real-time processing. While in post processing, the inversion of Q_{X_i} and X_i at each epoch can be omitted by using Eq. (5.11), the accumulation of the coefficient matrices only need to be solved at the last epoch, which shows significant superiority in computing efficiency compared to using Eq. (5.1). In accordance with Eq. (5.11) and the equivalence principle, the multi-GNSS combined PPP algorithm will be derived in the following section.

5.3 Multi-Constellation Combined PPP Algorithm Based on the Equivalence Principle

5.3.1 Multi-Constellation Combined PPP Algorithm

Based on the equivalence principle, the unknown parameters can be divided into two groups.

One group can be eliminated directly through constructing the equivalently eliminated observation equation (cf. Sect. 2.3).

Similar to the form of Eq. (2.38), the unknown parameter vector X in Eq. (4.3) can be divided into X_1 and X_2, thus one has

$$V = \begin{pmatrix} A & B \end{pmatrix} \begin{pmatrix} X_1 \\ X_2 \end{pmatrix} - L, \qquad P \tag{5.12}$$

where X_1 denotes the parameter varying with time, which is changeable between epochs and refers to the receiver clock offset in PPP. X_2 denotes the fixed parameters that do not change over time and can be maintained between epochs, which refer to coordinates, tropospheric delay and ambiguities in static PPP. In practical processing, the tropospheric delay parameter is considered as a constant during a certain time period (e.g. 2 hours) under normal weather condition and should be reinitialized every certain period during the estimation. It should be also pointed out that in case of kinematic PPP, coordinates vary over time and can not be inherited directly for the next instant computation.

The normal equation of Eq. (5.12) can be formed as

$$\begin{pmatrix} M_{11} & M_{12} \\ M_{21} & M_{22} \end{pmatrix} \begin{pmatrix} X_1 \\ X_2 \end{pmatrix} = \begin{pmatrix} B_1 \\ B_2 \end{pmatrix} \tag{5.13}$$

where $M_{11} = A^T PA$, $M_{12} = A^T PB$, $M_{21} = B^T PA$, $M_{22} = B^T PB$, $B_1 = A^T PL$, $B_2 = B^T PL$.

Appling the equivalence algorithm (Xu, 2002; Xu, 2007; Zhou, 1985) (cf. Sect. 2.3), the equivalently eliminated equation of Eq. (5.13) can be formed as

$$\begin{pmatrix} M_{11} & M_{12} \\ 0 & M_2 \end{pmatrix} \begin{pmatrix} X_1 \\ X_2 \end{pmatrix} = \begin{pmatrix} B_1 \\ R_2 \end{pmatrix} \tag{5.14}$$

where $M_2 = M_{22} - M_{21} M_{11}^{-1} M_{12}$, $R_2 = B_2 - M_{21} M_{11}^{-1} B_1$.

Therefore the unknown parameter X_2 can be solved directly through the second equation of Eq. (5.14), that can be expressed as

$$M_2 X_2 = R_2 \tag{5.15}$$

The parameter X_1 can be solved through applying X_2 to the first equation of Eq. (5.14), that

$$M_{11} X_1 + M_{12} X_2 = B_1 \tag{5.16}$$

Referring to the accumulation form of the normal equation as Eq. (5.11), the recursion formulas of the PPP solution at epoch *i* can be formed as

$$\begin{cases} \tilde{M}_2^i = M_2^i + \tilde{M}_2^{i-1} \\ \tilde{R}_2^i = R_2^i + \tilde{R}_2^{i-1} \\ X_2^i = (\tilde{M}_2^i)^{-1} \tilde{R}_2^i \\ X_1^i = (M_{11}^i)^{-1} (B_1^i - M_{12}^i X_2^i) \\ Q_{X_2^i} = (\tilde{M}_2^i)^{-1} \\ Q_{X_1^i} = \left(M_{11}^i - M_{12}^i (\tilde{M}_{22}^i)^{-1} M_{21}^i \right)^{-1}, \ \tilde{M}_{22}^i = \tilde{M}_2^i + M_{21}^i (M_{11}^i)^{-1} M_{12}^i \end{cases} \tag{5.17}$$

Thus, the PPP algorithm of a single system based on the equivalence principle is derived.

For multi-Constellation combined PPP, the fixed unknown parameter X_2 should further be divided into two groups, that

$$X_2 = \begin{bmatrix} Y_1 \\ Y_2 \end{bmatrix} \tag{5.18}$$

where Y_1 denotes the shared parameters between GNSS systems as coordinates and tropospheric delay; Y_2 denotes the unshared parameter as ambiguities of different GNSS systems.

Thus M_2 and R_2 in Eq. (5.15) should be rewritten as

$$M_2 = \begin{bmatrix} N_{11} & N_{12} \\ N_{21} & N_{22} \end{bmatrix}, \ R_2 = \begin{bmatrix} D_1 \\ D_2 \end{bmatrix} \tag{5.19}$$

Then Eq. (5.15) can be rewritten as

$$\begin{bmatrix} N_{11} & N_{12} \\ N_{21} & N_{22} \end{bmatrix} \begin{bmatrix} Y_1 \\ Y_2 \end{bmatrix} = \begin{bmatrix} D_1 \\ D_2 \end{bmatrix} \tag{5.20}$$

Similarly, the equivalently eliminated equation of Eq. (5.20) can be obtained as

$$\begin{bmatrix} N_1 & 0 \\ N_{21} & N_{22} \end{bmatrix} \begin{bmatrix} Y_1 \\ Y_2 \end{bmatrix} = \begin{bmatrix} S_1 \\ D_2 \end{bmatrix} \tag{5.21}$$

where $N_1 = N_{11} - N_{12}N_{22}^{-1}N_{21}$, $S_1 = D_1 - N_{12}N_{22}^{-1}D_2$.

Therefore

$$N_1 Y_1 = S_1 \tag{5.22}$$

For GPS, GLONASS, Galileo and BeiDou systems, the normal equation of the shared unknown parameter Y_1 of each system can be expressed as

$$N_1^G Y_1 = S_1^G \ , \ N_1^R Y_1 = S_1^R \ , \ N_1^E Y_1 = S_1^E \ , \ N_1^C Y_1 = S_1^C \tag{5.23}$$

where indices *G*, *R*, *E* and *C* represent GPS, GLONASS, Galileo and BeiDou satellites, respectively.

Therefore, the normal equation of the multi-GNSS combined PPP can be obtained as

$$\sum_{k=1}^{m} N_1^k Y_1 = \sum_{k=1}^{m} S_1^k \tag{5.24}$$

where *m* denotes the number of GNSS systems.

After solving the shared parameter Y_1 by Eq. (5.24), Y_2 can be solved by the second equation of Eq. (5.21), thus X_2 can be obtained and so is X_1. In this way, the complete solution of multi-GNSS combined PPP can be obtained. Similar to Eq. (5.17), the recursion formulas of the combined PPP solution at epoch *i* can be formed as

$$
\begin{cases}
\tilde{\tilde{M}}_2^i = \tilde{M}_2^i + \begin{bmatrix} \sum_{k=1,k\neq s}^{m} N_1^k & 0 \\ 0 & 0 \end{bmatrix} \\
\tilde{\tilde{R}}_2^i = \tilde{R}_2^i + \begin{bmatrix} \sum_{k=1,k\neq s}^{m} S_1^k \\ 0 \end{bmatrix} \\
X_2^i = (\tilde{\tilde{M}}_2^i)^{-1}\tilde{\tilde{R}}_2^i \\
X_1^i = (M_{11}^i)^{-1}(B_1^i - M_{12}^i X_2^i) \\
Q_{X_2^i} = (\tilde{\tilde{M}}_2^i)^{-1} \\
Q_{X_1^i} = \left(M_{11}^i - M_{12}^i(\tilde{\tilde{M}}_{22}^i)^{-1}M_{21}^i\right)^{-1},\ \tilde{\tilde{M}}_{22}^i = \tilde{\tilde{M}}_2^i + M_{21}^i(M_{11}^i)^{-1}M_{12}^i
\end{cases}
\tag{5.25}
$$

where $\sum_{k=1,k\neq s}^{m} N_1^k$ and $\sum_{k=1,k\neq s}^{m} S_1^k$ denote the accumulation of the normal equations of other GNSS systems except the self-owned system in combined PPP.

5.3.2 Specific Analysis under Static and Kinematic Conditions

Eqs. (5.12) to (5.25) are the complete solution of multi-GNSS combined PPP based on the equivalence principle. In static combined PPP, X_1 denotes the receiver clock offset parameter, which is changeable between epochs; X_2 denotes the coordinates, zenith tropospheric delay and ambiguities, which are fixed parameters and can be inherited between epochs; Y_1 denotes the coordinates and zenith tropospheric delay, which are the shared parameters between different GNSS systems; Y_2 denotes the unshared parameters, such as ambiguities of different GNSS satellites from different systems. In case of kinematic combined PPP, X_1 denotes the receiver clock offset parameter and coordinates; X_2 denotes the zenith tropospheric delay and ambiguities; Y_1 denotes the zenith tropospheric delay; Y_2 denotes the ambiguities of different GNSS satellites from different systems.

On the other hand, if the state equation of the motion carrier is known formerly in kinematic combined PPP, the coordinates parameter should be predictable by the state equation in Kalman filter. In this case, X_1 denotes the receiver clock offset parameter; X_2

denotes the coordinates, tropospheric delay and ambiguities; Y_1 denotes the coordinates and tropospheric delay; Y_2 denotes the ambiguities of different GNSS satellites from different systems. Based on the state equation, the predicted value of the parameter $\bar{X}_2^i$ at epoch *i* can be obtained as

$$\bar{X}_2^i = \Phi_{i,i-1} X_2^{i-1} \tag{5.26}$$

where X_2^{i-1} is the estimated value at epoch *i*-1, and $\Phi_{i,i-1}$ is the state transition matrix.

Similar to the form of Eq. (5.17), the recursion formulas at epoch *i* for the equivalently eliminated normal Eq. (5.15) and Eq. (5.16) can be formed as

$$\begin{cases} \tilde{M}_2^i = M_2^i + \bar{M}_2^i,\ \bar{M}_2^i = (\Phi_{i.i-1}^T)^{-1} \tilde{M}_2^{i-1} (\Phi_{i,i-1})^{-1} \\ \tilde{R}_2^i = R_2^i + \bar{R}_2^i,\ \bar{R}_2^i = (\Phi_{i.i-1}^T)^{-1} \tilde{R}_2^{i-1} \\ X_2^i = (\tilde{M}_2^i)^{-1} \tilde{R}_2^i \\ X_1^i = (M_{11}^i)^{-1} (B_1^i - M_{12}^i X_2^i) \\ Q_{X_2^i} = (\tilde{M}_2^i)^{-1} \\ Q_{X_1^i} = \left(M_{11}^i - M_{12}^i (\tilde{M}_{22}^i)^{-1} M_{21}^i \right)^{-1},\ \tilde{M}_{22}^i = \tilde{M}_2^i + M_{21}^i (M_{11}^i)^{-1} M_{12}^i \end{cases} \tag{5.27}$$

where the predicted normal matrices $\bar{M}_2^i$ and $\bar{R}_2^i$ can be derived through using the error propagation law. The following solution for kinematic combined PPP has the same form as Eq. (5.25).

5.3.3 Efficiency Comparison of the Multi-GNSS Combined PPP Algorithms

To validate the computational efficiency of the combined PPP algorithm based on the equivalence principle, a simulation example was conducted in this section. The observations of GPS, GLONASS, Galileo and BDS were simulated, which contained 2000 epochs. The simulated observations were generated according to the precise ephemeris and a given station coordinates. Firstly the distance between satellites and the station can be derived and then we artificially added all kinds of errors to the distance to obtain the simulated observations. The sample rate of the simulated observations can be set as an arbitrary value, since it would not affect the efficiency of the computation. The number of visible satellites of each system at each epoch was all set as 10 and there was no satellite change during the observation period.

Two processing schemes were conducted to make comparison and analysis possible.

Scheme 1: The conventional multi-constellation combined PPP (cf. Sect. 5.2).

Scheme 2: The multi-constellation combined PPP based on the equivalence principle (cf. Sect. 5.3.1).

In the computation of both schemes the numbers of GNSS systems were set as 1, 2, 3 and 4, respectively. The processing was conducted with a high performance configuration computer. The computation time of the different number of GNSS systems needed for the processing of both schemes is indicated in Fig. 5.1.

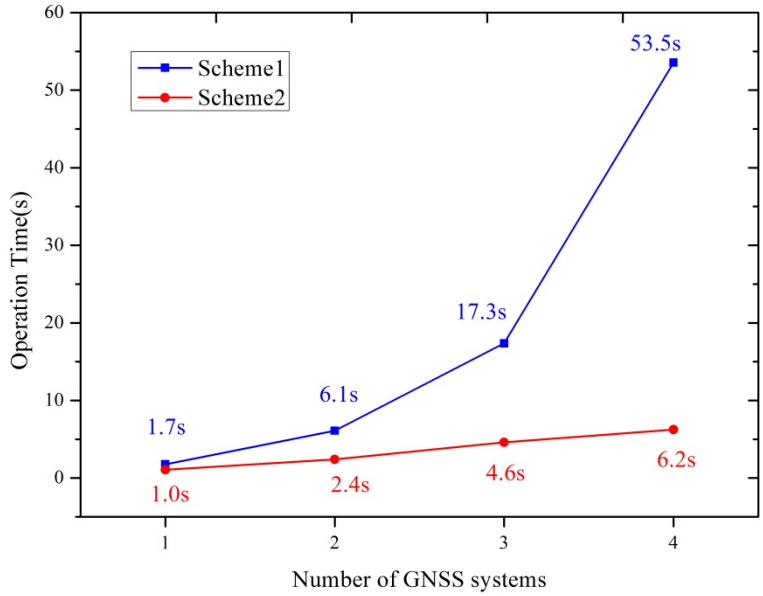

Fig. 5.1. Comparison of the operation time needed in the processing

From Fig. 5.1 it can be found that, with the advance of the GNSS systems and satellites, the operation time of the conventional combined PPP (Scheme 1) increases exponentially. By using the combined PPP based on the equivalence principle derived in this chapter (Scheme 2), the computation time increases linearly with more available GNSS systems and satellites, which leads to a greatly superior computation efficiency.

5.3.4 Examples and Analysis

1. Static combined PPP

To validate the combined PPP algorithm based on the equivalence principle, a set of 6 IGS stations (CAS1, GMSD, POHN, REUN, TUVA and XMIS) from MGEX (Multi-GNSS

Experiment) network were used to make the analysis. The GPS, GLONASS and BDS observations of these selected stations were during GPS weeks 1821 and 1822 with a sample interval of 30 s. The observation models and details of static PPP processing are listed in Table 5.1.

Table 5.1 Observation models and data processing strategies for PPP

Item	Models and Strategies
Observations	Un-differenced ionosphere-free code and phase combination
Observation weight	Elevation dependent weight
Elevation angle cutoff	7°
Precise orbit	Fixed, MGEX precise ephemeris from GFZ 15min
Precise clock biases	Fixed, MGEX combined precise clock from GFZ 5min
Tropospheric delay	Saastamoinen model & parameter estimation
Ionospheric delay	First order effect eliminated by ionosphere-free linear combination
Phase-windup effect	Corrected
Earth rotation parameter	Fixed, IGS ERP product
PCO & PCV	Satellite antenna and receiver antenna correction applied for GPS and GLONASS, not applied for BDS
Relativistic effects	IERS Convention 2010
Tidal displacement	Solid Earth tides, pole tides, ocean tides (IERS Convention 2010)
Phase ambiguity	Estimated as constant for each ambiguity arc
Time system	GPS Time
Terrestrial frame	ITRF2008

Four schemes were conducted to make comparison and analysis possible.

Scheme 1: GPS single system static PPP positioning (denoted as GPS in Fig. 5.2 - Fig. 5.7 and Table 5.2).

Scheme 2: GLONASS single system static PPP positioning (denoted as GLONASS in Fig. 5.2 - Fig. 5.7 and Table 5.2).

Scheme 3: BDS single system static PPP positioning (denoted as BDS in Fig. 5.2 - Fig. 5.7 and Table 5.2).

Scheme 4: GPS/GLONASS/BDS static combined PPP algorithm based on the equivalence principle (denoted as G+R+C in Fig. 5.2 - Fig. 5.7 and Table 5.2).

To make a comparison, the position coordinates published by IGS were treated as standard values to compute the bias and RMS of the position results of the four schemes in N, E and U

components. As examples, the bias of four schemes with respect to IGS published results in N, E and U components of the 6 stations for 9 days during the test period are shown in Fig. 5.2 - Fig. 5.7. The RMS results of GPS day 337 are given as an example in Table 5.2.

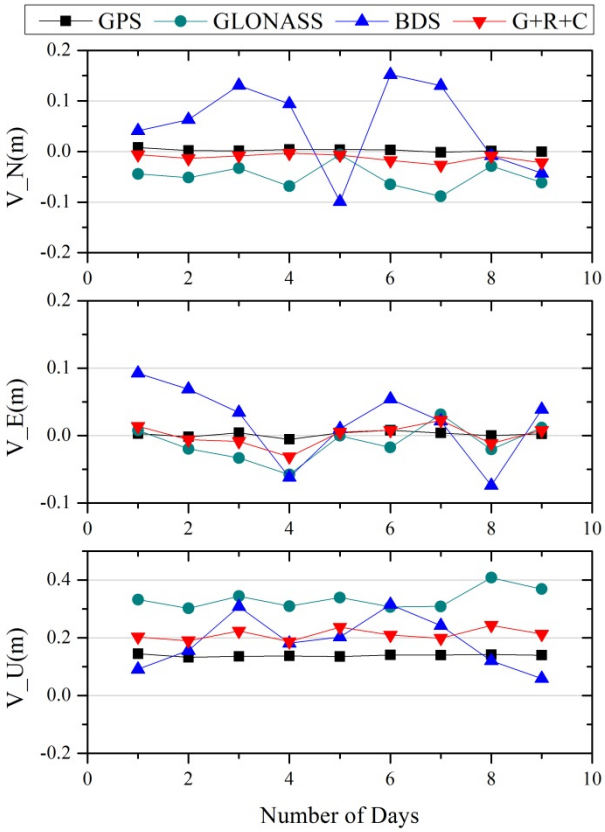

Fig. 5.2. Bias of four schemes with respect to IGS published results for station CAS1

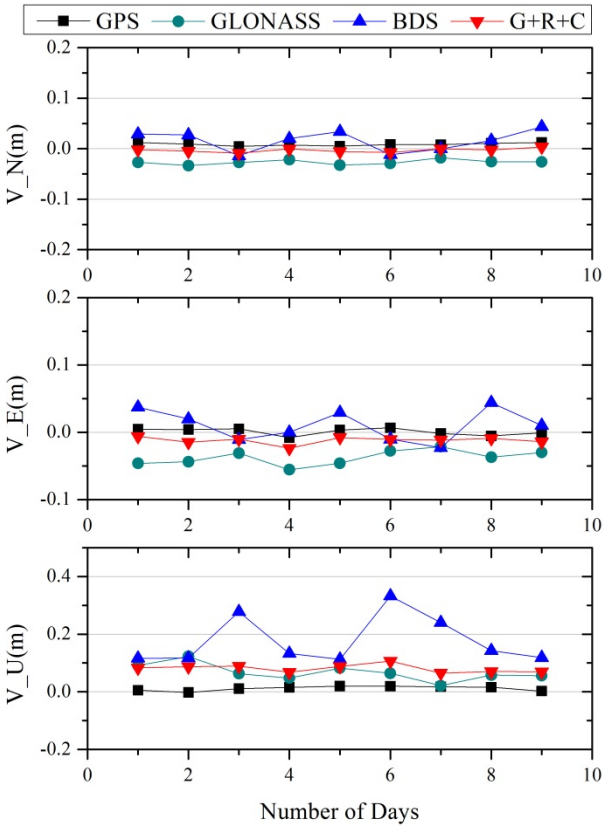

Fig. 5.3. Bias of four schemes with respect to IGS published results for station GMSD

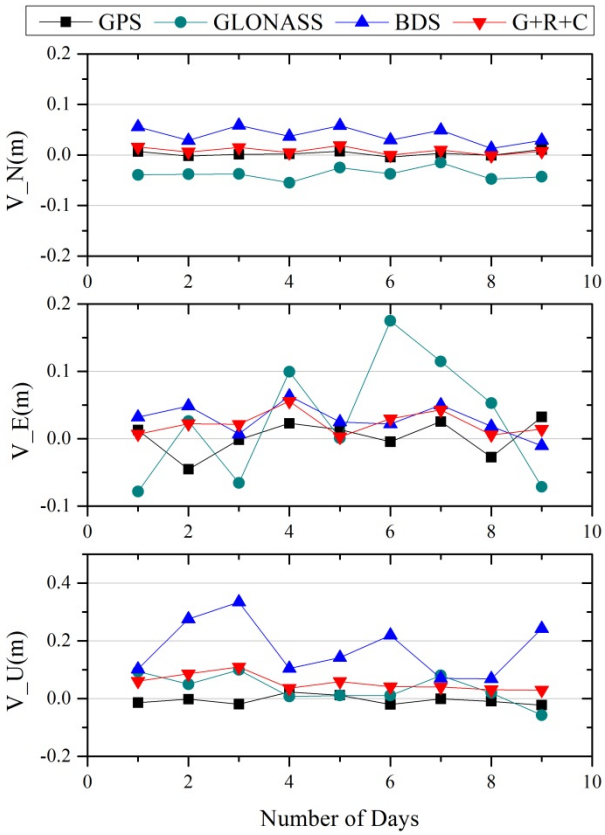

Fig. 5.4. Bias of four schemes with respect to IGS published results for station POHN

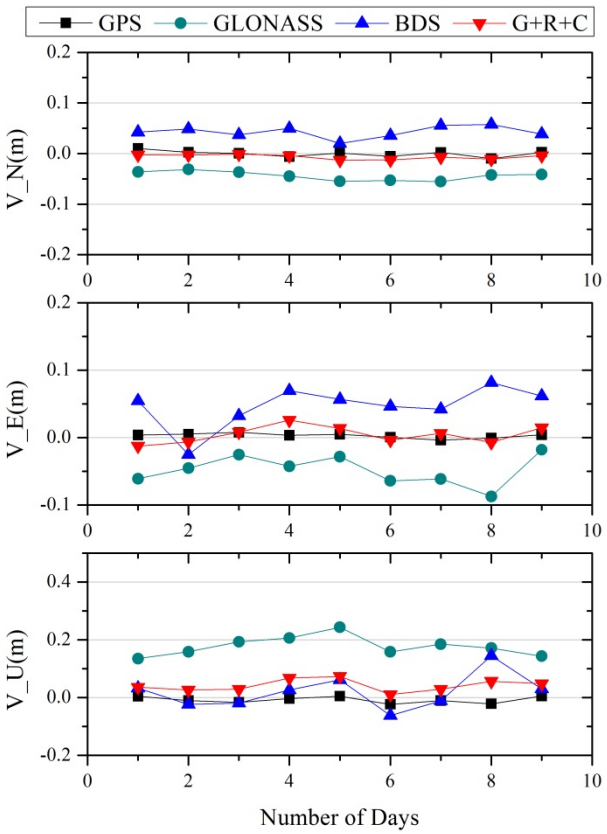

Fig. 5.5. Bias of four schemes with respect to IGS published results for station REUN

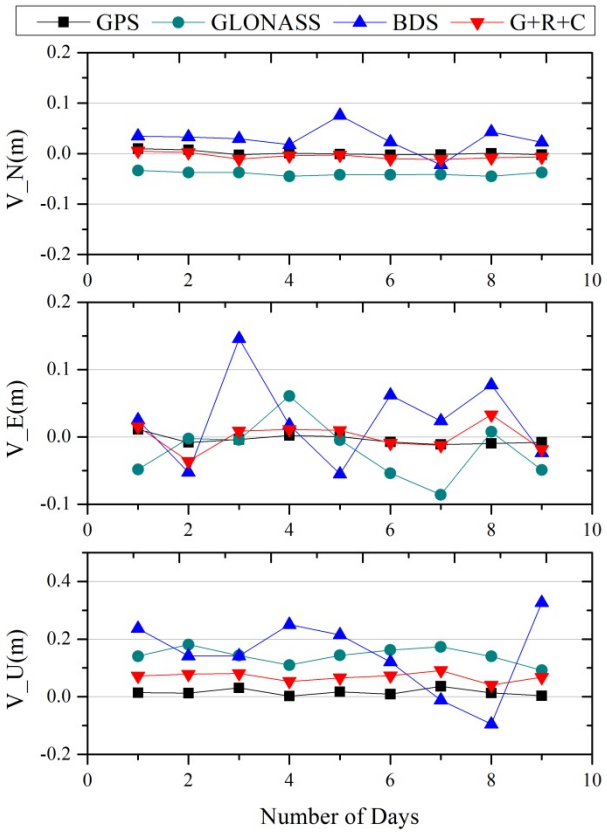

Fig. 5.6. Bias of four schemes with respect to IGS published results for station TUVA

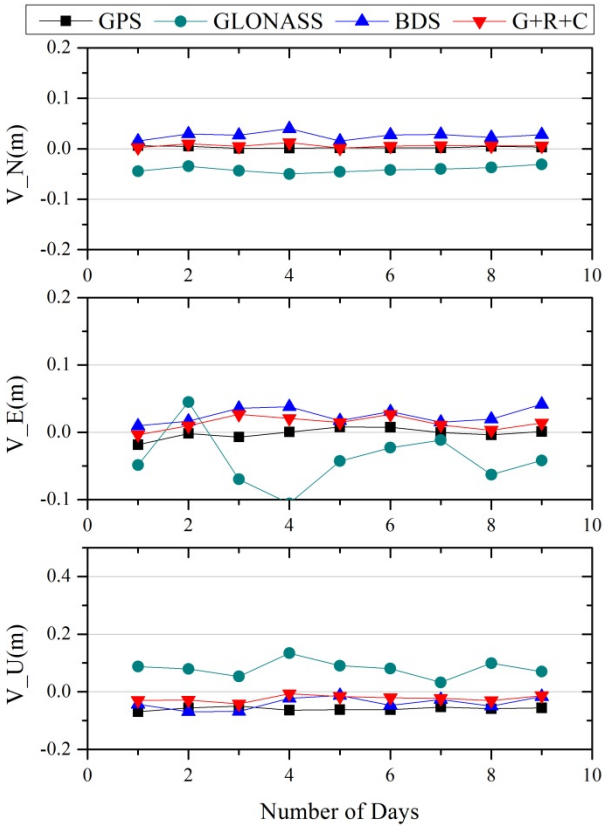

Fig. 5.7. Bias of four schemes with respect to IGS published results for station XMIS

Table 5.2 RMS with respect to IGS results (units: m)

Stations		GPS	GLONASS	BDS	G+R+C
CAS1	N	0.003	0.039	0.077	0.021
	E	0.006	0.046	0.054	0.018
	U	0.145	0.389	0.198	0.257
GMSD	N	0.006	0.054	0.009	0.022
	E	0.007	0.060	0.040	0.022
	U	0.008	0.151	0.187	0.111
POHN	N	0.005	0.058	0.050	0.014
	E	0.029	0.109	0.088	0.067
	U	0.041	0.169	0.356	0.103
REUN	N	0.002	0.027	0.028	0.004
	E	0.017	0.034	0.031	0.027
	U	0.022	0.270	0.047	0.066
TUVA	N	0.004	0.046	0.045	0.013
	E	0.019	0.117	0.183	0.019
	U	0.024	0.150	0.190	0.079
XMIS	N	0.003	0.037	0.019	0.002
	E	0.014	0.090	0.036	0.023
	U	0.059	0.169	0.116	0.052

From Fig. 5.2 - Fig. 5.7 and Table 5.2 it can be found that: (1) For single system

positioning, the precision of GPS solutions is superior to GLONASS and BDS solutions. Generally said, single GPS PPP can achieve an accuracy of mm in horizontal component and cm in vertical component, which indicates that PPP nowadays has high-precision. (2) It is noted that because of the location and the high latitude of station CAS1 (-66.28°), the RMS in U component reached up to 14.5 cm while in this case in N and E components they were 3 mm and 6 mm. This did not meet the normal accuracy relation regularity between horizontal and vertical components any more, which means that the vertical component of the RMS is generally the double of the horizontal component. That is because the station CAS1 is located in the Antarctic and due to the specificity of Antarctic positioning mentioned in Chapter 3, there are more observations with lower elevation angles in this region, and observations with lower elevation angles are more significantly influenced by the tropospheric delay. Thus the error effects of the tropospheric delay contained in the observations increase greatly and are used in the computation and lead to a degrading of the precision in U component. (3) Compared to single GLONASS or single BDS PPP, the positioning precision is improved significantly by GPS/GLONASS/BDS combination. However, the single GPS PPP solutions are still superior to combined PPP. That is because the combination of GPS, GLONASS and BDS systems are based on the equal weight ratio in this case. The contribution of each system to the combination is deemed to be identical, thus the precision of the combination results are influenced and degraded by GLONASS and BDS, which is inferior to single GPS but better than single GLONASS or BDS. (4) Based on the analysis, in combined PPP it is necessary to take into account a specific weight ratio rather than an identical one of each system, which could make the contribution of each system to the combined result more reasonable and improve the precision of combination. The related work has been done and will be described in Sect. 6.4 and Sect. 6.5.

2. Kinematic combined PPP

In case of kinematic combined PPP, the high-rate GPS/GLONASS/BDS observations of MGEX station GMSD on GPS day 334 in 2014 were used to validate the algorithm and make the analysis. The sample interval of the data is 1 s and the observed period is 8 hours. The difference between static and kinematic combined PPP is that the coordinate parameters can

not be directly inherited between epochs but should be reinitialized at each epoch. The observation models and details of kinematic PPP processing are similar to the static case which is referred to in Table 5.1.

Like in the static case, four schemes were conducted to make comparison and analysis possible.

Scheme 1: GPS single system kinematic PPP positioning (denoted as GPS in Fig. 5.8 and Table 5.3).

Scheme 2: GLONASS single system kinematic PPP positioning (denoted as GLONASS in Fig. 5.8 and Table 5.3).

Scheme 3: BDS single system kinematic PPP positioning (denoted as BDS in Fig. 5.8 and Table 5.3).

Scheme 4: GPS/GLONASS/BDS kinematic combined PPP algorithm based on the equivalence principle (denoted as G+R+C in Fig. 5.8 and Table 5.3).

To make a comparison, the position coordinates published by IGS were treated as standard values to compute the bias and RMS of the position results of the four schemes in N, E and U components. The bias of all four schemes with respect to IGS published results in N, E and U components is shown in Fig. 5.8. The RMS results are given in Table 5.3.

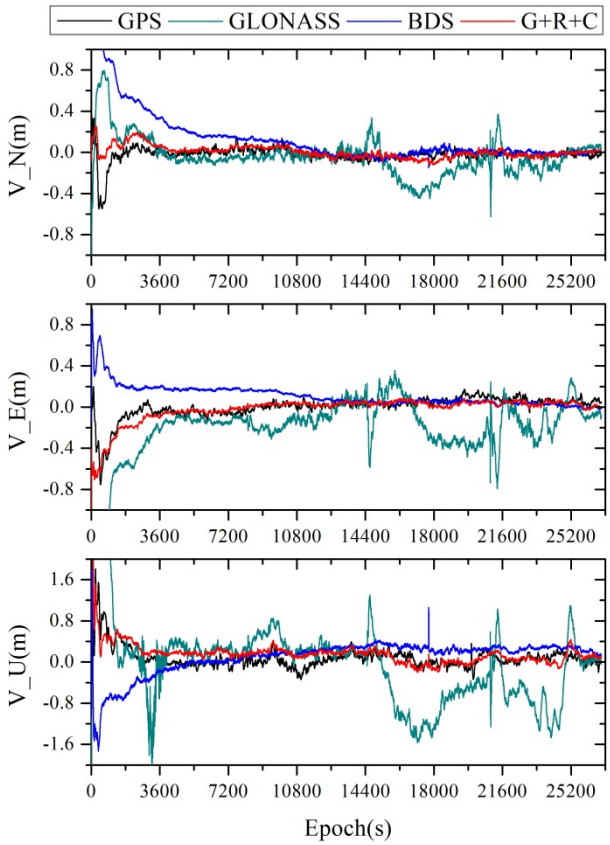

Fig. 5.8. Bias of four schemes with respect to IGS published results

Table 5.3 RMS with respect to IGS results (units: m)

RMS	GPS	GLONASS	BDS	G+R+C
N	0.042	0.150	0.102	0.041
E	0.059	0.206	0.103	0.041
U	0.112	0.615	0.229	0.157

From Fig. 5.8 and Table 5.3 it can be found that: (1) Similar to the static positioning, the precision of single GPS solutions is also superior to single GLONASS and single BDS solutions. (2) Compared to the single system positioning, the horizontal precision of kinematic PPP is improved by GPS/GLONASS/BDS combination, which is superior to any single system PPP. However, the height precision of combined PPP is still inferior to single GPS kinematic PPP. It is inferred to be influenced and degraded by GLONASS and BDS, especially GLONASS solutions with obvious fluctuation in this case. The results indicate that combined multi-systems PPP has the dominant advantage of improving the horizontal precision of kinematic positioning. (3) From Table 5.2 and Table 5.3, it can be found that generally in Asia-Pacific area the positioning accuracy of a single BDS system is in between single GPS and single GLONASS, which is worse than single GPS but better than single

GLONASS.

5.4 Fast BDS Ambiguity Determination Based on the Contribution of GPS Observations

5.4.1 Introduction

As mentioned in Sect. 5.1, with the rapid development of GNSS, PPP technique is advancing forward from mainly using GPS measurements towards multi-GNSS combinations, with newly available precise orbit and clock data for GNSS satellites. The Chinese BeiDou navigation satellite system (BDS) is steadily advancing forward towards being an operational global navigation satellite system, which is planned to be completed by 2020. And at present, the Multi-GNSS Experiment (MGEX) network which tracks multi-GNSS constellations and conducts tracking data analysis has basically achieved global distribution. However, since BDS system is under construction, four or more satellites are still not available at the same time in a plurality of regions (He et al., 2013; Zhang et al., 2015). In this case, the additional GPS observations can be applied to augment BDS for reducing the convergence time and improving positioning accuracy, reliability and availability compared to single BDS PPP. On this basis, similar to BDS/GPS combined PPP, a method which can speed up the determination of the ambiguities parameters of BDS through applying the contribution of GPS observations is proposed and analyzed in this section. In this method, the coordinates computed formerly by GPS observations are used as a priori information in the computation of BDS PPP, which improves the convergent speed eventually.

5.4.2 Methodology

The complete solution of the PPP algorithm based on the equivalence principle is derived and described in Sect. 5.3, where X_1 denotes the receiver clock offset parameter and X_2 denotes the coordinates, tropospheric delay and ambiguities parameters in Eq. (5.17). On this basis, the coordinates computed formerly by GPS observations are used as a priori information in the BDS PPP computation. Referring to the a priori constrained PPP algorithm derived in Sect. 4.2.1, the a priori constraint from GPS observations can be represented as

$$0 = CX_2 - W, \quad P_2 \tag{5.28}$$

where C is the coefficient matrix; X_2 has the same meaning as in Eq. (5.17); W is the constant vector; P_2 is the a priori weight matrix.

Thus the new normal equation coefficients with respect to parameter X_2 for Eq. (5.17) can be formed as

$$M_2' = M_2 + C^T P_2 C \tag{5.29}$$

$$R_2' = R_2 + C^T P_2 W \tag{5.30}$$

Substituting Eq. (5.29) and Eq. (5.30) into Eq. (5.17), the new PPP solution with a priori constrain is obtained. In case of applying the coordinates result from GPS observations, the coefficient matrix C and constant vector W in Eq. (5.28) can be referred to Eq. (4.24) and Eq. (4.25) in Sect. 4.3.1, that C=I is a three-dimensional identity matrix, $W = \begin{pmatrix} x_0 & y_0 & z_0 \end{pmatrix}^T$ is the known three-dimensional coordinates with the variance of $P_2^{-1} = \begin{pmatrix} \sigma_{x_0}^2 & & \\ & \sigma_{y_0}^2 & \\ & & \sigma_{z_0}^2 \end{pmatrix}$ obtained from the processing of GPS observations.

Therefore the contribution of GPS observations to the BDS PPP solution can be analyzed as follows.

According to Eq. (5.17), the PPP solution except receiver clock offset of a single BDS system can be expressed as

$$X_2 = (\tilde{M}_2)^{-1} \tilde{R}_2 \tag{5.31}$$

$$Q_{X_2} = (\tilde{M}_2)^{-1} \tag{5.32}$$

where X_2 includes the coordinates, tropospheric delay, and ambiguities parameters; Q_{X_2} denotes the coefficient matrix of X_2.

In accordance with Eq. (5.29) and Eq. (5.30), the new BDS PPP solution based on the GPS observations can be expressed as

$$X_2' = \left(\tilde{M}_2 + C^T P_2 C\right)^{-1}\left(\tilde{R}_2 + C^T P_2 W\right) \tag{5.33}$$

$$Q_{X_2}' = \left(\tilde{M}_2 + C^T P_2 C\right)^{-1} \tag{5.34}$$

Therefore, contribution of the GPS observations to the coordinates, tropospheric delay and ambiguities parameters in BDS computation can be expressed as

$$dX_2 = X_2' - X_2 = \left(\tilde{M}_2 + C^T P_2 C\right)^{-1}\left(\tilde{R}_2 + C^T P_2 W\right) - (\tilde{M}_2)^{-1}\tilde{R}_2 \tag{5.35}$$

To assess the precision of the estimated parameter, the covariance matrix of the parameter can be formed as

$$\sum_{X_2} = Q_{X_2}\sigma^2 \tag{5.36}$$

$$\sum_{X_2}' = Q_{X_2}'\sigma^2 \tag{5.37}$$

where σ denotes the standard deviation and can be computed by

$$\sigma = \sqrt{\frac{V^T PV}{n-m}} \tag{5.38}$$

where n is the number of BDS observations, m is the number of coordinates, tropospheric delay and ambiguity parameters of BDS.

Therefore, contribution of the GPS observations to the estimation precision of coordinates, tropospheric delay and ambiguities parameters in BDS PPP computation can be expressed as

$$\Delta\sum_{X_2} = \sum_{X_2} - \sum_{X_2}' \tag{5.39}$$

Thus, through using the coordinates computed formerly by GPS observations as a priori information in the BDS PPP, it can be expected that convergent speed and positioning precision will be improved. The convergence time of BDS computation is reduced if there is a priori information provided by GPS or other sensors and can be applied in the beginning of the computation. In practical, such algorithm is especially useful in applications of tracking particular vehicles and carriers under severe environment. For instance, in the canyon where there are less or lack of visible GPS satellites, while BDS satellites are observed due to its special constellation constitution (e.g. GEO satellites), in this case such as for weaponry launching, the GPS observations before launching (in static condition) can be used to speed

up the convergence time in the beginning, then the equipment can rely on itself by using BDS observations after launching and break away from its base platform.

5.4.3 Example and Analysis

The GPS/BDS observations of IGS station GMSD on GPS day 281 in 2014 were used to validate the method derived in Sect. 5.4.2. The sample interval of the data is 30 s. The observation models and details of PPP processing are indicated in Table 5.1. Two computation schemes were conducted to make comparison and analysis possible.

Scheme 1: BDS single system kinematic PPP.

Scheme 2: BDS fast positioning based on GPS observations (cf. Sect. 5.4.2).

To compare convergence conditions in the two schemes, the ionosphere-free ambiguities of satellites C04, C09 and C11 are shown in Fig. 5.9 - Fig. 5.11, respectively, where C04 is GEO satellite, C09 is IGSO satellite, C11 is MEO satellite of BDS system. Furthermore, to make a comparison, the position coordinates published by IGS were treated as standard values to compute the bias of the position results of the two schemes in N, E and U components. The bias and RMS of two schemes with respect to IGS published results are shown in Fig. 5.12 and Table 5.4.

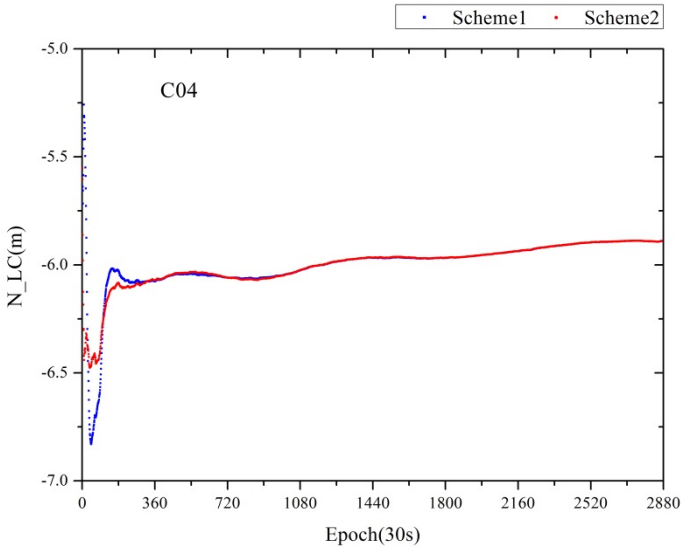

Fig. 5.9. Ionosphere-free ambiguity of satellite C04

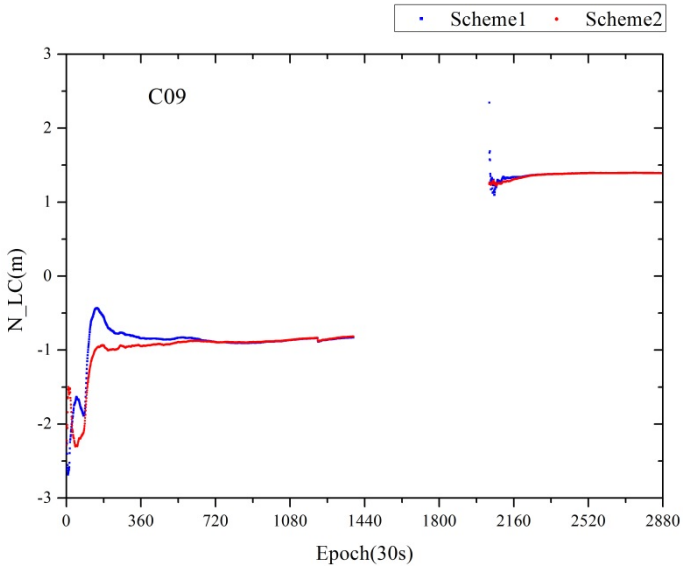

Fig. 5.10. Ionosphere-free ambiguity of satellite C09

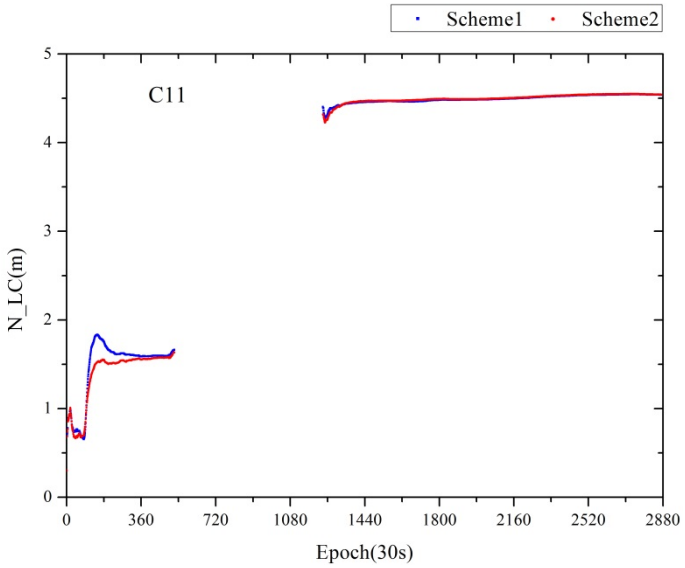

Fig. 5.11. Ionosphere-free ambiguity of satellite C11

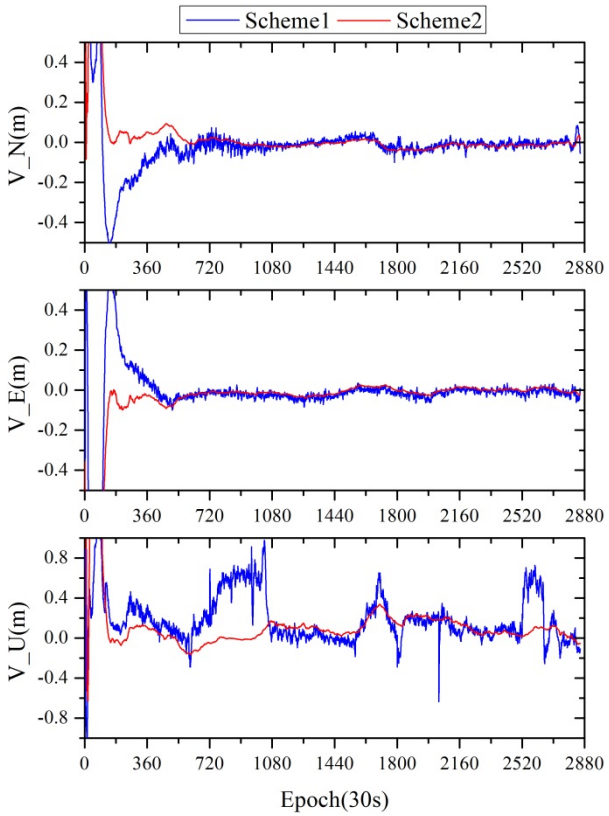

Fig. 5.12. Bias with respect to IGS published results

Table 5.4 RMS comparison of two schemes (units: cm)

RMS	N	E	U
Scheme 1	2.1	2.1	25.9
Scheme 2	1.8	1.9	12.8

From Fig. 5.9 - Fig. 5.12 and Table 5.4 it can be found that, ionosphere-free ambiguities of BDS satellites can be determined and converged to stable more quickly because of the contribution of GPS observations; the convergence time of Scheme 2 is greatly reduced compared to Scheme 1. Based on GPS observation, coordinates parameters can be obtained in advance and used as a priori information for the computation of BDS observation. Thus it shows significant superiority in convergent speed of computation. The positioning accuracy in N, E and U components are improved by 14%, 10% and 50%, respectively. It is useful for BDS computation if there is a priori information provided by GPS or other sensors and can be applied in the beginning of the computation.

5.5 GPS/BDS Combined PPP Algorithm with Inter-system Bias Parameter

5.5.1 Methodology

The Chinese BeiDou navigation satellite system (BDS) is providing coverage of the Asia-Pacific area positioning and navigation service since December 2012. With the combination of BDS, the GNSS PPP can improve its positioning precision, availability, and reliability. However, in order to achieve the best positioning solutions, the inter-system bias (ISB) between GPS and BDS should be resolved as precisely as possible (Jiang et al., 2016). In this section, a GPS/BDS combined PPP algorithm with inter-system bias parameter is derived.

Similar as described in Sect. 4.2, the ionosphere-free code and phase observation equations for GPS and BDS combination can be expressed as

$$P_{IF}^{G} = \rho^{G} + c \cdot dt^{G} + d_{trop}^{G} + dm_{IF}^{G} + \varepsilon_{P_{IF}}^{G} \tag{5.40}$$

$$\Phi_{IF}^{G} = \rho^{G} + c \cdot dt^{G} + d_{trop}^{G} + \lambda_{IF}^{G} \cdot N_{IF}^{G} + \delta m_{IF}^{G} + \varepsilon_{\Phi_{IF}}^{G} \tag{5.41}$$

$$P_{IF}^{C} = \rho^{C} + c \cdot dt^{C} + d_{trop}^{C} + dm_{IF}^{C} + \varepsilon_{P_{IF}}^{C} \tag{5.42}$$

$$\Phi_{IF}^{C} = \rho^{C} + c \cdot dt^{C} + d_{trop}^{C} + \lambda_{IF}^{C} \cdot N_{IF}^{C} + \delta m_{IF}^{C} + \varepsilon_{\Phi_{IF}}^{C} \tag{5.43}$$

where indices *G* and *C* represent GPS and BeiDou satellites, respectively. The meanings of the terms are the same as in Eq. (4.1) and Eq. (4.2). Due to the different time systems used by GPS and BDS, the receiver clock offset of GPS dt^{G} and BDS dt^{C} should be estimated separately. Alternatively, it is possible to treat the receiver clock offset of GPS as a reference, thus the receiver clock offset of BDS can be expressed as a form of receiver clock offset of GPS as follows

$$dt^{C} = dt^{G} + t_{sys}^{gc} \tag{5.44}$$

where t_{sys}^{gc} is the time system bias between GPS and BDS, which is the so-called ISB. Thus the unknown parameters to be estimated in GPS/BDS combined PPP include three-dimensional coordinates (x, y, z), the receiver clock offset of GPS dt^{G}, the ISB

parameter between GPS and BDS t_{sys}^{gc}, the tropospheric delay d_{trop}, the ambiguities parameters of GPS satellites N_{IF}^{G}, and the ambiguities parameters of BDS satellites N_{IF}^{C}.

To express the linearized error equation of the observation as

$$V = AX - L \tag{5.45}$$

Therefore the parameter vector X to be estimated can be expressed as

$$X = \left[x, y, z, dt^{G}, t_{sys}^{gc}, d_{trop}, N_{IF}^{G1}, \cdots, N_{IF}^{Gn}, N_{IF}^{C1}, \cdots, N_{IF}^{Cm} \right]^{T} \tag{5.46}$$

where n is the number of GPS satellites, m is the number of BDS satellites.

Therefore, GPS/BDS combined PPP with ISB parameter can be realized through solving Eq. (5.45).

The estimation of the ISB parameter t_{sys}^{gc} can be performed in three different ways: as epoch-wise variable, piece-wise constant, or daily constant. For rigorous data analysis, ISB should be estimated on an epoch-wise basis. However this approach will introduce too many unknown parameters and reduce the efficiency of the solution. Through a detailed analysis of ISB estimation by making double-differences using measurements from various receivers, Paziewski and Wielgosz (2015) have shown that the ISB values estimated as a constant parameter for "longer pieces" show better repeatability than estimating an epoch-varying parameter. Considering current PPP accuracy limits and computing speed, the piece-wise constant ISB model is chosen here as the optimal approach.

Furthermore, the GPS/BDS combined PPP with the ISB constraints is proposed in this section. The ISB value estimated at the day before is used as an a priori constraint for the processing of the next day. The superiority of the a priori ISB constraint in the GPS/BDS combined PPP is validated in the following example.

5.5.2 Example and Analysis

A set of 3 IGS stations (NNOR, REUN and XMIS) from MGEX network during GPS week 1811 were used to validate the GPS/BDS combined PPP with the ISB inter-system bias parameter. The sample interval of the data is 30 s. The observation models and details of PPP

processing are referred to in Table 5.1. The ISB parameter is estimated as an hourly piece-wise constant. Two computation schemes were conducted to make comparison and analysis possible.

Scheme 1: The observation data of GPS week 1811 was processed through GPS/BDS combined PPP with a day by day ISB.

Scheme 2: The observation data of three days was processed through PPP with a priori ISB constraint. The ISB estimated on the day before was used as the a priori value for the next day. In this case, the ISB estimated on GPS day 264 was used as the a priori value for day 265; the ISB estimated on GPS day 265 was used as the a priori value for day 266.

To make a comparison, the position coordinates published by IGS were considered as standard values to compute the bias and RMS of the position results of the two schemes in N, E and U components. The RMS of both schemes with respect to IGS published results on day 265 and 266 are given in Table 5.5. The comparison of the convergence time in N, E and U components using both schemes on day 265 and 266 are analyzed and shown in Fig. 5.13 and Fig. 5.14, respectively. The convergence criterion is defined as the bias of the first moment and its following 20 epochs in N, E and U components are less than 0.1 m.

Table 5.5 RMS comparison of two schemes (units: cm)

Day of Year	Station	Without ISB constraint			With ISB constraint		
		N	E	U	N	E	U
265	NNOR	0.4	1.1	2.6	0.4	1.2	2.5
	REUN	0.5	2.0	0.6	0.6	1.2	0.6
	XMIS	0.3	1.2	3.3	0.3	1.1	3.0
266	NNOR	0.4	1.3	2.1	0.3	1.2	2.1
	REUN	0.7	1.7	1.2	0.7	1.1	1.1
	XMIS	0.3	1.4	2.5	0.3	1.4	2.4
MEAN		0.43	1.45	2.05	0.43	1.20	1.95

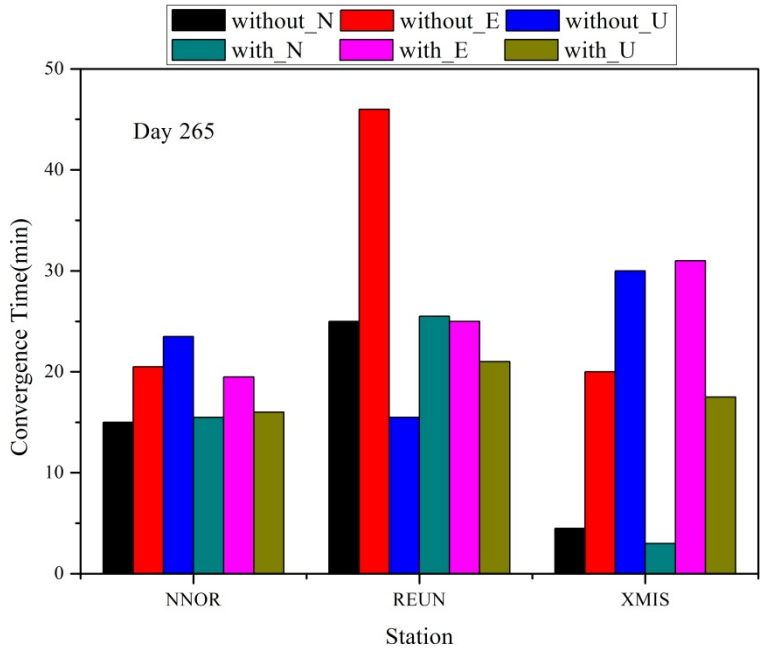

Fig. 5.13. Comparison of the convergence time of two schemes on day 265

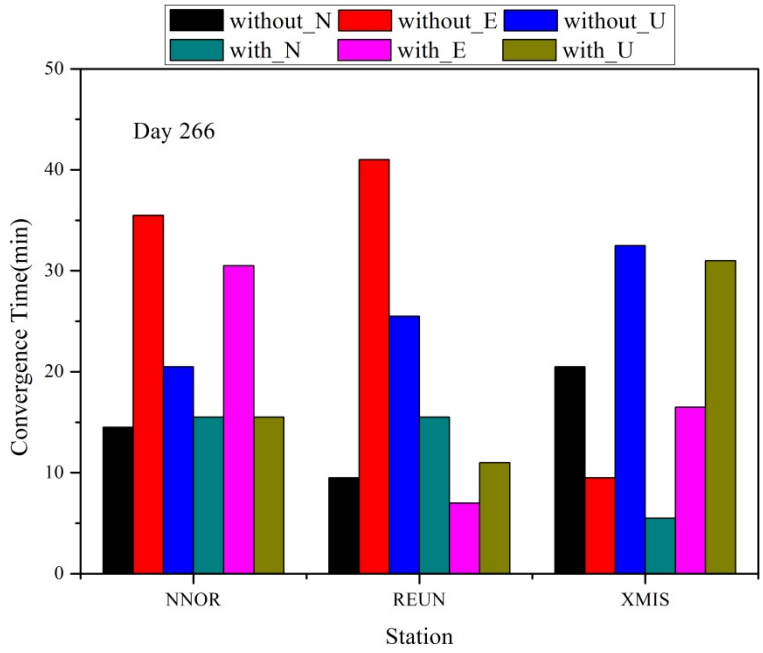

Fig. 5.14. Comparison of the convergence time of two schemes on day 266

From Table 5.5 and Fig. 5.13 - Fig. 5.14 it can be found that: (1) The mean RMS of of PPP processing without a priori ISB constraint are 0.43, 1.45 and 2.05 cm in N, E and U components, respectively. By using the a priori ISB constraint, the mean RMS are 0.43, 1.20 and 1.95 cm in three components, respectively. The average positioning accuracy has an improvement of 17% in E component and 5% in U component while in N component stays nearly the same. (2) The average convergence time of PPP processing without a priori ISB

constraint are 14.8, 28.7 and 24.5 minutes in N, E and U components, respectively. When using ISB as an a priori constraint, mean convergence time in the three components are 13.4, 21.5 and 18.6 minutes, respectively. The convergence speed in N, E and U components are improved by 9%, 25% and 24%, respectively. Thus it can be concluded, that the a priori constraint of ISB is superior in convergence time of PPP processing and can mainly improve the positioning accuracy in E component.

5.6 Conclusions

A multi-constellation combined PPP algorithm based on the equivalence principle was derived in this chapter. Being different from traditional multi-constellation combined PPP, the new algorithm firstly decomposes the entire combined computation into independent computing of each single system. Then the normal equations of the shared parameters of different GNSS systems, which are equivalently eliminated through the normal equation of single system, were directly and simply accumulated to obtain the combined solutions. Numerical examples were conducted to validate the efficiency and accuracy of the algorithm. By using this derived algorithm, the exponentially increased computational load of traditional multi-GNSS PPP algorithm can be reduced to the single linear increase when more GNSS satellites are available and used for combined computation. Results show that the GPS/GLONASS/BDS combination with the identical weight ratio in Sect. 5.3 can improve positioning accuracy compared to single GLONASS and single BDS. However, positioning accuracy in this case is inferior to single GPS. That is because the precision of the combined results is degraded by GLONASS and BDS due to the identical weight ratio of each system. Therefore it was found that it is necessary to consider a specific weight ratio to make the contribution of each system to combined results more reasonable and improve the accuracy of combination. The related work can be referred to in Sect. 6.4 and Sect. 6.5.

A method to speed up the determination of ambiguities parameters of BDS through applying the contribution of GPS observations was proposed and analyzed. The coordinates computed formerly by GPS observations were used as a priori information in the computation of BDS PPP. Thus it was found that the ionosphere-free ambiguities of BDS satellites could be determined and converged to stable more quickly. In addition, the convergence time could

be greatly reduced. It can be said that the method is useful for BDS computation if there is a priori information provided by GPS or other sensors and can be applied in the beginning of the computation.

The GPS/BDS combined PPP algorithm with inter-system bias parameter was also derived in this chapter. Furthermore, using the estimated ISB as a priori constraint in the GPS/BDS combined PPP was proposed. Results of the example demonstrate that the a priori constraint of ISB is superior in convergence time of PPP processing and can mainly improve the positioning accuracy in E component.

6 Adaptively Multi-Constellation Combined Precise Point Positioning Based on the Equivalence Principle

6.1 Introduction

A new adaptively robust filter with application in kinematic navigation and positioning has been systematically established and developed in recent years (Yang et al., 2013). The adaptively robust filter applies a robust estimation principle to resist the effects of measurement outliers and introduces an adaptive factor to control the influence of dynamic model disturbances. It can balance the contribution of the dynamic model information and the measurements in accordance with the magnitudes of their discrepancy (Yang et al., 2001). In this chapter, the principle of the adaptively robust filter, its developments and applications are firstly summarized and introduced. Then the adaptively robust PPP of a single system is derived. Due to the defect of the multi-GNSS combination with equal weight ratio (cf. Sect. 5.3), two kinds of adaptively multi-GNSS combined PPP based on the equivalence principle are derived. With these an adaptive adjustment of the weight ratio of each system in the multi-GNSS combination can easily be achieved. The posteriori covariance matrix of the shared parameters of each single system and the Helmert variance components are used to adaptively adjust the weight ratio of each system in the multi-GNSS combination, respectively. Numerical examples are conducted to validate the derived algorithms.

6.2 Main Progress of the Adaptively Robust Theory in Satellite Navigation and Positioning

6.2.1 Principle of the Adaptively Robust Filter

Supposing the linear dynamic model and observation model are

$$X_i = \Phi_{i,i-1} X_{i-1} + W_i \tag{6.1}$$

$$L_i = A_i X_i + e_i \tag{6.2}$$

where subscript i and i-1 denote epoch time; X_{i-1} and X_i are the state vectors of

dimension m at epoch i-1 and epoch i, respectively; $\Phi_{i,i-1}$ is the state transition matrix of dimension $m \times m$; W_i is the residual vector of dimension m of the system state model with zero expectation and covariance matrix $\sum_{W_i}$; L_i is the observational vector of dimension n_i; A_i is the coefficient matrix of dimension $n_i \times m$; e_i is the error vector of observations with zero expectation and covariance matrix $\sum_i$, here $\sum_i = \sigma_0^2 P_i^{-1}$; P_i denotes the weight matrix of L_i; σ_0^2 is the variance of the unit weight; m is the number of unknown parameters; n_i is the number of observations at epoch i. W_i and e_i are mutually uncorrelated. It is further assumed that V_i is the residual vector of the observation of dimension n_i, $\overline{X}_i$ is the predicted state vector, thus the observation error equation and the state predicted equation are

$$V_i = A_i \hat{X}_i - L_i \tag{6.3}$$

$$\overline{X}_i = \Phi_{i,i-1} \hat{X}_{i-1} \tag{6.4}$$

where $\hat{X}_i$ and $\hat{X}_{i-1}$ denote the estimated state vectors at epoch i and i-1, respectively. The covariance matrix $\sum_{\overline{X}_i}$ of the predicted state vector $\overline{X}_i$ can be obtained by using the covariance propagation law as

$$\sum_{\overline{X}_i} = \Phi_{i,i-1} \sum_{\hat{X}_{i-1}} \Phi_{i,i-1}^T + \sum_{W_i} \tag{6.5}$$

The principle of the adaptively robust filter can be expressed as (Yang, 2006)

$$V_i^T \overline{P}_i V_i + \alpha_i \left(\hat{X}_i - \overline{X}_i \right)^T P_{\overline{X}_i} \left(\hat{X}_i - \overline{X}_i \right) = \min \tag{6.6}$$

where $\overline{P}_i = \overline{\sum}_i^{-1}$ is the robust equivalent weight matrix of L_i; $\alpha_i (0 \le \alpha_i \le 1)$ is the adaptive factor; $P_{\overline{X}_i} = \sum_{\overline{X}_i}^{-1}$ is the weight matrix of the predicted state vector $\overline{X}_i$.

By solving Eq. (6.6) , the estimator of the adaptively robust filter can be obtained as

$$\hat{X}_i = (A_i^T \overline{P}_i A_i + \alpha_i P_{\overline{X}_i})^{-1} (A_i^T \overline{P}_i L_i + \alpha_i P_{\overline{X}_i} \overline{X}_i) \tag{6.7}$$

An alternative expression to Eq. (6.7) is

$$\hat{X}_i = \bar{X}_i + \bar{K}_i(L_i - A_i\bar{X}_i) \tag{6.8}$$

where $\bar{K}_i$ is the gain matrix based on the equivalent weight matrix of observations, that

$$K_i = \frac{1}{\alpha_i}\sum_{\bar{X}_i} A_i^T(\frac{1}{\alpha_i}A_i\sum_{\bar{X}_i}A_i^T + \bar{\sum}_i)^{-1} \tag{6.9}$$

The posteriori covariance matrix of the state vector $\hat{X}_i$ is

$$\sum_{\hat{X}_i} = (I - \bar{K}_i A_i)\sum_{\bar{X}_i}/\alpha_i \tag{6.10}$$

6.2.2 Determination of the Robust Equivalent Weight Matrix and the Adaptive Factor

The equivalent weight matrix $\bar{P}_i$ in Eq. (6.7) can be calculated commonly by the Huber weight function (Huber, 1981) or the IGG (Institute of Geodesy and Geophysics) series functions (Yang, 1994; Yang, 1999; Yang et al., 2002; Zhou, 1989). In case of independent observations, $\bar{P}_i$ is a diagonal matrix with elements $\bar{p}_{i_k}\ (k = 1,2,...,n_i)$. According to the IGG Ⅲ function (Yang et al., 2002), $\bar{p}_{i_k}$ can be defined as

$$\bar{p}_{i_k} = \begin{cases} p_{i_k} & |\tilde{V}_k| \le k_0 \\ p_{i_k}\dfrac{k_0}{|\tilde{V}_k|}\left(\dfrac{k_1 - |\tilde{V}_k|}{k_1 - k_0}\right)^2 & k_0 < |\tilde{V}_k| \le k_1 \\ 0 & |\tilde{V}_k| > k_1 \end{cases} \tag{6.11}$$

where V_k is the residual of the observation L_{i_k}; $\tilde{V}_k$ is the standard residual corresponding to V_k; k_0 and k_1 are two constants which are usually chosen as $k_0 = 1.0 \sim 1.5$ and $k_1 = 2.5 \sim 8.0$. $\bar{p}_{i_k}$ is a descending function with respect to the standard residual $\tilde{V}_k$, therefore the outlier in observation L_{i_k} can be controlled. Other equivalent weight functions can be chosen or constructed according to particular situations. The dependent equivalent weight matrix was also researched by Yang (1994) in case of dependent observations.

An appropriate adaptive factor should be sensitive to disturbances of predicted parameters or dynamic model errors. Several statistics of error judgement, i.e. the discrepancy between

the predicted and estimated state vector (Yang et al., 2001), the predicted residual (Xu and Yang, 2000; Yang and Gao, 2006b), the ratio of the Helmert variance components of the predicted state vector and observations (Yang and Xu, 2003), and the discrepancy between predicted and estimated velocities of the dynamic model (Cui and Yang, 2006) can be used to construct the adaptive factor. For instance, based on the statistics of discrepancy between predicted and estimated state vector, a three-segment function, similar to the IGG Ⅲ function, is presented for adaptation as defined below.

$$\alpha_i = \begin{cases} 1 & \Delta\tilde{X}_i \le c_0 \\ \dfrac{c_0}{\Delta\tilde{X}_i}\left(\dfrac{c_1 - \Delta\tilde{X}_i}{c_1 - c_0}\right)^2 & c_0 < \Delta\tilde{X}_i \le c_1 \\ 0 & \Delta\tilde{X}_i > c_1 \end{cases} \tag{6.12}$$

where c_0 and c_1 are two constants, which are usually chosen as $c_0 = 1.0 \sim 1.5$ and $c_1 = 2.5 \sim 8.0$; $\Delta\tilde{X}_i$ is the discrepancy between predicted and estimated state vector, expressed as

$$\Delta\tilde{X}_i = \frac{\left\| \tilde{X}_i - \overline{X}_i \right\|}{\sqrt{\mathrm{tr}\left(\Sigma_{\overline{X}_i}\right)}} \tag{6.13}$$

where $\tilde{X}_i$ is the estimated state vector, $\overline{X}_i$ is the predicted state vector.

6.2.3 Special Estimators

Eq. (6.7) is the general estimator of an adaptively robust filter. With differing adaptive factors α_i and differing equivalent weight matrices $\overline{P}_i$, several kinds of estimators can be formed.

Case 1. If $\alpha_i = 0$ and $\overline{P}_i = P_i$, than

$$\hat{X}_i = (A_i^T P_i A_i)^{-1} A_i^T P_i L_i \tag{6.14}$$

Eq. (6.14) is an LS estimator using only the new observations at epoch *i*. The estimator is suitable when observations are not contaminated by outliers, the updated parameters are biased so much that the $\Delta\tilde{X}_i$ in Eq. (6.12) is larger than c_1, and the information of the updated parameters is completely ignored.

Case 2. If $\alpha_i = 1$ and $\overline{P}_i = P_i$, than

$$\hat{X}_i = (A_i^T P_i A_i + P_{\overline{X}_i})^{-1}(A_i^T P_i L_i + P_{\overline{X}_i}\overline{X}_i) \tag{6.15}$$

Eq. (6.15) is a general estimator of the classic Kalman filter.

Case 3. If α_i varies between 0 and 1, which is determined by Eq. (6.12) and $\overline{P}_i = P_i$, than

$$\hat{X}_i = (A_i^T P_i A_i + \alpha_i P_{\overline{X}_i})^{-1}(A_i^T P_i L_i + \alpha_i P_{\overline{X}_i}\overline{X}_i) \tag{6.16}$$

Eq. (6.16) is an adaptive LS estimator of the Kalman filter. It balances the contributions of the updated parameters and the observations.

Case 4. If $\alpha_i = 0$, than

$$\hat{X}_i = (A_i^T \overline{P}_i A_i)^{-1} A_i^T \overline{P}_i L_i \tag{6.17}$$

Eq. (6.17) is a robust estimator using only the new observations at epoch *i* (Yang, 1994; Yang et al., 2002).

Case 5. If $\alpha_i = 1$, than

$$\hat{X}_i = (A_i^T \overline{P}_i A_i + P_{\overline{X}_i})^{-1}(A_i^T \overline{P}_i L_i + P_{\overline{X}_i}\overline{X}_i) \tag{6.18}$$

Eq. (6.18) is an M-LS filter estimator (Yang, 1997).

Case 6. If the covariance matrices of the observations L_i and the predicted state vector $\overline{X}_i$ are calculated based on the Sage windowing method (Deng, 2003; Yang and Xu, 2003), which are presented as $\hat{\Sigma}_i$ and $\hat{\Sigma}_{\overline{X}_i}$, given by

$$\hat{\Sigma}_i = \frac{1}{m}\sum_{j=0}^{m} \overline{V}_{i-j}\overline{V}_{i-j}^T - A_i \Sigma_{\overline{X}_i} A_i^T \tag{6.19}$$

$$\hat{\Sigma}_{\Delta X} = \frac{1}{m}\sum_{j=0}^{m} \Delta X_{i-j}\Delta X_{i-j}^T \tag{6.20}$$

where *m* is the window width; $\overline{V}_i$ is the predicted residual; ΔX_i denotes the discrepancy between the predicted and estimated state vector, then

$$\overline{V}_i = A_i \overline{X}_i - L_i \tag{6.21}$$

$$\Delta X_i = \hat{X}_i - \overline{X}_i \tag{6.22}$$

In this case the adaptively robust filter turns out to be an adaptive Sage filter.

6.2.4 Development of the Adaptively Robust Filter and Its Applications

After the adaptive filter was developed, the construction of a suitable adaptive factor for balancing the contribution of the measurements and the predicted dynamic model information has been a key problem. Two optimal adaptive factors are established, which satisfy the conditions that the theoretical uncertainty of the predicted state outputted from adaptive filtering equals or nearly equals to its actual estimated uncertainty, or the theoretical uncertainty of the predicted residual vector equals or nearly equals its actual estimated uncertainty (Yang and Gao, 2006a). Furthermore, an adaptively robust filter with classified adaptive factors (Cui and Yang, 2006) is developed, which is more effective in tracking disturbances of vehicle movements. An adaptively robust filter with multi-adaptive factors (Yang and Cui, 2008) is also set up, which is more general in theory and contains adaptively robust filters with a single adaptive factor and classified adaptive factors.

To control influences of measurement outliers and disturbances of the dynamic model, an adaptively robust filter based on the current statistical model (Gao et al., 2006b) is developed. In addition, an adaptively robust filter based on neural network (Gao et al., 2007a; Gao et al., 2007b) is studied to solve the construction of the dynamic model. An adaptively robust filter can also be integrated with error detection, identification and adaptation (DIA). To control the nonlinear disturbances of the dynamic model, an adaptive UKF (unscented Kalman Filter) algorithm for improving the generalization of neural network (Gao et al., 2008) and an adaptively robust filter based on the Bancroft algorithm (Zhang et al., 2007) are derived.

In terms of application, the adaptively robust filter has been successfully applied to the satellite orbit determination (Yang and Wen, 2004) and data processing of repeated observations of geodetic networks (Sui et al., 2007). Moreover, an adaptively robust filter with constraints has also been studied for navigation applications (Yang et al., 2011). In the integrated navigation application an adaptive Kalman filtering algorithm for the IMU/GPS

integrated navigation system (Gao et al., 2006a) and a two-step adaptively robust Kalman filtering algorithm for GPS/INS integrated navigation system (Wu and Yang, 2010) are developed. The comparison of several adaptive filtering algorithms in controlling the influence of colored noises is analyzed in order to simultaneously control the influence of colored noises and dynamic model disturbances (Cui et al., 2006). In research of the estimation and prediction of the satellite clock offset an adaptively robust sequential adjustment with opening window classified adaptive factors (Huang et al., 2011) and an adaptively robust Kalman filter with classified adaptive factors for real-time estimation of satellite clock offset (Huang and Zhang, 2012) are derived. Adaptive filtering is also applied to make progress on the estimation of the crustal deformation parameter by using geophysical models and geometrical measurements (Yang and Zeng, 2009).

6.3 Adaptively Robust PPP of A Single System Based on the Equivalence Principle

The PPP of a single system based on the parameter equivalent elimination principle can be briefly summarized as follows (cf. Sect. 5.3).

The linearized error equation can be formed as

$$V = \begin{pmatrix} A & B \end{pmatrix} \begin{pmatrix} \hat{X}_1 \\ \hat{X}_2 \end{pmatrix} - L, \qquad P \tag{6.23}$$

where the meanings of the characters can be referred to in Sect.5.3.1.

The normal equation can be formed as

$$\begin{pmatrix} M_{11} & M_{12} \\ M_{21} & M_{22} \end{pmatrix} \begin{pmatrix} \hat{X}_1 \\ \hat{X}_2 \end{pmatrix} = \begin{pmatrix} B_1 \\ B_2 \end{pmatrix} \tag{6.24}$$

where $M_{11} = A^T PA$, $M_{12} = A^T PB$, $M_{21} = B^T PA$, $M_{22} = B^T PB$, $B_1 = A^T PL$, $B_2 = B^T PL$.

Then the equivalently eliminated equation of Eq. (6.24) can be formed as

$$\begin{pmatrix} M_{11} & M_{12} \\ 0 & M_2 \end{pmatrix} \begin{pmatrix} \hat{X}_1 \\ \hat{X}_2 \end{pmatrix} = \begin{pmatrix} B_1 \\ R_2 \end{pmatrix} \tag{6.25}$$

where $M_2 = M_{22} - M_{21} M_{11}^{-1} M_{12}$, $R_2 = B_2 - M_{21} M_{11}^{-1} B_1$.

Thus one has

$$M_2\hat{X}_2 = R_2 \tag{6.26}$$

$$M_{11}\hat{X}_1 + M_{12}\hat{X}_2 = B_1 \tag{6.27}$$

The recursion formulas of PPP at epoch *i* can be formed as

$$\begin{cases} \tilde{M}_2^i = M_2^i + \tilde{M}_2^{i-1} \\ \tilde{R}_2^i = R_2^i + \tilde{R}_2^{i-1} \\ \hat{X}_2^i = (\tilde{M}_2^i)^{-1}\tilde{R}_2^i \\ \hat{X}_1^i = (M_{11}^i)^{-1}(B_1^i - M_{12}^i\hat{X}_2^i) \\ Q_{X_2^i} = (\tilde{M}_2^i)^{-1} \\ Q_{X_1^i} = \left(M_{11}^i - M_{12}^i(\tilde{M}_{22}^i)^{-1}M_{21}^i\right)^{-1},\ \tilde{M}_{22}^i = \tilde{M}_2^i + M_{21}^i(M_{11}^i)^{-1}M_{12}^i \end{cases} \tag{6.28}$$

Through Eq. (6.28) the sequential solution of a single system PPP based on the parameter equivalent elimination principle can be obtained. For the sake of resisting the effects of observation outliers and controlling the anomalous disturbances of the a priori information, the adaptively robust PPP can be derived as follows.

Referring to the principle of the adaptively robust filter in Sect. 6.2.1, we make $\bar{M}_{11} = A^T\bar{P}A$, $\bar{M}_{12} = A^T\bar{P}B$, $\bar{M}_{21} = B^T\bar{P}A$, $\bar{M}_{22} = B^T\bar{P}B$, $\bar{B}_1 = A^T\bar{P}L$, $\bar{B}_2 = B^T\bar{P}L$, where $\bar{P}$ denotes the robust equivalent weight which can be determined by Eq. (6.11), then one has $\bar{M}_2 = \bar{M}_{22} - \bar{M}_{21}\bar{M}_{11}^{-1}\bar{M}_{12}$, $\bar{R}_2 = \bar{B}_2 - \bar{M}_{21}\bar{M}_{11}^{-1}\bar{B}_1$. An adaptive factor $\alpha_i(0 \le \alpha_i \le 1)$ which can be determined by Eq. (6.12) is introduced to balance the contribution of the a priori information. Therefore the adaptively robust PPP based on the parameter equivalent elimination principle can be formed as

$$\begin{cases} \tilde{M}_2^i = \bar{M}_2^i + \alpha_i\tilde{M}_2^{i-1} \\ \tilde{R}_2^i = \bar{R}_2^i + \alpha_i\tilde{R}_2^{i-1} \\ \hat{X}_2^i = (\tilde{M}_2^i)^{-1}\tilde{R}_2^i \\ \hat{X}_1^i = (\bar{M}_{11}^i)^{-1}(\bar{B}_1^i - \bar{M}_{12}^i\hat{X}_2^i) \\ Q_{X_2^i} = (\tilde{M}_2^i)^{-1} \\ Q_{X_1^i} = \left(\bar{M}_{11}^i - \bar{M}_{12}^i(\tilde{M}_{22}^i)^{-1}\bar{M}_{21}^i\right)^{-1},\ \tilde{M}_{22}^i = \tilde{M}_2^i + \bar{M}_{21}^i(\bar{M}_{11}^i)^{-1}\bar{M}_{12}^i \end{cases} \tag{6.29}$$

where

$$\alpha_i = \begin{cases} 1 & \Delta\tilde{X}_i \le c_0 \\ \dfrac{c_0}{\Delta\tilde{X}_i}\left(\dfrac{c_1 - \Delta\tilde{X}_i}{c_1 - c_0}\right)^2 & c_0 < \Delta\tilde{X}_i \le c_1 \\ 0 & \Delta\tilde{X}_i > c_1 \end{cases} \tag{6.30}$$

$$\Delta\tilde{X}_i = \frac{\left\| \tilde{X}_i - \hat{X}_{i-1} \right\|}{\sqrt{\mathrm{tr}\left(\sum_{\hat{X}_{i-1}}\right)}} \tag{6.31}$$

where c_0 and c_1 are two constants, which are usually chosen as $c_0 = 1.0 \sim 1.5$ and $c_1 = 2.5 \sim 8.0$; $\Delta\tilde{X}_i$ can be computed through Eq. (6.31); $\tilde{X}_i$ is the estimated vector based on observations at epoch *i*; $\hat{X}_{i-1}$ and $\sum_{\hat{X}_{i-1}}$ are the sequential estimation solution and its covariance matrix at epoch *i*-1, respectively.

6.4 Adaptively Multi-Constellation Combined PPP Based on the Equivalence Principle

6.4.1 Methodology

In multi-constellation combined PPP with identical weight ratio (cf. Sect. 5.3), the results can sometimes be degraded and inferior to results of a single system. Thus it is necessary to consider and construct a more reasonable and specific weight ratio to improve the performance of the combination. In this case, the shared parameters (coordinates and tropospheric delay) and their precision information obtained by every single system can become highly valuable a priori information for combined data processing. Such information can be utilized as a judgement to determine the contribution and weight ratio of each single system to the final combined data processing. Therefore, an extra adaptive factor α_k between different GNSS systems is introduced. It provides the possibility to realize adaptively combined PPP of multi-GNSS systems. On basis of applying the equivalence principle, it is easier and more convenient to achieve such an adaptively combined PPP algorithm, compared to the traditional combined algorithm through constructing total calculation.

The normal equation of the shared parameters in multi-constellation combined PPP is derived and presented as Eq. (5.24). By introducing an adaptive factor for each GNSS system,

the normal equation of adaptively combined PPP of multi-GNSS systems can be formed as

$$\sum_{k=1}^{m} \alpha_k N_1^k Y_1 = \sum_{k=1}^{m} \alpha_k S_1^k \tag{6.32}$$

where α_k denotes the adaptive factor of system *k*. α_k can be determined as an unique adaptive factor or multi adaptive factors in accordance with different parameters (Huang et al., 2011; Huang and Zhang, 2012; Yang and Cui, 2008). For example, an unique adaptive factor can be determined directly by the posteriori covariance matrix $\sum_{\hat{X}_k}$ of the shared parameters obtained by a single system, that

$$\alpha_k = \frac{1}{\sqrt{tr\left(\sum_{\hat{X}_k}\right)}} = \frac{1}{\sqrt{\sigma_{X_k}^2 + \sigma_{Y_k}^2 + \sigma_{Z_k}^2 + \sigma_{ZTD_k}^2}} \tag{6.33}$$

The determination of the adaptive factor of each system as the form of Eq. (6.33) will be used in the examples given in Sect. 6.4.2. Another method to determine the adaptive factor α_k by variance components will be derived in Sect. 6.5.1.

Based on Eq. (6.32) and the multi-GNSS combined PPP solution (cf. Eq. (5.25)), the adaptively combined PPP of multi-GNSS systems based on the parameter equivalent elimination principle can be formed as

$$\begin{cases} \tilde{\tilde{M}}_2^i = \tilde{M}_2^i + \begin{bmatrix} \sum_{k=1,k\neq s}^{m} \alpha_k N_1^k & 0 \\ 0 & 0 \end{bmatrix} \\ \tilde{\tilde{R}}_2^i = \tilde{R}_2^i + \begin{bmatrix} \sum_{k=1,k\neq s}^{m} \alpha_k S_1^k \\ 0 \end{bmatrix} \\ \hat{X}_2^i = (\tilde{\tilde{M}}_2^i)^{-1} \tilde{\tilde{R}}_2^i \\ \hat{X}_1^i = (M_{11}^i)^{-1}(B_1^i - M_{12}^i \hat{X}_2^i) \\ Q_{X_2^i} = (\tilde{\tilde{M}}_2^i)^{-1} \\ Q_{X_1^i} = \left(M_{11}^i - M_{12}^i (\tilde{\tilde{M}}_{22}^i)^{-1} M_{21}^i\right)^{-1}, \ \tilde{\tilde{M}}_{22}^i = \tilde{\tilde{M}}_2^i + M_{21}^i (M_{11}^i)^{-1} M_{12}^i \end{cases} \tag{6.34}$$

where $\tilde{M}_2^i$ and $\tilde{R}_2^i$ are computed by Eq. (5.17).

By using Eqs. (6.32) - (6.34), the contribution of each system to the combined PPP solution can be adjusted adaptively according to the internal precision of each system in itself. In this

way the accuracy of the combined PPP solution will not be affected seriously when there are outliers in any single system, therefore the stability and precision of multi-GNSS combined PPP can be improved.

6.4.2 Example and Analysis

To validate the algorithm derived above (cf. Sect. 6.4.1), the GPS/GLONASS/BDS observations of MGEX stations (CAS1, GMSD, POHN, REUN, TUVA and XMIS) on GPS day 337 in 2014 and high-rate GPS/GLONASS/BDS observations of MGEX station GMSD (with an interval of 1 s) on GPS day 334 in 2014 were used for the case of static and kinematic combined PPP, respectively. The observation models and details of data processing can be referred to in Table 5.1 given in Sect. 5.3.4.

Two schemes were conducted to make comparison and analysis possible.

Scheme 1: GPS/GLONASS/BDS combined PPP with identical weight ratio of each system (cf. Sect. 5.3.4).

Scheme 2: Adaptively GPS/GLONASS/BDS combined PPP with adaptive factor determined by the posteriori covariance of shared parameters of each single system (cf. Eq. (6.33)).

To make a comparison, the position coordinates published by IGS were treated as standard values to compute the bias and RMS of the position results of both schemes in N, E and U components. The RMS results in the static case are given in Table 6.1. The bias and RMS results of station GMSD in the kinematic case are shown in Fig. 6.1 and given in Table 6.2.

Table 6.1 RMS with respect to IGS results (units: m)

Stations		CAS1	GMSD	POHN	REUN	TUVA	XMIS
Scheme1	N	0.021	0.022	0.014	0.004	0.013	0.002
	E	0.018	0.022	0.067	0.027	0.019	0.023
	U	0.257	0.111	0.103	0.066	0.079	0.052
Scheme2	N	0.008	0.006	0.007	0.002	0.005	0.003
	E	0.007	0.010	0.039	0.020	0.019	0.013
	U	0.184	0.035	0.029	0.006	0.029	0.058

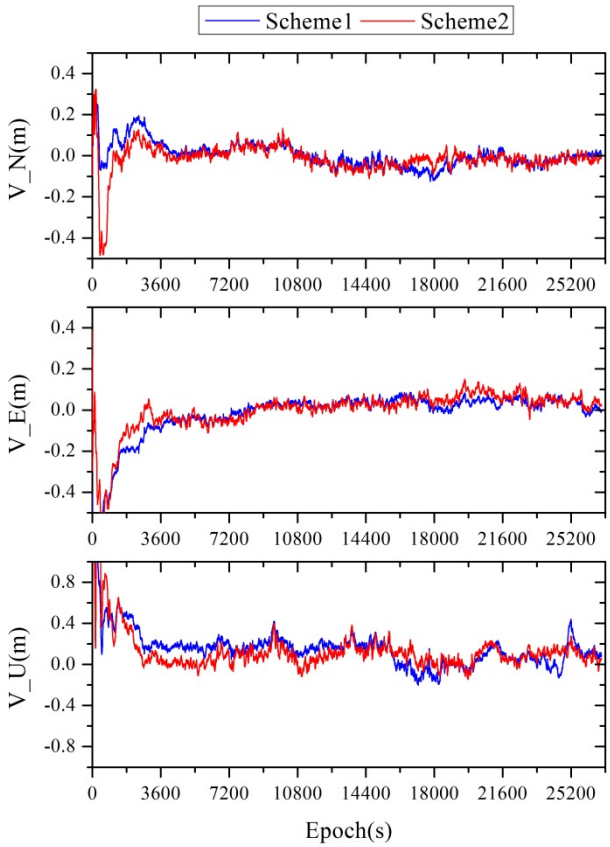

Fig. 6.1. Bias of two schemes with respect to IGS published results

Table 6.2 RMS with respect to IGS results (units: m)

Station		Scheme1	Scheme2
GMSD	N	0.041	0.039
	E	0.041	0.041
	U	0.157	0.114

From Fig. 6.1 and Table 6.1-6.2 it can be found that, compared to Scheme 1, Scheme 2 improves the precision in N, E and U components significantly. In the given example, by applying the adaptive factor determined by the posteriori covariance of the shared parameters of each system in the combined PPP, the precision in U component for stations CAS1, GMSD, POHN, REUN and TUVA in the static case improved by 28%, 68%, 72%, 91% and 63%, respectively; while in the kinematic case the precision in U component for station GMSD improved by 27% in this example. It can be concluded that the adaptive factor determined by covariance of each system (cf. Eq. (6.33)) is superior regarding the accuracy of the multi-constellation combined PPP, compared to using equal weight ratio combination directly (Scheme 1, cf. Sect. 5.3.4).

6.5 Adaptively Combined PPP Based on the Variance Component Estimation

6.5.1 Methodology

As described in Sect. 5.3.4, it is necessary to give a specific and reasonable weight ratio for the observations of each system in multi-GNSS combined PPP. The unreasonable weight ratio will cause the least squares solution losing the property of minimum variance and degrade the accuracy of combined positioning. It is known that the values of weight ratio depend on the random noise of the observations, thus to process combined positioning with an a priori constant or an identical weight ratio is obviously irrational. The Helmert variance components estimation (Koch, 2000; Koch and Kusche, 2002) is a widely applied posteriori variance component estimation method, which can adaptively determine the weight ratio of different observations through iteration computation. Therefore, in this section the Helmert variance component estimation is applied to adjust the weight ratio of mixed observations reasonably and to improve the accuracy and reliability of the positioning.

Assuming L_1 and L_2 are two types of independent observations, P_1 and P_2 are their weight matrices, thus the error equations can be formed as

$$\begin{aligned} V_1 &= B_1\hat{X} - L_1, \quad P_1 \\ V_2 &= B_2\hat{X} - L_2, \quad P_2 \end{aligned} \tag{6.35}$$

The initial weights P_1 and P_2 determined by a priori variance may not be appropriate, thus its corresponding unit weight variance σ_{01}^2 and σ_{02}^2 may not be equal, which has

$$\begin{aligned} D(L_1) &= \sigma_{01}^2 P_1^{-1} \\ D(L_2) &= \sigma_{02}^2 P_2^{-1} \end{aligned} \tag{6.36}$$

The normal equation of Eq. (6.35) can be formed as

$$N\hat{X} = W \tag{6.37}$$

where $N = N_1 + N_2 = A_1^T P_1 A_1 + A_2^T P_2 A_2$, $W = W_1 + W_2 = A_1^T P_1 L_1 + A_2^T P_2 L_2$. According to the quadratic expectation formula, the Helmert variance components estimation can be derived as

$$S\hat{\theta} = W_\theta \tag{6.38}$$

where

$$S = \begin{bmatrix} n_1 - 2tr(N^{-1}N_1) + tr(N^{-1}N_1N^{-1}N_1) & tr(N^{-1}N_1N^{-1}N_2) \\ tr(N^{-1}N_1N^{-1}N_2) & n_2 - 2tr(N^{-1}N_2) + tr(N^{-1}N_2N^{-1}N_2) \end{bmatrix} \tag{6.39}$$

$$\hat{\theta} = \begin{bmatrix} \sigma_{01}^2 & \sigma_{02}^2 \end{bmatrix}^T,\ W_\theta = \begin{bmatrix} V_1^T P_1 V_1 & V_2^T P_2 V_2 \end{bmatrix}^T \tag{6.40}$$

Eqs. (6.38) - (6.40) are the Helmert variance components estimation formulas for two types of observations. In case of expanding to *m* types of observations, the coefficient matrix *S* of variance estimation can be formed as

$$S = \begin{bmatrix} n_1 - 2tr(N^{-1}N_1) + tr(N^{-1}N_1N^{-1}N_1) & tr(N^{-1}N_1N^{-1}N_2) & \cdots & tr(N^{-1}N_1N^{-1}N_m) \\ tr(N^{-1}N_1N^{-1}N_2) & n_2 - 2tr(N^{-1}N_2) + tr(N^{-1}N_2N^{-1}N_2) & \cdots & tr(N^{-1}N_2N^{-1}N_m) \\ \vdots & \vdots & \ddots & \vdots \\ tr(N^{-1}N_1N^{-1}N_m) & tr(N^{-1}N_2N^{-1}N_m) & \cdots & n_m - 2tr(N^{-1}N_m) + tr(N^{-1}N_mN^{-1}N_m) \end{bmatrix} \tag{6.41}$$

$$\hat{\theta} = \begin{bmatrix} \sigma_{01}^2 & \sigma_{02}^2 \cdots & \sigma_{0m}^2 \end{bmatrix}^T,\ W_\theta = \begin{bmatrix} V_1^T P_1 V_1 & V_2^T P_2 V_2 \cdots & V_m^T P_m V_m \end{bmatrix}^T \tag{6.42}$$

By using Eq. (6.38), Eq. (6.41) and Eq. (6.42), the variance components for *m* types of observations can be estimated. The procedures of Helmert variance components estimation can be summarized as follows:

1. Determining the corresponding initial weights $P_i (i = 1,2,...,m)$ of various types of independent observations;
2. Computing the respect $V_i^T P_i V_i (i = 1,2,...,m)$ of various kinds of observations after the first adjustment;
3. Estimating the variance components $\sigma_i^2 (i = 1,2,...,m)$ of various kinds of observations by Eq. (6.38), then resetting the weight by $P_i^{(k+1)} = \frac{c}{\hat{\sigma}_i^2} P_i^{(k)} (i = 1,2,...,m)$, where *c* is a constant, which is usually set as one value of $\sigma_i^2 (i = 1,2,...,m)$;
4. Repeating procedures 2 and 3 until $\hat{\sigma}_1^2 = \hat{\sigma}_2^2 = \cdots = \hat{\sigma}_i^2 (i = 1,2,...,m)$.

In the adaptively combined PPP of multi-GNSS systems, the adaptive factor α_k of system

k can be determined by variance components. The Helmert variance components of each system can be computed and used to adaptively adjust the contribution of the observations of each system to the combined PPP.

Considering four kinds of observational vectors from four GNSS systems respectively, their simplified Helmert variance components can be approximately computed by

$$\hat{\sigma}_{0G}^2 = \frac{V_G^T P_G V_G}{n_G} \tag{6.43}$$

$$\hat{\sigma}_{0R}^2 = \frac{V_R^T P_R V_R}{n_R} \tag{6.44}$$

$$\hat{\sigma}_{0E}^2 = \frac{V_E^T P_E V_E}{n_E} \tag{6.45}$$

$$\hat{\sigma}_{0C}^2 = \frac{V_C^T P_C V_C}{n_C} \tag{6.46}$$

where $\hat{\sigma}_{0G}^2$, $\hat{\sigma}_{0R}^2$, $\hat{\sigma}_{0E}^2$ and $\hat{\sigma}_{0C}^2$ are the variance components of GNSS observations; the subscripts G, R, E and C represent GPS, GLONASS, Galileo and BeiDou systems, respectively; n denotes the number of observations of each GNSS system; V and P denotes the residual vector and the weight matrix of each GNSS system.

Therefore, the adaptive factor $\alpha_k(\alpha_R, \alpha_E, \alpha_C)$ of each system can be formed as

$$\alpha_R = \frac{\hat{\sigma}_{0R}^2}{\hat{\sigma}_{0G}^2},\ \alpha_E = \frac{\hat{\sigma}_{0E}^2}{\hat{\sigma}_{0G}^2},\ \alpha_C = \frac{\hat{\sigma}_{0C}^2}{\hat{\sigma}_{0G}^2} \tag{6.47}$$

where α_R, α_E and α_C denote the adaptive factors for GLONASS, Galileo and Beidou systems, respectively. Substituting the adaptive factors into Eq. (6.32) and (6.34), the adaptively combined PPP based on the variance components estimation can be realized.

6.5.2 Example and Analysis

The same high-rate GPS/GLONASS/BDS observations of MGEX station GMSD (with an interval of 1 s) on GPS day 334 in 2014 were used to validate the algorithm derived above (cf. Sect.6.5.1). The observation models and details of data processing can be referred to in Table

5.1 given in Sect. 5.3.4.

The kinematic PPP of each single system was processed. In addition, two schemes of kinematic combined PPP were conducted to make comparison and analysis possible. Therefore the computational schemes can be summarized as follows.

Scheme 1: GPS single system kinematic PPP (denoted as GPS in Table 6.3 and Fig. 6.2).

Scheme 2: GLONASS single system kinematic PPP.

Scheme3: BDS single system kinematic PPP.

Scheme 4: GPS/GLONASS/BDS kinematic combined PPP with identical weight ratio of each system (denoted as G+R+C in Table 6.3 and Fig. 6.2, cf. Sect. 5.3.4).

Scheme 5: GPS/GLONASS/BDS kinematic combined PPP with adaptive factors based on the variance component estimation (denoted as G+R+C_adaptively in Table 6.3 and Fig. 6.2, cf. Sect. 6.5.1).

As before, the position coordinates published by IGS were considered as standard values to compute the bias and RMS of the position results in N, E and U components. The RMS results of kinematic PPP of each single system and two schemes of kinematic combined PPP are given in Table 6.3. The bias of GPS single system kinematic PPP and two schemes of kinematic combined PPP are shown in Fig. 6.2.

Table 6.3 RMS with respect to IGS results (units: m)

RMS	GPS	GLONASS	BDS	G+R+C	G+R+C _adaptively
N	0.042	0.150	0.102	0.041	0.040
E	0.059	0.206	0.103	0.041	0.058
U	0.112	0.615	0.229	0.157	0.104

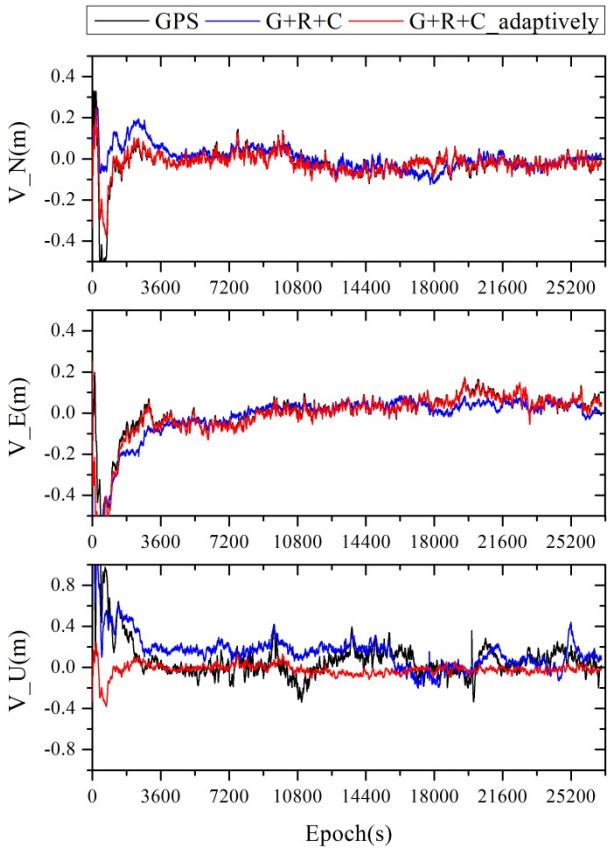

Fig. 6.2. Bias of two schemes with respect to IGS published results

From Table 6.3 and Fig. 6.2 it can be found that: (1) The kinematic combined PPP with adaptive factors based on the variance component estimation (Scheme 5) is significantly superior to other computational schemes and especially improves the precision of U component. In this case, the precision in U component can be improved by 33% compared to using equal weight ratio combination directly (Scheme 4). (2) The precision of the combined PPP based on the equal weight ratio (Scheme 4) is influenced and degraded by GLONASS and BDS, which is inferior to single GPS but better than single GLONASS or BDS. However, the adaptive factors based on the variance component estimation can adjust the weight ratio of combined observations more reasonable to determine the contribution of each system to the combined results. It enlarges the weight ratio of single GPS solution in the combination due to the highest accuracy of GPS, which makes the combination results very close to single GPS solution. Thus in combined PPP the weight ratio of each system should be considered carefully to make the contribution of each system to the combined result more reasonable and improve the precision of combination.

6.6 Conclusions

In this chapter, the principle of the adaptively robust filter, its developing progress and applications were summarized and introduced. Based on the equivalence principle, an adaptively robust PPP algorithm of a single system was derived. Due to the defect of the multi-GNSS combination with identical weight ratio, which leads to results that can sometimes be degraded and inferior to a single system, a more reasonable and specific weight ratio determined by the posteriori covariance matrix of the shared parameters of each single system adaptively was derived to improve the performance of combination. It shows that such an adaptive algorithm can be constructed and realized easily through applying the equivalence principle. Results show that through using such adaptive factors in combination, the precision in U component can be improved by an average of 58% compared to using the identical weight ratio combination directly. In addition, an adaptively combined PPP based on the variance component estimation, was derived. It was shown that it allows an accuracy improvement of 33% in U component compared to using the equal weight combination. Therefore it is concluded that the derived adaptively combined PPP algorithms, which can adjust the weight ratio of each system adaptively, and more reasonably, are significantly superior in the precision of combination.

7 Summary and Future Work

7.1 Summary

To achieve the objective of this thesis, which was to explore high-performance PPP algorithms and to develop GNSS algorithms with application of the equivalence principle, specific research has been done and the main achievements can be summarized as follows.

On the basis of the equivalence principle and the equivalence property of un-differenced and differencing algorithms, the specific equivalence of un-differenced and time differencing PPP algorithms is proved theoretically in this thesis for the first time. Meanwhile, as a supplement to the equivalence property of the triple differences, an alternative method is proposed and derived to prove the equivalence between triple differences and zero-difference which up to now was missing. The main idea of such a method is to regard triple differences as to firstly make time differencing of the same satellite between two adjacent epochs at one station and then to be formed by double differences.

As a consequence of above conducted theoretical study, a time differencing PPP algorithm based on the equivalence principle was derived and can be used to obtain the coordinates difference and average velocity between two adjacent epochs. Such a time differencing PPP algorithm is able to provide both position and velocity results from the phase and code observations. The obtained coordinates difference and velocity can keep stable from the beginning of computation, which is superior to making position difference of PPP because that always needs convergence time. Thus the results can be useful in different types of applications, such as airborne gravimetry, earthquake monitoring. Such a time differencing PPP algorithm could also be an efficient method to detect cycle slips in data processing.

The influence of tropospheric delay on PPP, especially in the context of observations in the polar region or with low elevation cut-off angles, where the position results of the observations are more significantly affected by tropospheric delay, was analyzed and a methodology for minimizing its effect is proposed. Due to the specificity of Antarctic

positioning, the actual meteorological data were used and proved to be beneficial for improving PPP precision in the Antarctic region. When the elevation cut-off angle is lower, the effect of the actual meteorological observations on the positioning precision is more significant in Antarctic due to the retention of low elevation angle observations. The effect of the tropospheric horizontal gradient correction on PPP was also analyzed and verified to remarkably improve PPP precision under lower elevation cut-off angles and higher humidity conditions.

A priori constrained PPP algorithms were proposed and derived in this thesis to improve the efficiency and precision of PPP. The a priori information concerning the geometric and physical properties of observations, which is known with a certain a priori precision, was applied in the PPP algorithms. The contribution of different a priori information constraints on different parameters to PPP solution was analyzed and validated. The a priori constraints as employed in the PPP were specified according to coordinates-, receiver clock offset-, tropospheric delay- and ambiguities-constraints, respectively. The validation of the derived PPP algorithms shows a significant improvement concerning convergence time and positioning accuracy. And moreover, the applications of different constraints under specific conditions were also discussed and validated. PPP with a priori coordinates accuracy and time period constraint is particularly beneficial to the convergence time and accuracy of the real-time slow-motion carriers positioning, such as landslide, urban land subsidence and structural monitoring. That is because it fully accounts for characteristics of slow-motion carriers. As deformation during geological disasters is generally continuous and in slow-motion, the monitoring station can be considered as stationary and the coordinates between epochs can be inherited like static positioning during a certain period. PPP with receiver clock offset constraint helps to solve the day-boundary discontinuities which are un-neglectable in precise timing and time transfer service. With coordinates and clock offset constraint, the results achieve convergent more quickly and more stable and continuous clock offset series can be obtained. PPP with tropospheric delay constraint removes the effect of the tropospheric delay on PPP height solution to improve the positioning accuracy in height component. PPP with ambiguities constraint is greatly superior in reducing the convergence

time of positioning.

A multi-constellation combined PPP algorithm based on the equivalence principle was proposed and derived in this thesis. Being different from traditional multi-GNSS combined PPP, the new algorithm firstly decomposes the entire combined computation into independent computing of each single system. Then the normal equations of the shared parameters of different GNSS systems, which are equivalently eliminated through the normal equation of single system, are directly and simply accumulated to obtain the combined solutions. With such an algorithm, the exponentially increased computational load of traditional multi-GNSS PPP algorithm can be reduced to the single linear increase when more GNSS satellites are available and used for combined computation.

A method to speed up the determination of the ambiguities parameters of BDS through applying the contribution of GPS observations was proposed. The coordinates computed formerly by GPS observations were used as a priori information in the computation of BDS PPP. Thus it was found that the ionosphere-free ambiguities of BDS satellites can be determined and converged to stable more quickly. In addition, the convergence time is greatly reduced. It can be said the method is useful for BDS computation if there is a priori information provided by GPS or other sensors and can be applied in the beginning of the computation.

The GPS/BDS combined PPP algorithm with inter-system bias parameter was derived. Furthermore, using the estimated ISB as a priori constraint in the GPS/BDS combined PPP was proposed. Results demonstrate that the a priori constraint of ISB is superior in convergence time of PPP processing and can mainly improve the positioning accuracy in E component.

In traditional multi-constellation combined PPP, it is difficult to adaptively adjust the contribution of each single system to the combination through constructing total calculation, which will lead to the deterioration in the combination accuracy. In this context, the adaptively combined PPP algorithms based on the equivalence principle were proposed and derived, which can easily achieve an adaptive adjustment of the weight ratio of each system in multi-GNSS combination. By using the posteriori covariance matrix of the shared

parameters of each single system and the Helmert variance components to adaptively adjust the weight ratio of each system, the derived algorithms can improve the accuracy of combination significantly, compared to combined PPP with identical weight ratio.

The developed algorithms are net applicable and can be used for cloud computation for internet GNSS service which is considered significant for commercial applications.

7.2 Future Work

In accordance with the research progress and achievements of this thesis, several main points and ideas for subsequent studies are considered and proposed as recommendations, which can be summarized as follows.

Due to the characteristics of Antarctic positioning, where there are much more lower elevation angle observations compared to mid-low latitude regions, a more accurate and reliable tropospheric model for the Antarctic area is essential to be explored and conducted in the future. An alternative idea is to make full use of a mass of real meteorological data to modelling or to apply such meteorological observations as a prior constraint in data processing.

The a priori constrained PPP algorithms derived in this thesis are specified according to coordinates-, receiver clock offset-, tropospheric delay- and ambiguities-constraint. The cases of other constraints, such as ionospheric delay-, baseline length-, as well as the combination of several constraints should be studied further.

With the rapid development of multiple GNSS systems, the developing features of GNSS precise positioning have changed from single GPS-only positioning over the past decades to multi-GNSS systems combined positioning nowadays. The study on PPP ambiguity resolution of multi-GNSS combination needs to be researched further. Moreover, the analysis, especially in case of BDS PPP will also have great significance in the future.

References

Berg, H., 1948. Allgemeine Meteorologie. Ferdinand Duemmler Verlag, Bohn.

Bertiger, W., Desai, S.D., Haines, B., Harvey, N., Moore, A.W., Owen, S. and Weiss, J.P., 2010. Single receiver phase ambiguity resolution with GPS data. Journal of Geodesy, 84(5): 327-337.

Bisnath, S. and Gao, Y., 2009. Current state of precise point positioning and future prospects and limitations, Observing our Changing Earth. International Association of Geodesy Symposia. Springer Berlin Heidelberg, Berlin, pp. 615-623.

Bisnath, S. and Langley, R., 2002. High-precision platform-independent positioning with a single GPS receiver. Navigation, 29(3): 161-169.

Bisnath, S., Wells, D. and Dodd, D., 2003. Evaluation of commercial carrier phase-based WADGPS services for marine applications, ION GPS/GNSS, Portland, Oregon, pp. 17-27.

Boehm, J., Heinkelmann, R. and Schuh, H., 2007. Short Note: A global model of pressure and temperature for geodetic applications. Journal of Geodesy, 81(10): 679-683.

Boehm, J., Niell, A., Tregoning, P. and Schuh, H., 2006a. Global Mapping Function (GMF): A new empirical mapping function based on numerical weather model data. Geophysical Research Letters, 33(7): L07304.

Boehm, J., Werl, B. and Schuh, H., 2006b. Troposphere mapping functions for GPS and very long baseline interferometry from European Centre for Medium-Range Weather Forecasts operational analysis data. Journal of Geophysical Research, 111: B02406.

Brown, R. and Hwang, P., 1992. Introduction to random signals and applied kalman filtering. John Wiley and Sons, Inc. New York.

Brunner, F. and Welsch, W., 1993. Effect of the troposphere on GPS Measurements. GPS World, 4(1): 42-51.

Byun, S.H. and Bar-Sever, Y.E., 2009. A new type of troposphere zenith path delay product of the international GNSS service. Journal of Geodesy, 83(3-4): 1-7.

Cai, C. and Gao, Y., 2013. Modeling and assessment of combined GPS/GLONASS precise point positioning. GPS Solutions, 17(2): 223-236.

Caissy, M., Agrotis, L., Weber, G., Hernandez-Pajares, M. and Hugentobler, U., 2012. The International GNSS Real-time Service. GPS World.

Cao, W., Guo, J., Xie, X., Zhou, M. and Jia, X., 2014. Influence of horizontal gradients on precise point positioning. Bulletin of Surveying and Mapping, 2: 13-15.

Cerretto, G., Lahaye, F., Tavella, P. and Vitrano, S., 2010. Precise Point Positioning: implementation of the constrained clock model and analysis of its effects in T/F transfer, EFTF-2010 24th European Frequency and Time Forum. IEEE, Noordwi jk, pp. 1-5.

Chen, G. and Herring, T., 1997. Effects of atmospheric azimuthal asymmetry on the analysis of space geodetic data. Journal of Geophysical Research, 102(B9): 20489.

Chen, J. and Wang, J., 2007. Kinematic precise orbit determination of low earth orbiter based on epoch-difference strategy. Journal of Geodesy and Geodynamics, 27(4): 57-61.

Chen, Y., 2010. Research on Bayes Filtering Algorithm in Kinematic Positioning with Prior Information, Central South University, Changsha, China.

CNAGA, 2014.

Collins, J. and Langley, R., 1997. Estimating the residual tropospheric delay for airborne differential GPS positioning, ION GPS 1997, Kansas City.

Cui, X. and Yang, Y., 2006. Adaptively Robust Filtering with Classified Adaptive Factors. Progress in Natural Science, 16(8): 846-851.

Cui, X., Yang, Y. and Gao, W., 2006. Comparison of Adaptive Filter Arithmetics in Controlling Influence of Colored Noises. Geomatics and Information Science of Wuhan University, 31(8): 731-735.

Dach, R., Hugentobler, U., Fridez, P. and Meindl, M., 2007. Bernese GPS software version 5.0. In: U.o.B. Astronomical Institute (Editor).

Dai, W., Chen, Z., Kuang, C. and Cai, C., 2011. Modeling Regional Precise Tropospheric Delay. Geomatics and Information Science of Wuhan University, 36(4): 392-396.

Defraigne, P. and Bruyninx, C., 2007. On the link between GPS pseudorange noise and day-boundary discontinuities in geodetic time transfer solutions. GPS Solutions, 11(4): 239-249.

Defraigne, P., Bruyninx, C. and Guyennon, N., 2007. GLONASS and GPS PPP for time and frequency transfer, Geneva, Switzerland, pp. 909-913.

Defraigne, P., Guyennon, N. and Bruyninx, C., 2008. GPS Time and Frequency Transfer: PPP and Phase-Only Analysis. Journal of Navigation and Observation: 1-7.

Deng, Z., 2003. Self-tuning Filtering Theory with Applications -- Modern Time Series Analysis Method. Press of Harbin Institute of Technology, Harbin.

Dixon, K., 2006. StarFireTM: A global SBAS for sub-decimetre precise point positioning, ION GNSS 2006, Fort Worth, Texas, pp. 2286-2296.

Dodd, D., Howden, S. and Bisnath, S., 2006. Implementation of Ionosphere and Troposphere Models for High-Precision GPS Positioning of a Buoy During Hurricane Katrina, ION GNSS 2006, Fort Worth, Texas, pp. 2006-2016.

Dow, J., Neilan, R. and Rizos, C., 2009. The International GNSS Service in a changing landscape of global navigation satellite systems. Journal of Geodesy, 83(3): 191-198.

Elsobeiey, M. and Al-Harbi, S., 2015. Performance of real-time Precise Point Positioning using IGS real-time service. GPS Solutions.

ESA, 2015.

ESA, 2016.

Gandolfi, S., Tavasci, L. and Poluzzi, L., 2015. Improved PPP performance in regional networks. GPS Solutions.

Gao, W., Feng, X. and Zhu, D., 2007a. GPS/INS Adaptively Integrated Navigation Algorithm Based on Neural Network. Journal of Geodesy and Geodynamics, 27(2): 64-67.

Gao, W., Yang, Y., Cui, X. and Zhang, S., 2006a. Application of Adaptive Kalman Filtering Algorithm in IMU/GPS Integrated Navigation System. Geomatics and Information Science of Wuhan University, 31(5): 466-469.

Gao, W., Yang, Y. and Zhang, S., 2006b. Adaptive Robust Kalman Filter Based on the Current Statistical Model. Acta Geodaetica et Cartographica Sinica, 35(1): 15-18.

Gao, W., Yang, Y. and Zhang, T., 2007b. Neural Network Aided Adaptive Filtering for

GPS/INS Integrated Navigation. Acta Geodaetica et Cartographica Sinica, 36(1): 26-30.

Gao, W., Yang, Y. and Zhang, T., 2008. An Adaptive UKF Algorithms for Improving the Generalizaiton of Neural Network. Geomatics and Information Science of Wuhan University, 33(5): 500-503.

Gao, Y., Skone, S., Chen, K., Nicholson, N.A. and Muellerschoen, R., 2004. Real-time sensing atmospheric water vapor using precise GPS orbit and clock products, ION GNSS 2004, Long Beach, California, pp. 2343-2352.

Gao, Y., Wojciechowski, A. and Chen, K., 2005. Airborne kinematic positioning using precise point positioning methodology. Geomatica, 59(1): 275-282.

Ge, M. and Liu, J., 1996. The estimation methods for tropospheric delays in global poitioning system. Acta Geodaetica et Cartographica Sinica, 25(4): 285-291.

Gelb, A., 1986. Applied optimal estimation. M. I. T. Press.

Geng, J., Teferle, F.N., Meng, X. and Dodson, A.H., 2010. Kinematic precise point positioning at remote marine platforms. GPS Solutions, 14(4): 343-350.

Griffiths, J. and Ray, J.R., 2009. On the precision and accuracy of IGS orbits. Journal of Geodesy, 83(3-4): 277-287.

Grinter, T. and Roberts, C., 2011. Precise point positioning: where are we now? , International Global Navigation Satellite Systems Society IGNSS symposium 2011, Sydney, NSW, Australia.

Grinter, T. and Roberts, C., 2013. Real time precise point positioning: are we there jet?, International Global Navigation Satellite Systems Society IGNSS symposium 2013, Gold Coast, QLD, Australia.

Guo, Q., 2014. Precision comparison and analysis of four online free PPP services in static positioning and tropospheric delay estimation. GPS Solutions, 19(4): 537-544.

Hadas, T., Kazmierski, K. and Bosy, J., 2015. On troposphere delay constraining in real-time GNSS Precise Point Positioning, EGU2015 European Geosciences Union General Assembly, Vienna, Austria.

He, L., Ge, M., Wang, J., Wickert, J. and Schuh, H., 2013. Experimental study on the precise orbit determination of the BeiDou navigation satellite system. Sensors, 13(3): 2911-2928.

Herring, T., 1992. Modeling atmospheric delays in the analysis of space geodetic data. In: M. J. and S. T. (Editors), Netherlands Geodetic Commision, Delft, pp. 157-164.

Hesselbarth, A., 2011. Statische und kinematische GNSS-Auswertung mittels Precise Point Positioning (PPP), Technischen Universitaet Dresden.

Hoffmann-Wellenhof, B., Lichtenegger, H. and Collins, J., 2001. GPS Theory and Practice. Springer, Wien.

Hoffmann-Wellenhof, B., Lichtenegger, H. and Wasle, E., 2008. GNSS - Global Navigation Satellite Systems. Springer Vienna.

Huang, G., 2012. Research on Algorithms of Precise Clock Offset and Quality Evaluation of GNSS Satellite Clock, Chang'an University, Xi'an, China.

Huang, G., Yang, Y., Liu, C., Zhang, Q. and Zhang, S., 2013. GNSS Precise Point Positioning Algorithm Based on Parameter Equivalent Reduction Principle, China Satellite Navigation Conference (CSNC) 2013. Springer-Verlag Berlin Heidelberg, pp.

449-469.
Huang, G., Yang, Y. and Zhang, Q., 2011. Estimate and Predict Satellite Clock Error Using Adaptively Robust Sequential Adjustment with Classified Adaptive Factors Based on Opening Windows. Acta Geodaetica et Cartographica Sinica, 40(1): 15-21.
Huang, G. and Zhang, Q., 2012. Real-time estimation of satellite clock offset using adaptively robust Kalman filter with classified adaptive factors. GPS Solutions, 16(4): 531-539.
Huber, P., 1981. Robust Statistics. John Wiley, New York.
IAC, 2015.
Jiang, N., Xu, Y., Xu, T., Xu, G., Sun, Z. and Schuh, H., 2016. GPS/BDS short-term ISB modelling and prediction. GPS Solutions.
Jokinen, A., Feng, S., Milner, C., Schuster, W. and Ochieng, W., 2011. Precise Point Positioning and Integrity Monitoring with GPS and GLONASS, European Navigation Conference 2011, London, United Kingdom.
Kjørsvik, N., Gjevestad, J. and Øvstedal, O., 2006. Handling of the tropospheric delay in kinematic precise point positioning, Meeting of the Satellie Division of the Institute of Navigation, pp. 2279-2285.
Koch, K. and Yang, Y., 1998. Robust Kalman filter for rank deficient observation models. Journal of Geodesy, 72: 436-441.
Koch, K.R., 2000. Einfuehrung in die Bayes-Statistik. Springer, Berlin Heidelberg New York.
Koch, K.R. and Kusche, J., 2002. Regularization of geopotential determination from satellite data by variance components. Journal of Geodesy, 76(5): 259-268.
Kouba, J., 2009b. Testing of global pressure/temperature (GPT) model and global mapping function (GMF) in GPS analyses. Journal of Geodesy, 83(3-4): 199-208.
Kouba, J. and Héroux, P., 2001. Precise point positioning using IGS orbit and clock products. GPS Solutions, 5(2): 12-28.
Lagler, K., Schindelegger, M., Bohm, J., Krasna, H. and Nilsson, T., 2013. GPT2: Empirical slant delay model for radio space geodetic techniques. Geophys Res Lett, 40(6): 1069-1073.
Leandro, R.F., Santos, M.C. and Langley, R., 2007. PPP-based ionospheric activity monitoring, Meeting of the Satellite Division of The Institute of Navigation, pp. 2849-2853.
Leandro, R.F., Santos, M.C. and Langley, R.B., 2010. Analyzing GNSS data in precise point positioning software. GPS Solutions, 15(1): 1-13.
Leick, A., 2004. GPS Satellite Surveying, 3rd Edition. John Wiley, New York.
Leick, A., Rapoport, L. and Tatarnikov, D., 2015. GPS Satellite Surveying, 4th Edition. John Wiley, New York.
Li, B. and Shen, Y., 2009. Fast GPS Ambiguity Resolution Constraint to Available Conditions. Geomatics and Information Science of Wuhan University, 34(1): 117-121.
Li, H., 2012. Research on the Single Station Time Service and Time Offset based on the GPS and GLONASS data, Chang'an University, Xi'an, China.
Li, H., Wang, J., Hu, C. and Chen, J., 2010. The Research on Precise Point Positioning Based on the Epoch-difference. Journal of Astronautics, 31(3): 748-752.
Li, L., Kuang, C., Zhu, J., Chen, Y. and Li, H., 2011. Influence analysis of horizontal gradients and mapping functions on tropospheric delay estimation. Geotechnical

Investigation and Surveying, 39(5): 52-56.
Li, X., 2013. Rapid Ambiguity Resolution in GNSS Precise Point Positioning, Wuhan University.
Li, X., Zhang, X., Ren, X., Fritsche, M., Wickert, J. and Schuh, H., 2015. Precise positioning with current multi-constellation Global Navigation Satellite Systems: GPS, GLONASS, Galileo and BeiDou. Scientific reports, 5: 8328.
MacMillan, D., 1995. Atmospheric gradients from very long baseline interferometry observations. Geophysical Research Letters, 22: 1041-1044.
MacMillan, D. and Ma, C., 1994. Evaluation of very long baseline interferometry atmospheric modeling improvements. Journal of Geophysical Research, 99(B1): 637-651.
Miyazaki, S.i., Iwabuchi, T., Heki, K. and Naito, I., 2003. An impact of estimating tropospheric delay gradients on precise positioning in the summer using the Japanese nationwide GPS array. Journal of Geophysical Research: Solid Earth, 108(B7): 2335-2345.
Moreno Monge, B., Rodríguez-Caderot, G. and de Lacy, M.C., 2013. Multifrequency algorithms for precise point positioning: MAP3. GPS Solutions.
Niell, A., 1996. Global mapping functions for the atmosphere delay at radio wavelengths. Journal of Geophysical Research, 101(B2): 3227-3246.
Paziewski, J. and Wielgosz, P., 2015. Accounting for Galileo-GPS inter-system biases in precise satellite positioning. Journal of Geodesy, 89(1): 81-93.
Petrovello, M., 2006. Narrowlane: is it worth it? GPS Solutions.
Ren, C., Peng, J., She, D. and Wu, W., 2011. Effects of low GPS satellite elevation mask angle on estimation of tropospheric delay. Journal of Geodesy and Geodynamics, 31(6): 124-127.
Saastamoinen, J., 1972. Atmospheric correction for the troposphere ans stratosphere in radio ranging of satellites. Geophysical Monograph Series, 15: 247-251.
Schwarz, K., Cannon, M. and Wong, R., 1989. A comparison of GPS kinematic models for the determination of position and velocity along a trajectory. Manuscripta Geodaetica, 14(6): 345-353.
She, D., Xie, S. and Peng, J., 2011. The influence of satellite elevation angle changing on atmospheric refraction. GNSS World of China, 02: 25-28.
Shen, Y., Li, B. and Xu, G., 2008. Simplified equivalent multiple baseline solutions with elevation-dependent weights. GPS Solutions, 13(3): 165-171.
Shen, Y. and Xu, G., 2007. Simplified equivalent representation of GPS observation equations. GPS Solutions, 12(2): 99-108.
Shi, J. and Gao, Y., 2014. A Troposphere Constraint Method to Improve PPP Ambiguity-Resolved Height Solution. Journal of Navigation, 67: 249-262.
Someswar, G., Rao, T. and Chigurukota, D., 2013. Global Navigation Satellite Systems and Their Applications. International Journal of Software and Web Sciences, 3(1): 17-23.
Sui, L., Liu, Y. and Wang, W., 2007. Adaptive Sequential Adjustment and Its Application. Geomatics and Information Science of Wuhan University, 32(1): 51-54.
Teke, K., Böhm, J., Nilsson, T., Schuh, H., Steigenberger, P., Dach, R., Heinkelmann, R., Willis, P., Haas, R., García-Espada, S., Hobiger, T., Ichikawa, R. and Shimizu, S.,

2011. Multi-technique comparison of troposphere zenith delays and gradients during CONT08. Journal of Geodesy, 85(7): 395-413.

Teunissen, P., 2003. Towards a unified theory of GPS ambiguity resolution. GPS Solutions, 2(1): 1-12.

Teunissen, P., 2005. GNSS ambiguity resolution with optimally controlled failure-rate. Artificial Satellites, 40(4): 219-227.

Teunissen, P., Jonge, P. and Tiberius, C., 1997. Performance of the LAMBDA method for fast GPS ambiguity resolution. J Inst Navig, 44(3): 373-383.

Tregoning, P. and Herring, T.A., 2006. Impact of a priori zenith hydrostatic delay errors on GPS estimates of station heights and zenith total delays. Geophysical Research Letters, 33: L23303.

Tsujii, T., Wang, J., Rizos, C., Harigae, M. and Inagaki, T., 2000. Estimation of Residual Tropospheric Delay for High-Altitude Vehicles: Towards Precise Positioning of a Stratosphere Airship, ION GPS 2000, Utah.

Wang, J., Rizos, C., Stewart, M.P. and Leick, A., 2001. GPS and GLONASS integration-Modeling and Ambiguity Resolution Issues. GPS Solutions, 5(1): 55-64.

Wang, L., 2014. A Study on Key Technology of High Precision GPS Monitoring for Geological Hazard, Chang'an University, Xi'an, China.

Wanninger, L., 2012. Carrier-phase inter-frequency biases of GLONASS receivers. Journal of Geodesy, 86: 139-148.

Wu, F. and Yang, Y., 2010. A New Two-Step Adaptive Robust Kalman Filtering in GPS/INS Integrated Navigation System. Acta Geodaetica et Cartographica Sinica, 39(5): 522-533.

Xie, J., 2014. Theory of surveying data processing with prior information and its applications in geodesy, Central South University, Changsha, China.

Xu, C. and Wu, S., 2009. Tropospheric gradient estimation model and its effect in the GPS precise point positioning. Journal of Minjiang University, 30(2): 95-98.

Xu, G., 2002. GPS data processing with equivalent observation equations. GPS Solutions, 6(1-2): 28-33.

Xu, G., 2003. A diagonalization algorithm and its application in ambiguity search. Journal of Global Positioning Systems, 2(1): 35-41.

Xu, G., 2007. GPS Theory, Algorithms and Applications, 2nd Edition. Springer, Berlin Heidelberg.

Xu, G., Shen, Y., Yang, Y., Sun, H., Zhang, Q., Guo, J. and Yeh, T.-K., 2010. Equivalence of GPS Algorithms and Its Inference. In: G. Xu (Editor), Sciences of Geodesy-I: Adavances and Future Directions. Springer-Verlag Berlin Heidelberg.

Xu, T. and Yang, Y., 2000. The Improved Method of Sage Adaptive Filtering. Science of Surveying and Mapping, 25(3): 22-24.

Xu, Y., 2012. Studies on Antarctic GNSS Precise Positioning, Chang'an University, Xi'an, China.

Xu, Y., Jiang, N., Xu, G., Yang, Y. and Schuh, H., 2015. Influence of meteorological data and horizontal gradient of tropospheric model on precise point positioning. Advances in Space Research, 56(11): 2374-2383.

Xu, Y., Yang, Y. and Xu, G., 2012. Precise determination of GNSS trajectory in the Antarctic

airborne kinematic positioning, China Satellite Navigation Conference. Springer, Guangzhou, China, pp. 95-105.

Xu, Y., Yang, Y. and Xu, G., 2014. Analysis on tropospheric delay in Antarctic GPS positioning. Journal of Geodesy and Geodynamics, 34(1): 104-107.

Yang, Y., 1994. Robust Estimation for Dependent Observations. Manuscripta Geodaetica(19): 10-17.

Yang, Y., 1997. Robust Kalman Filter for Dynamic Systems. Journal of the PLA Institute of Surveying and Mapping, 14(2): 79-84.

Yang, Y., 1999. Robust Estimation of Geodetic Datum Transformation. Journal of Geodesy, 73(5): 268-274.

Yang, Y., 2006. Adaptive Navigation and Kinematic Positioning. Surveying and Mapping Press, Beijing.

Yang, Y., 2010. Progress, Contribution and Challenges of Compass/Beidou Satellite Navigation System. Acta Geodaetica et Cartographica Sinica, 39(1): 1-6.

Yang, Y. and Cui, X., 2008. Adaptively Robust Filter with Multi Adaptive Factors. Survey Review, 40(309): 260-270.

Yang, Y. and Gao, W., 2006a. A New Learning Statistic for Adaptive Filter Based on Predicted Residuals. Progress in Natural Science, 16(8): 833-837.

Yang, Y. and Gao, W., 2006b. An Optimal Adaptive Kalman Filter. Journal of Geodesy, 80(4): 177-183.

Yang, Y., He, H. and Xu, G., 2001. Adaptively robust filtering for kinematic geodetic positioning. Journal of Geodesy, 75(2-3): 109-116.

Yang, Y., Li, J., Wang, A., Xu, J., He, H., Guo, H., Shen, J. and Dai, X., 2014. Preliminary assessment of the navigation and positioning performance of BeiDou regional navigation satellite system. Science China: Earth Sciences, 57: 144-152.

Yang, Y., Ren, X. and Xu, Y., 2013. Main Progress of Adaptively Robust Filter with Application in Navigation. Journal of Navigation and Positioning, 1(1): 9-15.

Yang, Y., Song, L. and Xu, T., 2002. Robust Estimator for Correlated Observations Based on Bifactor Equivalent Weights. Journal of Geodesy, 76(6-7): 353-358.

Yang, Y. and Wen, Y., 2004. Synthetically adaptive robust filtering for satellite orbit determination. Science in China Series D Earth Sciences, 47(7): 585-592.

Yang, Y. and Xu, T., 2003. An Adaptive Kalman Filter Based on Sage Windowing Weights and Variance Components. Journal of Navigation, 56(2): 231-240.

Yang, Y. and Zeng, A., 2009. Adaptive Filtering for Deformation Parameter Estimation in Consideration of Geometrical Measurements and Geopgysical Models. Science in China Series D Earth Sciences, 52(8): 1216-1222.

Yang, Y., Zhang, X. and Xu, J., 2011. Adaptively Constrained Kalman Filtering for Navigation Applications. Survey Review, 43(322): 370-381.

Ye, S., Zhang, S. and Liu, J., 2008. Precise Analysis of Precise Point Positioning Based Tropospheric Delay Estimation. Geomatics and Information Science of Wuhan University, 33(8): 788-791.

Zang, N., Zhang, Q., Li, S., Huang, G. and Zhang, S., 2014. GNSS Dynamic PPP Based on Additional Priori Coordinate and Epoch Constraints Information, China Satellie Navigation Conference (CSNC) 2014. Springer-Verlag Berlin Heidelberg, pp.

269-283.

Zhang, R., Zhang, Q., Huang, G., Wang, L. and Qu, W., 2015. Impact of tracking station distribution structure on BeiDou satellite orbit determination. Advances in Space Research, 56(10): 2177-2187.

Zhang, S., Yang, Y. and Zhang, Q., 2007. An Adaptively Robust Filter Based on Bancroft Algorithm in GPS Navigation. Geomatics and Information Science of Wuhan University, 32(4): 309-311.

Zhou, J., 1985. On the Jie Factor. Acta Geodaetica et Geophysica, 5.

Zhou, J., 1989. Classical Theory of Errors and Robust Estimation. Acta Geodaetica et Cartographica Sinica, 18(2): 115-120.

Zumberge, J., Heflin, M., Jefferson, D., Watkins, M. and Webb, F., 1997. Precise point positioning for the efficient and robust analysis of GPS data from large networks. Journal of Geophysical Research, 102(B3): 5005-5017.

Acknowledgements

The completion of this thesis would not be possible without the support of many people and organizations.

First of all I would like to express my profound respect and gratitude to my supervisors, Prof. Dr. Dr. h.c. Harald Schuh at TU Berlin and GFZ, Prof. Prof. h.c. Dr. Guochang Xu formerly at GFZ and now at Shandong University at Weihai China, for supervising this thesis, for their continuous support, guidance and encouragement of my studies and research. They are always willing to share their insights with me and are patient with every question. And also many thanks for their organization of my work and improvements of my publications.

I would like to thank Prof. Dr. Jürgen Oberst of TU Berlin for his work on my thesis defense. My special words of thanks would go to Prof. Dr. Luísa Bastos of Universität Porto and Prof. Dr. Roman Galas of TU Berlin for reviewing the thesis and attending the thesis defense. Thanks very much for their comments and works which are quite beneficial for this thesis.

I appreciate the friendly concerning from Prof. Dr. Frank Flechtner and Dr. Christoph Förste during my stay at GFZ. Dr. Christoph Förste is particularly thanked for improving the German abstract translation of this thesis. I am also grateful to Prof. Dr. Jens Wickert for his kindly help that I could start my PhD work at GFZ.

I would like to express my gratitude to my former advisors Prof. Yuanxi Yang and Prof. Qin Zhang, for their continuous support throughout the last years. I would like also to thank Dr. Tianhe Xu, for his helpful suggestions and discussions. I owe special thanks to Dr. Guanwen Huang, who always offers me detailed guidance and selfless help that I can advance forward successfully.

I would like also to thank my GFZ colleagues Dr. Svetozar Petrovic, Dr. Franz Barthelmes, Dr. Maiko Ritschel, Mr. Hartmut Pflug, Ms. Angelika Svarovsky, Dr. Rolf Koenig, Dr. Karl Neumayer, Dr. Grzegorz Michalak, Dr. Christian Gruber, Christoph Dahle, Ms. Karin Bogner. I have enjoyed working with them and I appreciate their friendly help very much. Many thanks are also expressed to the colleagues and students of GFZ and TU Berlin and Shandong

University at Weihai, Prof. Dr. Hermann Kaufmann, Dr. Nina Bösche, Dr. Kaifei He, Dr. Yumiao Tian, Dr. Kejie Chen, Min Li, Biao Lu, Jia Xu, Dr. Yujun Du, Dr. Fan Gao, Jing Qiao, Zhangzhen Sun, Wenlin Yan, Chunhua Jiang, Wenfeng Nie, Chaonan Ji, Taihao Wang and others, for their kindly help and discussions.

I am indebted to my host institute GFZ where I was doing my research from 2013 to 2016. TU Berlin is also thanked for my study during this period. Shandong University at Weihai is also appreciated for my short-term stay with doing research. The International GNSS Service (IGS) is thanked for providing GNSS data and products.

Gratefully acknowledged are the China Scholarship Council (CSC) and the Education Section of the Embassy of the People's Republic of China in the Federal Republic of Germany, which financially supported my PhD research work for four years.

Finally, I would like to express my best gratitude to my parents for their endless support and understanding of my works. The person I wish to thank most is my husband, Nan Jiang, who supports and accompanies me, gives me courage, confidence and love all the time.